Spring 4-24-2020

RESEARCH TOOLS AND THEIR USES FOR DETERMINING THE THERMAL INACTIVATION KINETICS OF SALMONELLA IN LOW-MOISTURE FOODS

Soon Kiat Lau
University of Nebraska-Lincoln, lskiat@huskers.unl.edu

RESEARCH TOOLS AND THEIR USES FOR DETERMINING THE THERMAL INACTIVATION KINETICS OF SALMONELLA IN LOW-MOISTURE FOODS

by

Soon Kiat Lau

A DISSERTATION

Presented to the Faculty of

The Graduate College at the University of Nebraska

In Partial Fulfillment of Requirements

For the Degree of Doctor of Philosophy

Majors: Food Science & Technology and Biological Engineering

Under the Supervision of Professors Curtis L. Weller and David D. Jones

Lincoln, Nebraska

April, 2020

RESEARCH TOOLS AND THEIR USES FOR DETERMINING THE THERMAL INACTIVATION KINETICS OF SALMONELLA IN LOW-MOISTURE FOODS

Soon Kiat Lau, Ph.D.

University of Nebraska, 2020

Advisers: Dr. Curtis L. Weller and Dr. David D. Jones

The reputation of low-moisture foods as safe foods has been crumbling over the past decade due to repeated involvement in foodborne illness outbreaks. Although various pasteurization technologies exist, a majority are thermal processes and have not been well-characterized for pasteurizing low-moisture foods. In addition, the nature of a low-moisture food matrix introduces various experimental complications that are not encountered in high-moisture foods. In this dissertation, the development, building instructions, and characterization of various open source tools for studying the inactivation kinetics of microorganisms in low-moisture foods are described. The first tool is the TDT Sandwich, a dry heating device for measuring the thermal inactivation kinetics of microorganisms. The second tool is the HumidOSH, a self-contained environmental chamber for adjusting the water activity of food samples. Accompanying these tools are two studies that characterized the thermal inactivation kinetics of *Salmonella* and *Enterococcus faecium* NRRL-B2354 in whole milk powder and chia seeds. The TDT Sandwich was shown to produce thermal inactivation kinetics that are comparable with commonly used methods while also demonstrating less variation in microbial data collected with this tool. The comparison of model parameters using statistical tests of significance is discussed with the use of Monte Carlo simulations. *E.*

faecium was shown to be a conservative surrogate to *Salmonella* in chia seeds. The variability between production lots of chia seeds was found to have a large impact on the inactivation kinetics of both *Salmonella* and *E. faecium*. The open source tools presented in this dissertation and the accompanying conclusions of the thermal inactivation studies can be used to accelerate scientific progress in understanding and improving the microbiological safety of low-moisture foods.

For the late D.F. and R., the Grand Magus

Acknowledgements

I've heard many a time from people who are far wiser than me that the time we spend in school is invaluable because we may never ever again enjoy such a low-risk environment for learning and making mistakes once we are unceremoniously plopped into the "real world." The one thing that I wasn't told, however, is how the learning is not limited to what's just on the books—we also learn how to communicate effectively, recognize the efforts and works of others, handle convoluted paperwork/procedures, and gain a profound appreciation of science in general. On the darker side of things, I've seen firsthand unethical practices, wasteful politics, and had to deal with stresses on my mental health. These bittersweet experiences have littered my academic journey with both stepping stones and pitfalls, but have ultimately redefined me as a person—both attitude and goals—and I must acknowledge the individuals who have been instrumental in my learning experiences, without whom I may never end up where I am today.

Dr. Jeyamkondan Subbiah has been one of the most prominent figures in my life since my time in my master's program and will continue to be for the foreseeable future. My doctoral program was off to a rocky start and went further downhill from there, but I was able to climb myself back up with Dr. Subbiah's guidance. Research is full of ups and downs, and the advices given by Dr. Subbiah—both life- and work-related—have pulled me back on track more than a few times. Yet, times change and people need to move forward, so it was a great personal loss when Dr. Subbiah had to advance his career at another university. However, he still spent time and effort to remotely advise not just me, but other students in our group. The lessons I've learned from Dr. Subbiah have been

invaluable, so if you are reading this, **THANK YOU** for everything that you have done for me!

When I was young, I was adamant to not be an engineer because I, like most teenagers, was rebellious against my parents and in particular my father's career choice as an engineer. Little did I know upon stepping into the world of food science that I would kindle a passion for engineering. This wasn't a purely personal effort, however, as the initial inspiration and subsequent learning experiences came from engineering faculty members. Once again, I am grateful to Dr. Subbiah here for his initial encouragement for me to get into the engineering side of things during my research. During my early days as a graduate student, Dr. Sohan Birla was also instrumental in shaping my views and sparking my passion for engineering. I've also had the opportunity to learn from Dr. Florin Bobaru, Dr. George Gogos, Dr. Ravi Saraf, and Dr. William Velander, all of whom concreted my belief that perfectionism is not a terrible thing; it is in fact much needed when it comes to the math side of engineering! My learning experiences in engineering culminated with Dr. Mehrdad Negahban who showed me the beauty that can be found in engineering, be it the way equations are derived, simplified, and modified to finally meld together in a monolithic block of statements or appreciating the theory and programming for finite element modeling.

Upon Dr. Subbiah's departure, a few selfless individuals stepped up and agreed to selflessly guide me through the remainder of my doctoral program. Dr. Curtis Weller and Dr. David Jones, both of whom respectively co-advise me for my Food Science and Biological Engineering majors, helped me at my times of need despite their busy

schedules. Dr. Byron Chaves gave some great advice for the microbiology portions of my project and implemented some safety measures in the laboratories of our group that helped put everyone at ease and focus on our work. I am also thankful that my committee members are willing to set aside time in their schedules for my meetings even though they do not have a personal stake in my projects.

A special shoutout to Dr. Chris Calkins, Felipe Azevedo Ribeiro, and many others from the Meat Science department whom I've worked and interacted with during my involvement with their beef dry aging project. Although this project isn't a part of my dissertation, the amount of knowledge I've gained from working with these amazing people have either affected my own work or improved my understanding of the food supply chain. I also appreciate the conversations I've had and life advice I've received from Dr. Calkins and Felipe during hard times in my academic journey.

I am extremely thankful to my current and past lab members Ryan Anderson, Emily Bender, Long Chen, Alisha Kar, Yawen Lin, Xinman Lou, Sabrina Vasquez, Tushar Verma, and Xinyao Wei, all of whom had taught me to find joys in life other than in work itself. I really appreciate the lunch and dinner outings we had and the scientific problems that we solved together. I am also thankful for their patience with me when I'm having the blues in my research program.

A lot of my research work would have been delayed or not been possible without the indirect help I've received from various staff members of the university. I am extremely thankful to Jodi Lathrop for her patience in dealing with my exorbitantly large

amount of purchases for research supplies and equipment. When things go bad in the third floor, Julie Reiling has always been there to get us immediate help from Tetrad. Receiving packages has always been a joy with the fun talks I had with Tom Dobesh. Finally, I want to mention my appreciation of Jerry Reif and Max Wheeler of the Nebraska Innovation Studio who gave great advice and guidance in building prototypes of the tools used in my dissertation research.

Last but not the least, I am thankful for my loved ones for sticking by and supporting me through the good and bad times. I can never be thankful enough for my partner Liya Mo, the pillar of my life, who lifted my spirits when I'm at rock bottom and helped me grow as a person. You are my motivation and my drive to push on even when it feels like the world is against us. To the GALAPAGO crew, always being there for both the jokes and the gloom, I hope that our friendship will only grow stronger over time. And of course, to my dear father, mother, and brother, all of whom have given me the opportunity to be where I am today, for which I will forever be grateful for.

Table of Contents

List of Tables

List of Figures

Chapter 1: Introduction and Review of Literature

1.1. Low-moisture Foods

The Food and Agriculture Organization of the United Nations defines low-moisture foods (LMF) as foods with a water activity of less than 0.85 (*7*). Since moisture content is related but does not always exactly correlate with water activity, LMF are also sometimes called low water activity foods. Water activity is a measure of the availability of water for any kind of reactions including biological ones, and thus a low water activity could halt the growth of or even inactivate microorganisms. It is of no surprise then that a lot of LMF are dried for preservation purposes *e.g.* dried meat, dried fruits, nuts, spices. With a lower water activity, the nutritional and sensory qualities of these foods are maintained for a longer period of time while minimizing microbiological activity. Many LMF (such as those previously listed) are also consumed without cooking due to their perceived safety. Yet, the reputation of LMF as safe foods has been tarnished over the past few decades due to the repeated association with foodborne illness outbreaks all over the US, be it as nuts (*16*, *18*, *25*, *27*), spreads (*21*, *22*, *26*, *28*, *30*, *33*), spices (*20*), ingredients (*17*, *24*, *31*, *32*), pet food (*19*, *29*, *34*), and even stimulants (*23*). The list does not end there; many more food products have been recalled due to suspicion of contamination with pathogenic microorganisms. Investigations into the food borne illness outbreaks revealed that the culprit microorganisms are commonly those that are able to adapt and survive in the low water activity environment of LMF.

1.2. *Salmonella* in Low-moisture Foods

The genus *Salmonella*, so-named in honor of the late Dr. Daniel Elmer Salmon, is part of the Enterobacteriaceae family which includes many bacteria that live in the intestines (*59*). Of particular concern to food safety is the non-typhoidal subspecies *Salmonella enterica* subsp. *enterica*. Within this subspecies, many serovars exist such as Enteritidis, Montevideo, Tennessee, and many more. For brevity purposes, a specific serovar of *Salmonella* is commonly shortened to its abbreviated genus and serovar *e.g.* *Salmonella enterica* subsp. *enterica* Serovar Enteritidis would be written as *S.* Enteritidis. Pathogenic non-typhoidal *Salmonella* serovars cause a variety of gastrointestinal complications collectively known as salmonellosis. Symptoms include inflammation of the digestive tract, nausea, diarrhea, and damage to the intestinal lining (*59*). If the infected individual has a compromised immune system, further health complications may arise leading to possible death. The infectious dose of *Salmonella* appears to be dependent on a variety of factors such as the consumer, food matrix, and *Salmonella* strain, with volunteer studies reporting infectious doses of up to 10^{10} cells while assessments on salmonellosis outbreak data indicated doses as low as 81 MPN (*10*, *48*). A large-scale survey published by the United Nations revealed that *Salmonella* contamination in LMF accounts for approximately 44.9% of worldwide foodborne illness outbreaks, primarily traced back to confectionary products, spices, nuts, and seeds (*7*). There is also a disturbing rising trend of antibiotic resistance in some *Salmonella* serovars (*4*).

The ubiquity of *Salmonella* in LMF is partly due to its ability to survive under the harshest conditions. Upon exposure to a dry environment, varying populations of *Salmonella* will activate a plethora of metabolic processes such as accumulating compatible solutes and osmoprotectants, entering a dormant state called viable but nonculturable (VBNC), forming filaments, cannibalizing ribosomal RNA for nutrients, and modifying the cell membrane (*13*, *43*). Like most other bacteria, *Salmonella* also acquires additional tolerance to other stresses after acclimatizing to desiccation stress. *Salmonella* has exhibited increased tolerance against heat in a variety of LMF such as almonds, cocoa, chocolate, corn flour, dry milk powder, egg products, hazelnut, peanut butter, wheat flour—the list goes on and is continuously expanding even now (*13*, *63*). As such, common pasteurization conditions that sufficiently eliminated *Salmonella* in high-moisture foods may not be applicable in LMF.

1.3. Thermal Pasteurization of Low-moisture Foods

Thermal pasteurization has historically been the most direct method for reducing bacterial populations in food products. **Table 1.1** gives a brief overview of some pasteurization technologies, both thermal and non-thermal, currently in use or being researched. Thermal pasteurization of LMF is particularly difficult because moist heat (*i.e.* steam) traditionally used by the food industry are not readily applicable on LMF due to its inherent dryness, unless the process is followed by a drying step. Additionally, thermal pasteurization processes can alter/reduce heat-sensitive components in spices and herbs. The problem is further convoluted by the increased thermal tolerance of *Salmonella* spp. in LMF as previously described. With all these disadvantages, it seems

Table 1.1. Common pasteurization technologies for food products.

Technology	Advantages	Disadvantages
Moist heat (saturated steam, superheated steam)	Readily available	High thermal resistance in *Salmonella* (*63*); degrades heat-labile volatile compounds; condensation could occur; unsuitable for pastes/spreads
Dry heat (hot air, plate heat exchanger)	Readily available; could be part of the production process (e.g. roasting, drying)	High thermal resistance in *Salmonella* (*63*); degrades heat-labile volatile compounds
Non-ionizing visible radiation (pulsed light, ultraviolet)	Usually non-thermal depending on process conditions	Microorganisms shaded from the light source would survive (*54*); unsuitable for pastes/spreads
Non-ionizing radiofrequency radiation (microwave, radiofrequency)	Volumetric process; suitable for most LMF	High thermal resistance in *Salmonella* (*63*); degrades heat-labile volatile compounds; heating efficiency highly dependent on dielectric properties (*62*)
Ionizing radiation (gamma, e-beam)	Non-thermal; Volumetric process; suitable for most LMF	Produces byproducts and off-flavors (*41*); mixed consumer acceptance and label requirements (*49*)
High pressure processing	Usually non-thermal depending on process conditions; volumetric process	Cost-intensive (*68*); Non-continuous process; food must be in flexible packaging
Cold plasma	Thermal/non-thermal, depending on distance from applicator	Indirect application (sample far from applicator) requires long process time (*50*)
Antimicrobial gases (chlorine dioxide, ethylene oxide, ozone, etc.)	Non-thermal, can diffuse into bulk of product	Risk of chemical byproducts depending on the gas and process conditions.

as if thermal pasteurization should not even be an option for LMF! However, the wide availability of thermal processing equipment and mature understanding of heat transfer physics means that thermal processing should still be considered, at least as a first attempt at pasteurizing a specific food product. In addition, the production of most LMF usually involves a drying step (*e.g.* hot air drying, spray drying, drum drying, roasting) which could be readily adjusted to harsher processing conditions to inactivate the pathogen(s) of interest. The literature is also rife with studies on the thermal inactivation kinetics of bacteria in LMF—some of these studies are listed in **Table 1.2**. Due to increasing regulatory pressure for food manufacturers to validate the microbial safety of their processes, the wide availability of resources for thermal pasteurization of LMF makes it the more attractive "first-step" approach.

Thermal pasteurization of foods is commonly characterized by the temperature of the process and the duration that the food is exposed to the treatment. Other parameters such as pH may also be applicable depending on the food matrix. In the context of LMF, however, moisture plays an extremely important role. Various studies have shown that the thermal resistance of various bacteria including *Salmonella* is decreased if the room temperature water activity of the inoculated LMF was increased (*74*). In addition, an increase of process humidity during a baking or roasting process has also been shown to dramatically reduce the thermal resistance of *Salmonella* (*15*, *69*). Therefore, the water activity and process humidity of LMF are important parameters to monitor and adjust for thermal pasteurization processes.

Table 1.2. A selection of studies on the thermal resistance of *Salmonella* in LMF.

Food product	Summary of results
Almond, whole	D-values of *Salmonella* ranged from 15.7 to 18.0 min depending on water activity (*45*)
Almond flour	D-values for *S.* Enteritidis PT30 at 80 °C ranged from 0.8 to 27.3 min depending on water activity (*78*)
Confectionary model food	Time taken to reduce an *Escherichia coli* cocktail by 5 logs between 80 to 110 °C ranged between 114.4 to 575.9 min (*36*)
Chicken powder	Time taken to reduce an *Escherichia coli* cocktail by 5 logs between 80 to 120 °C ranged between 60.7 to 879.2 min (*36*)
Peanut butter	• At 90 °C, *S.* Tennessee required 120 min to be reduced by 7 log while other *Salmonella* serovars needed between 55 to 86 min (*56*) • Reductions between 0.41 to more than 5.17 log CFU/g were achieved for *Escherichia coli* O157:H7, *S.* Typhimurium, and *Listeria monocytogenes* depending on applied microwave power (*71*)
Pecan	Inoculation procedure and heat treatment procedure affected the inactivation rate of *Salmonella* in pecan nutmeats (*9*)
Pet model food	Time taken to reduce an *Escherichia coli* cocktail by 5 logs between 80 to 110 °C ranged between 53.9 to 247.6 min (*36*)
Pistachio	Thermal resistance of *S.* Enteritidis PT30 was significantly reduced when the roasting process had higher humidity (*15*)
Walnut shell	D-values for *Staphylococcus aureus* ATCC 25923 between 56 to 70 °C ranged between 0.56 to 10.21 min depending on water activity (*79*)
Wheat flour	• D-values for *Escherichia coli* O121 between 70 to 80 °C ranged from 4.6 to 18.2 min (*72*) • D-values for *S.* Enteritidis PT30 at 80 °C ranged from 1.33 to 7.32 min depending on water activity and hydration/desiccation procedure (*70*) • D-values for *S.* Weltevreden between 60 to 65 °C ranged from 29 to 875 min depending on water activity (*5*) • D-values for *S.* Enteritidis PT30 at 80 °C ranged from 1.2 to 12.2 min depending on water activity (*78*) • δ-values for *Escherichia coli* O45, O121, and O145 between 55 to 70 °C ranged from 0.2 to 20.0 min. Corresponding δ-values for *Salmonella* ranged from 17.4 to 152.2 min (*44*)
Whey protein powder	D-values for *S.* Enteritidis PT30 at 80 °C ranged from 1.5 to 17.5 min depending on water activity (*78*)

1.4. Non-thermal Pasteurization of Low-moisture Foods

Non-thermal pasteurization, as the name suggests, involves subjecting food products to a treatment that inactivates microorganisms without the use of heat. However, some processes that produce some heat as a side effect (*e.g.* high-pressure processing) may also be categorized as non-thermal if heat isn't the main inactivation mechanism or if the product is actively cooled to remove heat. Non-thermal pasteurization is an attractive option due to its omission of heat which is important if a food product has heat-sensitive components or if microorganisms in the food product have high heat resistance, as commonly seen in LMF. As previously listed in **Table 1.1**, there are many types of non-thermal processes available in the modern age. However, as the list of disadvantages show, there is no "silver bullet" that could pasteurize all LMF.

Non-ionizing visible radiation utilize electromagnetic radiation in the visible region to inactivate microorganisms. Examples of technologies using this radiation include pulsed light and ultraviolet radiation. In a pulsed light treatment, food products are blasted with short bursts of highly-powered radiation in the visible range of the electromagnetic spectrum. Pulsed light has been tested for inactivating microorganisms in a few LMF such as chia seeds (*66*), peppercorns (*77*), and sesame seeds (*52*). This technology is favorable because of the absence of moving parts and chemicals. However, due to the nature of light, the design of the applicator must be optimized to ensure every part of the food product receive the light radiation. Ultraviolet is very similar to pulsed light but uses radiation at the lower end of the visible spectrum and is rarely pulsed. Ultraviolet radiation has investigated for pasteurizing black pepper (*42*) and wheat flour

(*35*, *42*). Due to its similarities to the pulsed light technology, ultraviolet radiation shares the advantages and disadvantages of pulsed light.

Ionizing radiation includes any radiation that may cause molecular changes within a food product. The application of ionizing radiation on food products is commonly called irradiation. Irradiation is commercially used on spices and has also been investigated for reducing microbial populations in apple pomace flour (*53*), black tea (*65*), halva (*61*), infant formula (*67*), tahini (*60*), and a variety of spices such as onion powder, oregano, cumin seeds and peppercorns (*6*). Irradiation is extremely effective at inactivating bacteria and has been emphasized by the World Health Organization to be an effective decontamination process (*76*). However, this technology has unfortunately been known to degrade quality of food products and has trouble finding consumer acceptance unless appropriate educational measures are put into place (*12*, *76*).

Cold plasma is the application of partially ionized gas to food products without the extreme temperatures seen in the generation of fully ionized gases and is commonly produced using a variety of methods such as corona discharge or dielectric barrier discharge (*11*). The generated plasma can be applied either directly or indirectly onto the treated food product. Cold plasma has been investigated for a variety of LMF such as almond (*39*, *58*), black peppercorn (*51*, *73*), brown rice (*55*), chickpea seed (*57*), hazelnut (*38*), maize (*37*), and wheat grain (*14*). The many ways to apply cold plasma to food products and high research interest make it an attractive technology for pasteurizing LMF, but there are some limitations such as high costs and negative impact on food quality attributes (*46*).

Antimicrobial gases are an array of gases that have been shown to be effective at inactivating microorganisms such as chlorine dioxide, vapor-phase hydrogen peroxide, and ozone. The main advantage of antimicrobial gases is the ability of gases to diffuse through air spaces and into pores, allowing the gases to effectively pasteurize irregularly shaped granular foods. Various antimicrobial gases have been investigated for LMF:

- Chlorine dioxide: seeds of cantaloupe, lettuce, and tomato (*75*)
- Ozone: black pepper (*40*), dried fig (*2*), flaked red pepper (*1*), pistachio (*3*), rice (*8*), and the seeds of cantaloupe, lettuce, and tomato (*75*)

Although the diffusivity of gases allows volumetric pasteurization of a food product, some preliminary studies have shown that the efficacy of antimicrobial gases may be affected by a variety of environmental factors such as temperature and relative humidity (*47*, *64*). The application of antimicrobial gases must thus be accompanied by strict control of the environmental parameters.

1.3. Objectives

This dissertation discusses considerations for developing pasteurization technologies for LMF. The overall goal is to develop a framework that allows the characterization and development of intervention technologies for ensuring the microbiological safety of LMF. This overall goal is broken down into two specific objectives:

- **Objective 1:** Develop a suite of open source research tools that can be utilized by other researchers to perform research into pasteurization technologies for LMF.

- **Objective 2:** Characterize the thermal inactivation kinetics of *Salmonella* and a nonpathogenic surrogate in a selection of LMF.

1.4. Dissertation Organization

This dissertation consists of six chapters. The first chapter is the introduction of the entire dissertation and provides a review of the literature on LMF pasteurization. The sixth chapter summarizes the dissertation and provides suggestions for future research. The middle four chapters contain the bulk of work that, as a whole, fulfill the dissertation objectives. Each of these four chapters is formatted as a research paper that is in the process of or have been published in peer-reviewed scientific journals.

Objective 1 is covered in Chapters 2 and 3. This objective is concerned with the development of robust scientific tools that are either necessary or would greatly improve the efficiency of the development of pasteurization technologies for LMF. Chapter 2 details the development of the TDT Sandwich, a system for applying dry heat to food samples with the aim of determining thermal inactivation kinetics of microorganisms. Chapter 3 describes the development of the HumidOSH, a relative-humidity controlled chamber for equilibrating food samples to a desired water activity for investigation into its effects on the inactivation kinetics of microorganisms.

Objective 2 is explored in both Chapters 4 and 5. The thermal inactivation kinetics of *Salmonella* is vital for the development of a reliable thermal processes that are intended to reduce or eliminate *Salmonella* in food products. In addition, by choosing a nonpathogenic surrogate, the developed process can be validated in actual food

processing environments which is an invaluable resource to the food industry. Chapter 4 compares the thermal inactivation kinetics of *Salmonella* in whole milk powder as measured by three methods. In Chapter 5, the thermal inactivation kinetics of *Salmonella* and a non-pathogenic surrogate, *Enterococcus faecium* NRRL-B2354, are characterized in whole chia seeds. Both of these chapters used the tools developed in Chapters 2 and 3.

1.5. References

1. Akbas, M. Y., and M. Ozdemir. 2008. Effect of gaseous ozone on microbial inactivation and sensory of flaked red peppers. *Int. J. Food Sci. Technol.* 43:1657–1662.
2. Akbas, M. Y., and M. Ozdemir. 2008. Application of gaseous ozone to control populations of *Escherichia coli*, *Bacillus cereus* and *Bacillus cereus* spores in dried figs. *Food Microbiol.* 25:386–391.
3. Akbas, M. Y., and M. Ozdemir. 2006. Effectiveness of ozone for inactivation of *Escherichia coli* and *Bacillus cereus* in pistachios. *Int. J. Food Sci. Technol.* 41:513–519.
4. Angelo, K. M., J. Reynolds, B. E. Karp, R. M. Hoekstra, C. M. Scheel, and C. Friedman. 2016. Antimicrobial Resistance Among Nontyphoidal *Salmonella* Isolated From Blood in the United States, 2003–2013. *J. Infect. Dis.* 214:1565–1570.
5. Archer, J., E. T. Jervis, J. Bird, and J. E. Gaze. 1998. Heat Resistance of *Salmonella* weltevreden in Low-Moisture Environments. *J. Food Prot.* 61:969–973.
6. Arias-Rios, E. V., G. R. Acuff, A. Castillo, L. M. Lucia, S. E. Niebuhr, and J. S. Dickson. 2019. Identification of a surrogate to validate irradiation processing of selected spices. *LWT* 102:136–141.
7. Batz, M., P. Cook, J.-L. Cordier, M. Danyluk, J. Farber, L. J. Harris, E. Margas, G. Montibeller, S. Igimi, L. Waddell, I. Young, V. Carolissen-Mackay, P. Desmarchelier, L. Dysart, and A. Rajić. 2014. Ranking of Low Moisture Foods in Support of Microbiological Risk Management. Food and Agriculture Organization.

8. Beber-Rodrigues, M., G. D. Savi, and V. M. Scussel. 2015. Ozone Effect on Fungi Proliferation and Genera Susceptibility of Treated Stored Dry Paddy Rice (Oryza sativa L.). *J. Food Saf.* 35:59–65.
9. Beuchat, L. R., and D. A. Mann. 2011. Inactivation of *Salmonella* on Pecan Nutmeats by Hot Air Treatment and Oil Roasting. *J. Food Prot.* 74:1441–1450.
10. Blaser, M. J., and L. S. Newman. 1982. A Review of Human Salmonellosis: I. Infective Dose. *Rev. Infect. Dis.* Oxford Academic 4:1096–1106.
11. Bourke, P., D. Ziuzina, L. Han, P. J. Cullen, and B. F. Gilmore. 2017. Microbiological interactions with cold plasma. *J. Appl. Microbiol.* 123:308–324.
12. Bruhn, C. M. 1998. Consumer acceptance of irradiated food: theory and reality. *Radiat. Phys. Chem.* 52:129–133.
13. Burgess, C. M., A. Gianotti, N. Gruzdev, J. Holah, S. Knøchel, A. Lehner, E. Margas, S. S. Esser, S. Sela (Saldinger), and O. Tresse. 2016. The response of foodborne pathogens to osmotic and desiccation stresses in the food chain. *Int. J. Food Microbiol.* 221:37–53.
14. Butscher, D., D. Zimmermann, M. Schuppler, and P. Rudolf von Rohr. 2016. Plasma inactivation of bacterial endospores on wheat grains and polymeric model substrates in a dielectric barrier discharge. *Food Control* 60:636–645.
15. Casulli, K. E., F. J. Garces-Vega, K. D. Dolan, E. T. Ryser, L. J. Harris, and B. P. Marks. 2018. Impact of Process Temperature, Humidity, and Initial Product Moisture on Thermal Inactivation of *Salmonella* Enteritidis PT 30 on Pistachios during Hot-Air Heating. *J. Food Prot.* Allen Press 81:1351–1356.

16. CDC. 2011. Multistate Outbreak of *E. coli* O157:H7 Infections Associated with In-Shell Hazelnuts (FINAL UPDATE).
17. CDC. 2013. Multistate outbreak of hepatitis A virus infections linked to pomegranate seeds from Turkey (Final Update).
18. CDC. 2011. Multistate Outbreak of Human *Salmonella* Enteritidis Infections Linked to Turkish Pine Nuts (Final Update).
19. CDC. 2019. Multistate Outbreak of Human *Salmonella* Infantis Infections Linked to Dry Dog Food (Final Update).
20. CDC. 2010. Multistate Outbreak of Human *Salmonella* Montevideo Infections (Final Update).
21. CDC. 2014. Multistate Outbreak of *Salmonella* Braenderup Infections Linked to Nut Butter Manufactured by nSpired Natural Foods, Inc. (Final Update).
22. CDC. 2012. Multistate Outbreak of *Salmonella* Bredeney Infections Linked to Peanut Butter Manufactured By Sunland, Inc. (Final Update).
23. CDC. 2018. Multistate Outbreak of *Salmonella* Infections Linked to Kratom (Final Update).
24. CDC. 2014. Multistate Outbreak of *Salmonella* Infections Linked to Organic Sprouted Chia Powder (Final Update).
25. CDC. 2009. Multistate Outbreak of *Salmonella* Infections Linked to Pistachio Nuts (FINAL UPDATE).
26. CDC. 2013. Multistate Outbreak of *Salmonella* Montevideo and *Salmonella* Mbandaka Infections Linked to Tahini Sesame Paste (Final Update).

27. CDC. 2016. Multistate Outbreak of *Salmonella* Montevideo and *Salmonella* Senftenberg Infections Linked to Wonderful Pistachios (Final Update).
28. CDC. 2016. Multistate Outbreak of *Salmonella* Paratyphi B variant L(+) tartrate(+) Infections Linked to JEM Raw Brand Sprouted Nut Butter Spreads (Final Update).
29. CDC. 2019. Multistate Outbreak of *Salmonella* Schwarzengrund Infections Linked to Dry Pet Food (FINAL UPDATE).
30. CDC. 2009. Multistate Outbreak of *Salmonella* Typhimurium Infections Linked to Peanut Butter, 2008-2009 (FINAL UPDATE).
31. CDC. 2016. Multistate Outbreak of *Salmonella* Virchow Infections Linked to Garden of Life RAW Meal Organic Shake & Meal Products (Final Update).
32. CDC. 2016. Multistate Outbreak of Shiga toxin-producing *Escherichia coli* Infections Linked to Flour (Final Update).
33. CDC. 2017. Multistate Outbreak of Shiga toxin-producing *Escherichia coli* O157:H7 Infections Linked to I.M. Healthy Brand SoyNut Butter (Final Update).
34. CDC. 2019. Outbreak of Multidrug-Resistant *Salmonella* Infections Linked to Contact with Pig Ear Pet Treats.
35. Condón-Abanto, S., S. Condón, J. Raso, J. G. Lyng, and I. Álvarez. 2016. Inactivation of *Salmonella* typhimurium and *Lactobacillus plantarum* by UV-C light in flour powder. *Innov. Food Sci. Emerg. Technol.* 35:1–8.
36. Daryaei, H., W. Peñaloza, I. Hildebrandt, K. Krishnamurthy, P. Thiruvengadam, and J. Wan. 2018. Heat inactivation of Shiga toxin-producing *Escherichia coli* in a selection of low moisture foods. *Food Control* 85:48–56.

37. Dasan, B. G., I. H. Boyaci, and M. Mutlu. 2016. Inactivation of aflatoxigenic fungi (*Aspergillus* spp.) on granular food model, maize, in an atmospheric pressure fluidized bed plasma system. *Food Control* 70:1–8.

38. Dasan, B. G., I. H. Boyaci, and M. Mutlu. 2017. Nonthermal plasma treatment of *Aspergillus* spp. spores on hazelnuts in an atmospheric pressure fluidized bed plasma system: Impact of process parameters and surveillance of the residual viability of spores. *J. Food Eng.* 196:139–149.

39. Deng, S., R. Ruan, C. K. Mok, G. Huang, X. Lin, and P. Chen. 2007. Inactivation of *Escherichia coli* on Almonds Using Nonthermal Plasma. *J. Food Sci.* 72:M62–M66.

40. Emer, Z., M. Y. Akbas, and M. Ozdemir. 2008. Bactericidal Activity of Ozone against *Escherichia coli* in Whole and Ground Black Peppers. *J. Food Prot.* 71:914–917.

41. Feliciano, C. P. 2018. High-dose irradiated food: Current progress, applications, and prospects. *Radiat. Phys. Chem.* 144:34–36.

42. Fine, F., and P. Gervais. 2004. Efficiency of Pulsed UV Light for Microbial Decontamination of Food Powders. *J. Food Prot.* Allen Press 67:787–792.

43. Finn, S., O. Condell, P. McClure, A. Amézquita, and S. Fanning. 2013. Mechanisms of survival, responses and sources of *Salmonella* in low-moisture environments. *Front. Microbiol.* 4.

44. Forghani, F., M. den Bakker, J.-Y. Liao, A. S. Payton, A. N. Futral, and F. Diez-Gonzalez. 2019. *Salmonella* and Enterohemorrhagic *Escherichia coli* Serogroups O45, O121, O145 in Wheat Flour: Effects of Long-Term Storage and Thermal Treatments. *Front. Microbiol.* 10:323.

45. Garces-Vega, F. J., E. T. Ryser, and B. P. Marks. 2019. Relationships of Water Activity and Moisture Content to the Thermal Inactivation Kinetics of *Salmonella* in Low-Moisture Foods. *J. Food Prot.* Allen Press 82:963–970.
46. Gavahian, M., and A. M. Khaneghah. 2019. Cold plasma as a tool for the elimination of food contaminants: Recent advances and future trends. *Crit. Rev. Food Sci. Nutr.* 0:1–12.
47. Guan, J., J. Tang, A. Lacombe, D. F. Bridges, B. Rane, S. Sablani, and V. C.-H. Wu. 2019. Identification of Nonpathogenic Surrogate Bacteria Applicable for Industrial-Scale Gaseous Chlorine Dioxide Treatment on Baby Carrots. IAFP.
48. Hara-Kudo, Y., and K. Takatori. 2011. Contamination level and ingestion dose of foodborne pathogens associated with infections. *Epidemiol. Infect.* Cambridge University Press 139:1505–1510.
49. Heddle, N. M., S. J. Lane, N. Sholapur, E. Arnold, B. Newbold, J. Eyles, and K. E. Webert. 2014. Implementation and public acceptability: lessons from food irradiation and how they might apply to pathogen reduction in blood products. *Vox Sang.* 107:50–59.
50. Hertwig, C., N. Meneses, and A. Mathys. 2018. Cold atmospheric pressure plasma and low energy electron beam as alternative nonthermal decontamination technologies for dry food surfaces: A review. *Trends Food Sci. Technol.* 77:131–142.
51. Hertwig, C., K. Reineke, J. Ehlbeck, D. Knorr, and O. Schlüter. 2015. Decontamination of whole black pepper using different cold atmospheric pressure plasma applications. *Food Control* 55:221–229.

52. Hwang, H.-J., C.-I. Cheigh, and M.-S. Chung. 2017. Construction of a pilot-scale continuous-flow intense pulsed light system and its efficacy in sterilizing sesame seeds. *Innov. Food Sci. Emerg. Technol.* 39:1–6.

53. Ito, V. C., A. A. Ferreira Zielinski, S. Avila, M. Spoto, A. Nogueira, E. Schnitzler, and L. G. Lacerda. 2017. Effects of gamma radiation on physicochemical, thermogravimetric, microstructural and microbiological properties during storage of apple pomace flour. *LWT - Food Sci. Technol.* 78:105–113.

54. Kramer, B., J. Wunderlich, and P. Muranyi. 2016. Recent findings in pulsed light disinfection. *J. Appl. Microbiol.* 122:830–856.

55. Lee, K. H., H.-J. Kim, K. S. Woo, C. Jo, J.-K. Kim, S. H. Kim, H. Y. Park, S.-K. Oh, and W. H. Kim. 2016. Evaluation of cold plasma treatments for improved microbial and physicochemical qualities of brown rice. *LWT* 73:442–447.

56. Ma, L., G. Zhang, P. Gerner-Smidt, V. Mantripragada, I. Ezeoke, and M. P. Doyle. 2009. Thermal Inactivation of *Salmonella* in Peanut Butter. *J. Food Prot.* 72:1596–1601.

57. Mitra, A., Y.-F. Li, T. G. Klämpfl, T. Shimizu, J. Jeon, G. E. Morfill, and J. L. Zimmermann. 2014. Inactivation of Surface-Borne Microorganisms and Increased Germination of Seed Specimen by Cold Atmospheric Plasma. *Food Bioprocess Technol.* 7:645–653.

58. Niemira, B. A. 2012. Cold Plasma Reduction of *Salmonella* and *Escherichia coli* O157:H7 on Almonds Using Ambient Pressure Gases. *J. Food Sci.* 77:M171–M175.

59. Norton, C. F. 1986. Microbiology, 2nd ed. Addison-Wesley, Reading, Mass.

60. Osaili, T. M., A. A. Al-Nabulsi, S. A. Abubakar, A. R. Alaboudi, and M. A. Al-Holy. 2016. Feasibility of Using Gamma Irradiation for Inactivation of Starvation-, Heat-, and Cold-Stressed *Salmonella* in Tahini. *J. Food Prot.* 79:963–969.

61. Osaili, T. M., A. A. Al-Nabulsi, T. F. Aljaafreh, and A. N. Olaimat. 2018. Use of gamma radiation to inactivate stressed *Salmonella* spp., *Escherichia coli* O157:H7 and *Listeria monocytogenes* in tahini halva. *LWT* 98:438–443.

62. Piyasena, P., C. Dussault, T. Koutchma, H. S. Ramaswamy, and G. B. Awuah. 2003. Radio Frequency Heating of Foods: Principles, Applications and Related Properties—A Review. *Crit. Rev. Food Sci. Nutr.* 43:587–606.

63. Podolak, R., E. Enache, W. Stone, D. G. Black, and P. H. Elliott. 2010. Sources and Risk Factors for Contamination, Survival, Persistence, and Heat Resistance of *Salmonella* in Low-Moisture Foods. *J. Food Prot.* 73:1919–1936.

64. Rane, B., A. Lacombe, S. Sablani, D. F. Bridges, J. Tang, J. Guan, and V. C.-H. Wu. 2019. Identifying Nonpathogenic *Salmonella* Surrogates for Industrial Scale Treatment of Almonds Using Gaseous Chlorine Dioxide. IAFP.

65. Rashid, Md. H., M. A. Z. Chowdhury, Z. Fardous, E. M. Tanvir, M. K. Pramanik, I. Jahan, Md. K. Alam, M. Moniruzzaman, and S. H. Gan. 2016. Microbial decontamination of gamma irradiated black tea and determination of major minerals in black tea, fresh tea leaves and tea garden soil. *LWT - Food Sci. Technol.* 73:185–190.

66. Reyes-Jurado, F., A. R. Navarro-Cruz, J. Méndez-Aguilar, C. E. Ochoa-Velasco, E. Mani-López, M. T. Jiménez-Munguía, E. Palou, A. López-Malo, and R. Ávila-Sosa.

2019. High-Intensity Light Pulses To Inactivate *Salmonella* Typhimurium on Mexican Chia (*Salvia hispanica L.*) Seeds. *J. Food Prot.* Allen Press 82:1272–1277.

67. Robichaud, V., L. Bagheri, B. R. Aguilar-Uscanga, M. Millette, and M. Lacroix. 2020. Effect of ɣ-irradiation on the microbial inactivation, nutritional value, and antioxidant activities of infant formula. *LWT* 125:109211.
68. Sevenich, R., C. Rauh, and D. Knorr. 2016. A scientific and interdisciplinary approach for high pressure processing as a future toolbox for safe and high quality products: A review. *Innov. Food Sci. Emerg. Technol.* 38:65–75.
69. Shrestha, S., W. Birbari, T. Sheehan, and K. A. Glass. 2016. Thermal Inactivation of *Salmonella* on Sesame-topped Bread during Baking Using High and Low Oven Humidity. *Food Prot. Trends* 36:116–124.
70. Smith, D. F., and B. P. Marks. 2015. Effect of Rapid Product Desiccation or Hydration on Thermal Resistance of *Salmonella enterica* Serovar Enteritidis PT 30 in Wheat Flour. *J. Food Prot.* 78:281–286.
71. Song, W.-J., and D.-H. Kang. 2016. Influence of water activity on inactivation of *Escherichia coli* O157:H7, *Salmonella* Typhimurium and *Listeria monocytogenes* in peanut butter by microwave heating. *Food Microbiol.* 60:104–111.
72. Suehr, Q. J., N. M. Anderson, and S. E. Keller. 2019. Desiccation and Thermal Resistance of *Escherichia coli* O121 in Wheat Flour. *J. Food Prot.* 82:1308–1313.
73. Sun, S., N. M. Anderson, and S. Keller. 2014. Atmospheric Pressure Plasma Treatment of Black Peppercorns Inoculated with *Salmonella* and Held Under Controlled Storage. *J. Food Sci.* 79:E2441–E2446.

74. Syamaladevi, R. M., J. Tang, R. Villa-Rojas, S. Sablani, B. Carter, and G. Campbell. 2016. Influence of Water Activity on Thermal Resistance of Microorganisms in Low-Moisture Foods: A Review. *Compr. Rev. Food Sci. Food Saf.* 15:353–370.

75. Trinetta, V., N. Vaidya, R. Linton, and M. Morgan. 2011. A comparative study on the effectiveness of chlorine dioxide gas, ozone gas and e-beam irradiation treatments for inactivation of pathogens inoculated onto tomato, cantaloupe and lettuce seeds. *Int. J. Food Microbiol.* 146:203–206.

76. Wilcock, A., and B. Ball. 2014. Food Safety, p. 11–29. *In* Practical Food Safety. Wiley-Blackwell.

77. Xie, J., and Y.-C. Hung. 2020. Efficacy of pulsed-ultraviolet light for inactivation of *Salmonella* spp on black peppercorns. *J. Food Sci.* 85:755–761.

78. Xu, J., J. Tang, Y. Jin, J. Song, R. Yang, S. S. Sablani, and M.-J. Zhu. 2019. High temperature water activity as a key factor influencing survival of *Salmonella* Enteritidis PT30 in thermal processing. *Food Control* 98:520–528.

79. Zhang, L., X. Kou, S. Zhang, T. Cheng, and S. Wang. 2018. Effect of water activity and heating rate on *Staphylococcus aureus* heat resistance in walnut shells. *Int. J. Food Microbiol.* 266:282–288.

Chapter 2: TDT Sandwich: An Open Source Dry Heat System for Characterizing the Thermal Resistance of Microorganisms

2.1. Introduction

A comprehensive understanding of the thermal death kinetics of pathogenic microorganisms is essential for designing and validating thermal pasteurization or sterilization technologies. By modeling the inactivation of microorganisms during a thermal treatment, the thermal death time (TDT) of the target microorganism can be calculated to characterize the robustness of the thermal treatment. The TDT is usually calculated from microbial death models containing one or more parameters that need to be determined experimentally using inoculated food samples and equipment with some form of temperature control.

In most cases, temperature-controlled liquid baths are used to control the temperature of samples in thermal death kinetics characterization studies because they are commercially available, user-friendly and suffice for most experimental needs. However, the use of liquid as a heating medium introduces the risk of water infiltration into samples which may affect results because water activity has been shown to affect the thermal resistance of bacteria in low-moisture foods (*42*). There are also operational disadvantages to liquid baths such as the need to pre-heat it and cleanup of liquid spillage.

There are few custom equipment that have been developed specifically for measuring the thermal death kinetics of microorganisms. The thermoresistometer mainly

consists of a vessel that has an injection port, sampling port, pressurizing port, heating coil, mixing propeller, thermocouple, and pH electrode (*8*, *9*, *10*, *15*, *32*, *36*). Initially, bacterial inoculum is injected into pre-heated sterile sample in the vessel to be heated to the target temperature. Samples are then extracted at specified time intervals from the sampling port. This instrument requires proper sample preparation to ensure that they can be stirred and flow through tubes, thus it may be unsuitable for dry and granular samples. The BUGDEATH apparatus utilizes a combination of hot dry air, steam, and cold air to heat or cool the surface of a sample (*12*, *13*, *14*, *23*, *24*, *29*). The use of the three heating/cooling systems allows reproduction of the dynamic temperature and relative humidity conditions experienced by microorganisms on the surface of a food product. However, the system is built to process only one sample at a time. The heating block system is an aluminum block padded with heating pads that has slots machined into its sides for drawers containing the samples (*4*, *5*, *22*, *44*, *45*). Each drawer has a well in which the sample is placed and then enclosed by a screw-on cap. Although the system allows the user to adjust the heating rate, the maximum heating rate of 13.3 °C/min means that it would take a while for the sample to reach the target temperature, during which some loss of the microorganism of interest may occur. Clearly, there is no silver bullet for characterizing the thermal death kinetics of microorganisms. The introduction of additional custom equipment would provide researchers with more options to choose from to satisfy their experimental objectives.

The come-up time (CUT) of a sample can be defined as the time needed for the temperature of the sample to reach within a certain threshold of the target treatment

temperature. CUT has been shown to affect the thermal resistance of bacteria and fungi in a variety of food products, with a longer CUT resulting in higher thermal resistance (*1*, *7*, *14*, *22*, *45*). If researchers are provided a research tool that allows control of CUT, it will open a path for investigation into its effects on inactivation kinetics of microorganisms.

This paper describes the design, construction, operation, and performance of the TDT Sandwich which was conceived to address the limitations and needs in existing systems and to expedite the laborious process of characterizing thermal death kinetics. The build instructions and software of the TDT Sandwich are open source and available for free to allow replication of the system by other researchers.

2.2. Hardware Description

The TDT Sandwich (**Fig. 2.1**) is a clamshell-like box that applies dry heat to a sample sandwiched between the internal heating pads. The system can raise the temperature of a sample to a desired target (up to 140 °C) and then maintain it within 0.2 °C of the target. The rate of temperature increase of the heating pads can be adjusted up to a maximum of approximately 100 °C/min. Temperature measurements are performed with type-T thermocouples with limits of error of ±0.5 °C. The electronics for the system are housed in an enclosure adhered to the top of the system that also displays the customizable identification number of the system. The TDT Sandwich connects to a computer or laptop via a USB cable and is controlled using the free software described in **Section 2.6.3**. Due to the wide availability of USB hubs, multiple TDT Sandwiches can be connected to a single computer or laptop and can be plugged in or out when not in operation, thus giving rise to its modular nature. Aside from the custom-order heaters and

printed circuit board, the TDT Sandwich is designed to be constructed from commercially available components to simplify the construction process. A single TDT Sandwich only costs about a tenth or less of scientific programmable water baths. The system is also mess-free, maintenance-free, have few moving parts, and is easy to operate. Samples treated in the TDT Sandwich are packaged in airtight pouches which create a closed environment for the sample during heating. Because it only has heating capabilities, the TDT Sandwich is not built to cool samples rapidly. Some possible usages of the TDT Sandwich include:

- Holding a sample at a target temperature for a given period of time to measure the amount of microorganisms inactivated by the heat treatment.
- Investigating the effects of CUT on the thermal resistance of a microorganism.
- Characterizing the effects of heat on quality changes in a food sample such as lipid oxidation, color change, enzyme inactivation, and destruction of heat-labile nutrients.
- General-purpose heating of samples.

2.3. Design Files

All the files necessary for the construction and operation of the TDT Sandwich are listed in **Table 2.1**. The printed circuit board (PCB) design files can be sent to a PCB manufacturer to fabricate the PCB. The Arduino code is uploaded to the microcontroller of the TDT Sandwich during the construction process. The computer program is a Windows executable file for controlling TDT Sandwiches. All the files are stored in an online repository with an accompanying “Wiki” that describes the files and their uses.

2.4. Bill of Materials

Tables 2.2 and **2.3** list all the materials needed for building a single TDT Sandwich. Some specialized tools or consumables used during the construction process are listed in **Table 2.4**. Once the TDT Sandwich has been constructed and is ready to be used, it is recommended to seal samples in the disposable pouches listed in **Table 2.5**. Decimal quantities are given for items that are sold in bulk but of which only one or a few units are needed.

2.5. Design and Construction

This section provides instructions for constructing the TDT Sandwich and the rationale behind certain design aspects of the system.

2.5.1. Build Instructions

The TDT Sandwich consists of multiple components, most of which can be constructed independently of each other before everything is assembled. Step-by-step instructions with accompanying pictures for constructing the system are provided at https://doi.org/10.17504/protocols.io.36agrae. The build instructions use the designators defined in **Tables 2.2** to **2.4**.

2.5.2. Design of Heating System

The TDT Sandwich was built around the use of dry heat that is applied through conduction to a sample sandwiched between its two heating pads. The rationale behind this design decision is to avoid the disadvantages associated with liquid as a heating medium such as spills and contamination of samples. However, avoiding the use of liquid

also means giving up its advantages such as uniform heating (when agitated) and large heatsinking capacity. Without a heatsink, the sample does not have a buffer against temperature fluctuations such as heat spikes from the heaters and heat loss to the environment. Since a uniform temperature profile is essential for ensuring the accuracy of thermal death kinetics data obtained from the TDT Sandwich, various components such as aluminum plates and insulation foam were added to the heaters in an effort to improve heating uniformity. In order to design the system for best heating performance, it would be necessary to construct multiple prototypes with varying physical configurations and run comprehensive tests on each one. To avoid this time-consuming process, a heat transfer model was developed to optimize the design of the heating system. The objective of the model was to investigate the effect of various physical configurations of the system on the heating performance. Specifically, three physical configurations were investigated: heater without aluminum plates, heater with sample-facing aluminum plate, and heater with both sample-facing and flanking aluminum plate. The model is not meant to be highly accurate and experimentally validated; instead its purpose is to provide direction for the final design of the system.

The heat conduction phenomenon in the heat transfer model is described by Fourier's law (*2*):

$$\rho c_p \frac{\partial T}{\partial t} = k\nabla^2 T \tag{2.1}$$

where ρ is the bulk density of the material (kg m^{-3}), c_p is the specific heat capacity of the material (J kg^{-1} K^{-1}), T is the local temperature (°C), t is the current time (s), and k is the

thermal conductivity of the material (W m^{-1} K^{-1}). The material properties are listed in **Table 2.6**.

As for the boundary conditions, a few characteristics of the system can be considered to simplify the model and its geometry:

- **Characteristic 1:** The heating pads are square in shape and can thus be divided into symmetrical quadrants, of which only one needs to be analyzed in the model.
- **Characteristic 2:** The two heating pads are essentially identical to each other and sandwich the sample from two opposite sides. Therefore, only one needs to be considered for the heat transfer model.
- **Characteristic 3:** Heat is generated by a resistive metal foil that forms a maze-like pattern within the heater. Due to the gaps within the maze-like pattern, heating is not strictly uniform. However, the gaps are small (2 mm) compared to the overall size of the heater (120 mm x 120 mm), therefore heating can be assumed to be uniform everywhere on the heater. The heaters are also extremely thin (0.16 mm).
- **Characteristic 4:** The insulation foam pads that flank the heaters are actually enclosed within a plastic box in the actual system. Aside from providing structural support to the TDT Sandwich, the plastic box also adds an additional layer of insulation in the form of air trapped between the walls of the box and the insulation foam pads. In this model, the worst-case-scenario is assumed where the plastic box is absent and the insulation foam pads are directly exposed to natural convection cooling by the environment.

Fig. 2.2 depicts the geometry, dimensions, and boundary conditions of the model based on the simplifications drawn from the characteristics of the system. Some dimensions such as thickness of the insulation foam and size of heater are fixed due to commercial availability of materials with those dimensions. To model the three investigated heater configurations, the following values as defined in **Fig. 2.2** were used:

- Heater without aluminum plates: $l_f = l_s = d_f = d_s = 0$ cm
- Heater with sample-facing aluminum plate: $l_s = 4$ cm, $d_s = 0.08128$ cm, $l_f = d_f = 0$ cm
- Heater with both sample-facing and flanking aluminum plates: $l_s = l_f = 4$ cm, $d_s = d_f = 0.08128$ cm

where l_f and l_s are one half of the side lengths of the flanking and sample-facing aluminum plates, respectively, while d_f and d_s are the thicknesses of the flanking and sample-facing aluminum plates, respectively. The above values were used due to material availability constraints (*e.g.* aluminum sheets are readily available in only a few thicknesses) and structural design considerations (*e.g.* thinner aluminum sheets deform too easily). Earlier prototypes of the TDT Sandwich also showed that a buffer zone between the edge of the heater and the edge of the sample is required to improve heating uniformity of the sample, therefore the size of the aluminum plates were adjusted to accommodate the sample while creating the aforementioned buffer zone.

The first and second TDT Sandwich characteristics are implemented in the geometry itself and with adiabatic boundary conditions at the symmetrical faces (*2*):

$$\boldsymbol{n} \cdot \boldsymbol{q} = 0 \tag{2.2}$$

where $\boldsymbol{n}$ is the surface unit normal vector pointing out of the domain enclosed by the boundary and $\boldsymbol{q}$ is the heat flux at the boundary (W m^{-2}). The third characteristic implies that the heater can be modeled as a boundary heat source (*2*):

$$-\boldsymbol{n} \cdot \boldsymbol{q} = Q_b \tag{2.3}$$

where Q_b is the boundary heat source (W m^{-2}). The negative sign implies that the heat generated by Q_b is entering the domain enclosed by the boundary. As per the assumption in the third characteristic, Q_b is assumed to be uniform over the entire heater surface. A constant temperature boundary was not used because the heater generates heat uniformly but does not guarantee a constant temperature everywhere. The value of Q_b varies during operation of the system and is modeled by a Proportional-Integral (PI) algorithm:

$$e(t) = T_{target} - T(t) \tag{2.4}$$

$$u(t) = K_P e(t) + K_I \int_0^t e(\tau)\, d\tau \tag{2.5}$$

$$s(t) = \begin{cases} 0, & if\ u(t) < 0 \\ 255, & if\ u(t) > 255 \\ u(t), & for\ other\ cases \end{cases} \tag{2.6}$$

$$Q_b(t) = \frac{s(t)}{255} Q_{max} \tag{2.7}$$

where $e(t)$ is the deviation of the process variable (in this case, temperature) from the desired target (°C), T_{target} is the desired temperature of the heater (°C), $T(t)$ is the instantaneous point temperature measured at a specific location on the heater (°C), $u(t)$

is the output of the PI algorithm, K_P is the PI proportional gain (°C^{-1}), K_I is the integral gain (°C^{-1} s^{-1}), $s(t)$ is the constrained PI output, and Q_{max} is the maximum power output of the heater (W m^{-2}). In this model and the actual TDT Sandwich system, $T_{control}$ is measured at the geometric center of the heater on the sample-facing side. The value of T_{target} was arbitrarily set to 70 °C to simulate a typical temperature used in heat inactivation studies in low-moisture foods. The values of K_p and K_i were set to 10 °C^{-1} and 0.01 °C^{-1} s^{-1}, respectively, based on some preliminary testing of the model. The PI output was not used directly as the power output of the heater; instead it was first constrained within 0 to 255 because this value range is utilized for PWM outputs in 8-bit microcontroller systems such as the Arduino Uno which is used in the TDT Sandwich system. It should be noted that the proportional term in the PI algorithm of the actual TDT Sandwich system is proportional-on-measurement instead of proportional-on-error (*47*), but this difference does not affect the findings of the heat transfer model.

The fourth system characteristic is modeled by convective heat flux boundary conditions on the outside-facing surfaces of the insulation foam pads (*2*):

$$-\boldsymbol{n} \cdot \boldsymbol{q} = h(T_a - T_s) \tag{2.8}$$

where h is the convective heat transfer coefficient (W m^{-2} K^{-1}), T_a is the ambient air temperature (°C), and T_s is the temperature at the surface (°C). A value of 25 W m^{-2} K^{-1} was assumed for h to simulate natural convection without external air currents (*2*). T_a was set to 25°C to emulate room temperature conditions.

The integrated heat transfer and PI model was solved in COMSOL Multiphysics® 5.4 (COMSOL, Inc., Burlington, MA) for a 90 s heating process. The geometry was meshed with tetrahedral elements between 0.14 to 0.76 cm in size. The time-dependent problem was solved using the Multifrontal Massively Parallel Sparse (MUMPS) direct solver. The simulations were performed on a computer with a Windows 7 64-bit operating system, two Intel E5-2630 processors, and 88 GB of RAM.

Fig. 2.3 shows the difference between T_{target} and the temperature at the center of the surface of the sample-facing aluminum plate (or the heater, if the sample-facing plate is absent), T_{center} during the simulated heating process. Without the aluminum plates, the target temperature was quickly achieved. However, the temperature was not maintained in a stable manner and experienced some disturbance around 50 and 75 s. This behavior was unexpected because no external temperature disturbances were programmed into the model. Further refinement of the model mesh did not remove the noise. It is thus likely that these artifacts were generated from a combination of the numerical solution process and absence of a heatsink. The solution to the PI algorithm requires instantaneous integration throughout the numerical solving process and is thus prone to numerical noises. In response to these noises, the PI algorithm adjusted the output of the heater. Due to the absence of a well-conducting heatsink, the resultant spikes in heater power were not suppressed and show up in the temperature measurements. The other two configurations did not show such noises possibly due to the presence of aluminum plates as heatsinks, but the time to reach the target temperature was longer. In fact, with the addition of the flanking plate, the time was delayed by at least 50 s.

Fig. 2.4 plots the difference between T_{center} and the temperature at the corner of a sample pouch (**Section 2.5.3**), T_{corner} during the heating process. Since the pouch measures 7.62 cm by 7.62 cm, the location of T_{corner} is thus located 5.39 cm diagonally from T_{center}. During the initial heating for the heater without aluminum plates, a large difference was induced between the center and corner points. This difference was quickly minimized and stabilized at approximately 1 °C throughout the remainder of the heating process. This non-uniformity in temperature between the center and corner is undesirable. On the other hand, as aluminum plates are added onto the heater, the discrepancy in temperature between the two points is minimized. The configuration with both sample-facing and flanking aluminum plates had the best overall performance with minimal difference during the initial heating phase and the subsequent temperature maintenance phase. In addition to these simulation results, real-life tests with physical prototypes showed that the sample-facing aluminum plate on heaters without the flanking aluminum plate often peeled off during use. The addition of the flanking aluminum plate helped to mechanically secure both aluminum plates to the heater. Therefore, the configuration with both sample-facing and flanking aluminum both was used in the final design of the TDT Sandwich. Although this resulted in a prolonged initial heating phase, the improved structural integrity and heating uniformity makes this configuration the desirable choice for the design objectives of the TDT Sandwich. The temperature contour plots (**Fig. 2.5**) of this configuration over the duration of the heating process shows that the largest difference in temperature on the sample-facing aluminum plate will always be between the center and corner. This observation can be used to evaluate the heating uniformity of

the physical prototypes of TDT Sandwich by placing one thermocouple at the center and another at a corner.

2.5.3. Choice of Sample Pouch

A thermal death kinetic study usually requires sealing the food sample in a sterile vessel to prevent contamination of the sample during the heating process. Various vessels for liquid and granular products have been used: test tubes (*1*, *7*, *21*, *43*), thin capillary tubes (*3*, *31*, *37*, *38*, *41*), and miniature vials such as PCR tubes (*18*, *33*). For irregular solids or viscous samples, it may be desirable to use vacuum or heat-sealed pouches (*11*, *16*, *20*, *25*, *27*, *28*, *35*) to ensure that the vessel conforms to the shape of the sample. Alternatively, reusable vessels such as the TDT disk could be used (*6*, *16*, *17*, *19*, *39*, *40*). In some cases, the food itself (e.g. shell eggs) is the vessel (*34*). The choice of vessel is important to ensure excellent heat transfer during heating while minimizing the risk of contamination of the sample. Since the TDT Sandwich was constructed to apply dry heat over a large flat surface, flat pouches (03MFW03TN, IMPAK Corp., Los Angeles, CA) were used as the sample vessels. These heat-sealable pouches measure 7.62 cm x 7.62 cm and are made of thin (0.1143 mm) Mylar film metallized with aluminum, thus giving it very low diffusion properties for water vapor (1.94×10^{-4} g m^{-2} h^{-1}). As a result, samples can be sealed in the pouches in advance of experiments and can be used for experiments over multiple days without significant changes to the water activity of the sample. The flexibility of the pouches makes it suitable for food products in the form of liquid, paste, or powder. As these pouches are meant to contain food samples, they can be used immediately without pre-sterilization. It should be noted that the impermeability of the

pouches preserves moisture content of the sample during heating, thus simulating a food product sealed in an airtight container undergoing a heating process.

Since the pouches would be subjected to high temperatures which could change the moisture permeability of the pouches, a study was performed to investigate the moisture loss from samples at elevated temperatures. Seven pouches were filled with 2.0 ± 0.1(SD) g of deionized water, sealed with a heat sealer (IPK-105H, IMPAK Corporation, Los Angeles, CA) set to level 6.5, and heated to 100°C for a total heating time of 45 min. After the heating process, the pouches were cooled to room temperature in a desiccator before being weighed to determine the mass change. There was minimal loss in moisture (0.20 ± 0.12(SD) mg), therefore the pouches can be considered impermeable to moisture migration during isothermal treatments.

When using the pouches for thermal inactivation studies, it is advisable to ensure that the contents of the pouches are distributed evenly to improve heating uniformity. This is especially important for powder samples which tend to settle towards one edge of the pouch. To distribute the sample evenly, simply hold the pouch on the edge where most of the sample has settled on and flick it up and down. This helps to distribute the sample away from the edge. Subsequently, shake the pouch horizontally to encourage uniform distribution of the sample. As for liquid or paste samples, the distribution of the sample can be improved by simply pinching parts of the pouch which seems to have more sample than other parts of the pouch. At the conclusion of the thermal treatment, the sample can be cooled very quickly by removing them from the TDT Sandwich and submerging them into an ice slurry bath. The author and other early users of the TDT

Sandwich have performed this transfer with typical thin disposable nitrile gloves on samples up to 90 °C without issues due to the low thermal mass of the pouch, though a pair of tongs could be used if the sample is too hot to the touch.

2.5.4. Proportional-Integral Algorithm

The heater output from the system in response to temperature readings from both heating pads are determined by a Proportional-Integral (PI) algorithm. As previously described in **Section 2.5.2**, the PI algorithm consists of a proportional and integral term. The proportional term responds to the immediate deviation of the process variable from the target while the integral term keeps track of the deviation over time. The TDT Sandwich uses a modified PI algorithm, whereby the proportional term is defined as proportional-on-measurement instead of proportional-on-error. With this change, the proportional term resists changes in the process variable to provide a slightly sluggish performance in exchange for improved stability and less overshoot (*47*). In addition, the system was better at maintaining the temperature of the sample at the target temperature if the proportional and integral gains were forced to certain values when the heating pad temperatures were close to the target temperature. As such, the resulting PI algorithm is as follows:

$$e_P(t) = T(t) - T(t = 0) \tag{2.9}$$

$$e_I(t) = T_{target} - T(t) \tag{2.10}$$

$$u(t) = -K_P e_P(t) + K_I \int_0^t e_I(\tau)\, d\tau \tag{2.11}$$

$$K_P = \begin{cases} K_{P,U}, & if\ e_I(t) > T_P \\ K_{P,C}, & otherwise \end{cases} \quad (2.12)$$

$$K_I = \begin{cases} K_{I,U}, & if\ e_I(t) > T_I \\ K_{I,C}, & otherwise \end{cases} \quad (2.13)$$

where $e_P(t)$ is the proportional error term (°C), $T(t)$ is the instantaneous temperature of the heating pad (°C), $T(t = 0)$ is the temperature of the heating pad at the start of the heating (°C), $e_I(t)$ is the integral error term (°C), T_{target} is the target temperature for the heating pads (°C), $u(t)$ is the output of the PI algorithm, K_P is the proportional gain ($°C^{-1}$), K_I is the integral gain ($°C^{-1}\text{-}s$), $K_{P,U}$ is the user-defined proportional gain during initial heating ($°C^{-1}$), and $K_{P,C}$ is the constant proportional gain that is used when $e_I(t)$ is within the threshold T_P. $K_{I,U}$, $K_{I,C}$, and T_I are similar to their proportional counterparts, but are defined for the integral term. The values of $K_{P,U}$ and $K_{I,U}$ can be modified by the user using the computer program described in **Section 2.6.3**, with default values of 25.0 and 1.7, respectively. $K_{P,C}$, T_P, $K_{I,C}$, and T_I are constant values hard-coded as 5.0, 0.0, 0.8, and 0.3, respectively, into the microcontroller program of the TDT Sandwich. These values were determined through trial-and-error and should not be modified unless the user wishes to adapt the TDT Sandwich to special use cases.

2.6. Operation Instructions

This section describes the steps for using the TDT Sandwich to heat a sample. The designators listed in **Tables 2.2** to **2.5** will be used to describe some components for brevity.

2.6.1. ID of TDT Sandwich

Before using a TDT Sandwich, its identification number (ID) should first be set. Every TDT Sandwich must have a unique ID; if two or more TDT Sandwiches share the same ID, only one of them would work properly. Before setting the ID, ensure that the TDT Sandwich is not turned on *i.e.* CB4 and CB5 are disconnected. To set the ID, an appropriate amount of CB6 must be placed on certain pins at the front of the control box. By referring to the labelled pins in **Fig. 2.6(A)**, the following equation can be used to determine which pins CB6 should be attached to:

$$n = \sum_{i=0}^{7} a_i 2^i \tag{2.14}$$

where n is the ID of the TDT Sandwich, i is the pin number as labelled in **Fig. 2.6(A)** and on the control box, and a_i is 1 if CB6 is attached to pin i and 0 otherwise. Internally, the ID is capped to a maximum of 99. The setting of ID with the pins actually follows a binary system. Therefore, the following steps can be used to determine which pins should be plugged with C6:

1. Determine the desired ID of the TDT Sandwich and denote this as m.
2. Determine the largest value of i where 2^i is still smaller or equal to m. Denote this value of i as k.
3. Plug a C6 into pin k.
4. Calculate $p = m - 2^k$. If p is zero, no further action is necessary. Otherwise, repeat steps 2 to 4 by replacing m with p.

For example, for an ID of 27, pins 4, 3, 1, and 0 will be plugged with C6 (**Fig. 2.6(B)**). When attaching C6 to the pins, it actually connects two pins vertically. Do not connect the pins horizontally. Subsequently, ensure that the TDT Sandwich is connected to an electrical outlet or power strip with CB5 and to a computer/laptop either directly or through a USB hub with CB4. When the computer/laptop or USB hub is switched on, there will be an approximately 5 second delay before the ID of the TDT Sandwich is displayed on the display at the front of the control box. If this number is not the correct ID, refer again to the steps above to set the correct ID.

2.6.2. Sample Preparation

If the TDT Sandwich is being used to heat a sample, it is recommended to package the sample in the pouches (P1) suggested in **Table 2.5** and **Section 2.5.3**. If an exact amount of sample is needed, then the filling process should be done on a weighing scale. Otherwise, kitchen measuring spoons of an appropriate volume can be used to fill the pouches with samples. Once a pouch has been filled, its opening should be sealed with a heat sealer. For some experiments such as measuring the time taken for the sample to reach the target temperature, it is desirable to have a thermocouple in the pouch to measure the temperature of the sample during heating. To insert the thermocouple, puncture one end of the pouch with a thin sharp object such as a push pin and insert the thermocouple to a desired location in the pouch. It is recommended to place a piece of tape on the hole on the pouch to immobilize the thermocouple and minimize sample leakage (**Fig. 2.7(A)**).

Once the sample pouch is ready, it should be placed at the geometric center of the bottom heating pad of the TDT Sandwich (**Fig. 2.7(B)**). If a thermocouple is inserted into the sample, it should be routed out through the slot hole at the front of the TDT Sandwich. Subsequently, the top half of the TDT Sandwich should be secured to the bottom half by applying downwards pressure on the top half and pushing in the plastic clip at the front (**Fig. 2.7(C)**). The plastic clip will make a snapping or clicking sound when pushed in properly. If a thermocouple was inserted into the sample, connect the thermocouple connector to the thermocouple jack at the front of the control box (**Fig. 2.7(D)**). The TDT Sandwich is now ready for operation using the computer program. Note that in most use cases, the sample thermocouple is unnecessary, therefore the preparation of the TDT Sandwich is as simple as placing the pouch containing sample at the geometric center of the bottom heating pad and snapping the TDT Sandwich close.

2.6.3. Computer Program

Instructions on downloading and installing any required files for the computer program are given in the build instructions described in **Section 2.5.1**. Throughout this section, elements in the program will be referred to using the labels in **Fig. 2.8**.

2.6.3.1. Overview

The physical TDT Sandwiches cannot be operated on their own and can only be controlled with the provided computer program. Before opening the computer program, all the TDT Sandwiches that will be used should first be connected to the computer/laptop, either directly or through USB hubs. Also, ensure that the ID for each TDT Sandwich is unique.

The computer program is a graphical user interface that contains buttons and text boxes for user input (**Fig. 2.8**). The menu bar at the top contains two items (**C0** and **P0**) that will expand to more items when they are clicked. The main body of the program lists "virtual" TDT Sandwiches. A virtual TDT Sandwich is a collection of temperature readings, heating settings, data recording functions, and various instructions to communicate with a physical TDT Sandwich. There is no limit to the amount of virtual TDT Sandwiches that can be added. In order to match a virtual TDT Sandwich to its virtual counterpart, the appropriate communication port must be assigned to it, as will be described in **Section 2.6.3.2**. If any errors are encountered during operation of the TDT Sandwich program, the details of the errors will be recorded in a file named "errorLog.txt" in the same directory as the TDT Sandwich program.

2.6.3.2. Basic Operation of TDT Sandwich

Pressing **C0** and then **C1** in the program window creates a virtual TDT Sandwich that would appear below the list of existing virtual TDT Sandwiches. The default ID (**I1**) of new virtual TDT Sandwiches is 0, which should be changed to match the physical TDT Sandwich by pressing the up or down arrows on **I1** to set the ID between 0 and 99. The user can add as many virtual TDT Sandwiches to match the number of physical TDT Sandwiches. For the program to communicate with the physical TDT Sandwich, the appropriate communication port must be given (**A3**). Instead of doing this manually, it is highly recommended to press **P0** and then **P1**, before pressing **P0** again and then **P2**. **P1** instructs the program to rebuild its list of active USB connections while **P2** sends out messages to each USB port to identify if the connected device is a TDT Sandwich, obtain

the ID of the connected TDT Sandwich, and populates **A3** with the appropriate communication port.

Once the virtual TDT Sandwiches have been matched to their physical counterparts, operation of the TDT Sandwiches can begin. If a thermocouple is inserted into the thermocouple jack in the front (*i.e.* the sample thermocouple), ensure that **D3** is checked so that the program would obtain and display the temperature readings of the sample (**D4**). Otherwise, keep **D3** unchecked to hide **D4**. Pressing **D5** will begin communication with the physical TDT Sandwich and acquisition of temperature readings from both heaters (**D1** and **D2**) and, if requested, the sample (**D4**). The background of the "DAQ" section will also change to green. If the incorrect communication port was selected, an error would pop up and the user should assign the appropriate port, either manually or automatically as described previously. If "Error" is displayed in either **D1**, **D2**, or **D3**, the thermocouple connection is compromised. This could be something simple like a loose connection or a serious issue like a broken thermocouple. If it was the former, the affected thermocouple should be unplugged, checked for any knots or kinks in its wire, then plugged back in. The latter requires repair or replacement of the broken thermocouple. The rate of data acquisition is affected by the number of thermocouple readings averaged (**A5**). At a default value of 8, the data acquisition rate is approximately 5 Hz. While data acquisition is active, **D5** can be pressed to stop data acquisition.

Once data acquisition has begun, the heating and recording options will be unlocked. The target temperature for the TDT Sandwich can be adjusted at **H1**, with a minimum value of 0 °C and maximum value of 140 °C. Note that this is the target

temperature for the heating pads; in normal use cases, the sample temperature will eventually reach this value. However, for extremely thick samples, the isothermal sample temperature may have an offset from the heating pad temperature; this needs to be verified using the sample thermocouple. By default, **H2** is checked to induce the maximum heating rate; unchecking it reveals an input (**H3**) for adjusting the heating rate for the TDT Sandwich between 0 to 100 °C/min. The TDT Sandwich will attempt to match the given heating rate but there will be some deviation during the start of heating and close to the target temperature due to efforts by the PI algorithm to prevent the heating pad temperature from overshooting the target temperature. For most use cases where it is desirable to heat the sample as fast as possible, it is recommended to leave **H2** checked. The duration for the heating can be adjusted with **H4**, **H5**, and **H6**. The maximum duration possible is 99 h, 59 min, and 59 s. Upon pressing **H7**, the TDT Sandwich will begin applying heat according to the given settings and changes the background of the "Heat" section to red. When the remaining heating duration is 10 s or less, the TDT Sandwich will beep and flash once every second until the heating is completed, upon which it will give out an extended beep and flash. While heating is active, **H7** can be pressed to stop the heating.

The recording section allows the user to record temperature readings from the TDT Sandwich into a file. **R2** opens a window for browsing to the location to save the recorded data and giving the name for the data file. The data file is a Comma Separated Value (CSV) file which can be opened by any text processing or spreadsheet software such as Microsoft Excel. Once the location of the file has been chosen, its path will

appear in **R1**. Pressing **R3** anytime while data acquisition is active, whether heating is active or not, will begin recording data to the file at the same rate that data is being acquired and changes the background of the "Record" section to yellow. Data is written into the file as new rows for each acquired data, with the first column being time (ms), second being temperature of heating pad 1 (°C), third being temperature of heating pad 2 (°C), and, if **D3** was checked, the fourth being temperature of the sample (°C). Fresh data is always appended to the end of the file; this means that if the user accidentally recorded data to an existing data file, the old contents will not be overwritten and the new data will be below the old data.

2.6.3.3. Configuration Files

After adding a desired amount of TDT Sandwiches and adjusting their operating parameters, it may be desirable to save the program state (*i.e.* number of virtual TDT Sandwiches, heating rate, target temperature, data record location, etc.) so that it can be reused in the future instead of manually redoing the entire process. The computer program implements this feature through the use of configuration files. To save the program state at any given time, press **C0** and then **C3**. A window would open in which the user should choose a location and file name to store the program state. To load the program state, press **C0**, then **C2** and browse to the desired configuration file. The program will inform the user that the current program state will be cleared before loading the program state defined in the configuration file.

Another method of using the configuration file is to have it loaded automatically upon opening the program. When opening the computer program, the program will

search for a file named “defaultConfig.csv” in the same directory as the program. If this file exists, the program will load the program state defined in that file it just like any other configuration file. This feature is useful when a known number of TDT Sandwiches with a set of default settings is to be used frequently. To use this feature, simply rename a desired configuration file to “defaultConfig.csv” without the quotes and place it in the same directory as the computer program.

2.6.3.4. Advanced Options

The steps described in **Section 2.6.3.2** would suffice for most use cases of the TDT Sandwich. However, if desired, there are more options available to modify behavior of the TDT Sandwich to the user’s needs. These advanced options are revealed by pressing **A0**. **A1** instructs the physical TDT Sandwich to flash for a few seconds. This is useful for checking if the correct communication port has been selected in **A3** or for finding the physical TDT Sandwich**.** Clicking **A2** removes the virtual TDT Sandwich from the list. **A3** is used to manually assign the communication port of the TDT Sandwich. **A4** and **A5** are settings affecting all the thermocouples, including the sample thermocouple. **A4** allows the user to choose a thermocouple of different type. Note that the bills of materials and build instructions utilize thermocouples of type T, so this setting should not be changed in most use cases. **A5** adjusts the number of raw thermocouple readings that are averaged to produce a final thermocouple reading *i.e.* the one that is displayed in the computer program and recorded. A smaller value increases data acquisition rate but reduces the precision of the acquired temperature reading. The default value of 8 results in a data acquisition rate of approximately 5 Hz. The proportional and

integral gains of the PI algorithm in the TDT Sandwich can be adjusted with **A6** and **A7**. The default values of 25.0 and 1.7 for **A6** and **A7**, respectively, were determined through trial-and-error and provide satisfactory heating speed and temperature maintenance. If desired, the user can adjust these settings to further optimize heating performance of the TDT Sandwich.

2.7. Validation and Characterization

The primary goal of the TDT Sandwich is to utilize dry heat to maintain a uniform temperature throughout the sample after achieving a desired CUT. However, innate variations due to manufacturing defects or human error during fabrication may affect the performance consistency among different TDT Sandwich units. It is thus necessary to verify that the system can consistently achieve its design goals under a variety of operating conditions, namely heating pad target temperature, heating pad heating rate, and sample amount.

The characterization study was performed with three heating pad target temperatures (70, 90, 110 °C), three heating pad heating rates (25, 50, ~100 °C/min) and three amounts of whole milk powder for the sample (0, 2, 4 g). To induce the maximum heating rate, the TDT Sandwiches were instructed to heat samples at 600 °C/min instead of exactly 100 °C/min in order to push the systems to their limits; the actual conservative maximum heating rate is approximately 100 °C/min. The samples masses of 2 and 4 g resulted in sample thicknesses of 1.10 ± 0.15(SD) mm and 2.00 ± 0.23(SD) mm, respectively. The experimental unit is a TDT Sandwich unit—12 units were used for this study. The

consistency and innate variations of the TDT Sandwich units were measured by four characteristics:

- t_{CUT} : The time (s) taken by the center of the sample to reach within 0.5 °C of the target temperature of the heating pads. Small variations in CUT for a set of TDT Sandwich units indicate minimal variation between the TDT Sandwich units.
- $T_u^{t_{CUT}} = T_{center}^{t_{CUT}} - T_{corner}^{t_{CUT}}$: The difference in temperature (°C) between the center and corner of the sample at the time when CUT was achieved. The smaller the difference, the more uniform the heating of the sample. If this number is negative, then the center of the sample is colder than the corner. The temperature measurement locations were chosen based on the heat transfer model in **Section 2.5.2** which predicted the largest temperature difference between the center and corner.
- $T_u^{t_{SS}} = T_{center}^{t_{SS}} - T_{corner}^{t_{SS}}$: Same as $T_U^{t_{CUT}}$, but 1 min after achieving CUT *i.e.* $t_{SS} = t_{CUT} + 1$ min. The time delay of 1 min was arbitrarily chosen to capture steady-state (SS) condition of the heating pad and sample within a reasonable time frame.
- $T_o^{t_{SS}} = T_{center}^{t_{SS}} - T_{target}^{t_{SS}}$: The difference between the temperature at the center of the sample and the target temperature of the heating pad 1 min after achieving CUT. A minimal value is desired so that the user does not have to apply offsets to the target temperature of the heating pad to achieve a desired sample temperature.

Type-T 40 gage thermocouples (T1X-WBWX-40G-EX-0.25-PFXX-40-STWL, Evolution Sensors and Controls, West Deptford, NJ) were held in place with aluminum

tape at the center and a corner of the sample pouches with one thermocouple per location. The pouches were then placed in the TDT Sandwich units. The thermocouples were connected to TDT Sandwiches that were not in use to acquire and record temperature readings at approximately 5 Hz.

The four characteristics for all operating parameter combinations are summarized in **Table 2.7**. In general, as the target temperature increased and/or heating rate decreased, t_{CUT} increased, which is expected due to larger heat requirement for a high target temperature and slower heating provided by a low heating rate. The standard deviation of t_{CUT} also appears to be the highest when the TDT Sandwich is operated at its maximum heating rate, with a maximum value of 6.8 s among all the operating conditions. At the CUT, the center of the sample was always colder than the corner, as evident by the negative $T_u^{t_{CUT}}$ values across all operating conditions, which agrees with the heat transfer model predictions from **Section 2.5.2**. In addition, $T_u^{t_{CUT}}$ appeared to increase if any one of the target temperatures, heating rates, or sample amounts increased. With a higher target temperature and heating rate, the system needs to provide more heat in a shorter time to bring the temperature of the heating pads up to the target. Since there is more sample mass at the center of the heating pad than the corner, the corner heats up faster and reaches a higher temperature. As the overall sample mass is increased, this discrepancy is aggravated. However, once the heating pads have reached the target temperature and enough time (1 min in this case) has been allowed for equilibration of the temperature of the sample, then the difference between the center and corner appears to be decreased, as evident by the smaller $T_u^{t_{SS}}$ values in comparison to $T_u^{t_{CUT}}$. At this

point in time, T_o^{tss} has also shrunk to almost zero, indicating that the heating pad temperature represents the temperature at the center of the sample at steady-state conditions. Therefore, it is not necessary to apply offsets to the target temperature when operating the TDT Sandwiches. The biggest exception to this is when the TDT Sandwiches were operated at maximum heating rate for samples with mass of 4 g. This observation arose because the sample had not yet achieved steady-state conditions at the 1 min mark, as will be discussed with **Fig. 2.9**.

The performance of the tested TDT Sandwich systems is visualized in **Fig. 2.9** for all the operating conditions. As mentioned previously, the large value of T_o^{tss} for 4 g samples heated at the maximum heating rate is caused by unsteady-state conditions; this can be seen in the lower three rows of **Fig. 2.9** where the center and corner temperatures could take upwards of 4 min to settle at the target temperature. Therefore, operation of the TDT Sandwich at its maximum heating rate with a large amount of sample is not recommended. In addition, it is also apparent that the corner temperature tends to overshoot by more than 0.2 °C of the target temperature whenever the target temperature is 110 °C. These observations indicate that the parameters of the PI algorithm of the TDT Sandwich need to be adjusted for higher target temperatures; as of now, these parameters are constant values. Therefore, future versions of the system should introduce temperature dependency into the PI algorithm parameters (**Section 2.5.4**) to prevent overshoot at higher temperatures. In any case, the expected use cases for the TDT Sandwich would not require temperatures above 100 °C in order to avoid boiling of the food sample, therefore the system should be able to maintain the temperature of the

sample within 0.2 ℃ of the target temperature. It is, however, advised to keep sample mass to minimum (2 g or less) to prevent the temperature overshoots as seen in the 4 g whole milk powder samples.

2.8. Acknowledgements

This material is based upon work that is supported by the National Institute of Food and Agriculture, U.S. Department of Agriculture, under award number 2015-68003-23415 and with partial support from the Nebraska Agricultural Experiment Station with funding from the Hatch Act (Accession Number 1006859) through the USDA National Institute of Food and Agriculture. Much appreciation is given to Kun Huang, Sierra Mendez, Raghavendra Singh, and Tushar Verma for their invaluable assistance during the process of manufacturing multiple TDT Sandwiches. Many thanks to The Nebraska Innovation Studio for allowing use of their prototyping facilities.

2.9. References

1. Al-Holy, M., Z. Quinde, D. Guan, J. Tang, and B. Rasco. 2004. Thermal Inactivation of *Listeria innocua* in Salmon (*Oncorhynchus keta*) Caviar Using Conventional Glass and Novel Aluminum Thermal-Death-Time Tubes. *J. Food Prot.* 67:383–386.
2. Bergman, T. L., A. S. Lavine, F. P. Incropera, and D. P. DeWitt. 2011. Fundamentals of Heat and Mass Transfer, 7th ed. Wiley, Hoboken, NJ.
3. Carlier, V., J. C. Augustin, and J. Rozier. 1996. Heat Resistance of *Listeria monocytogenes* (Phagovar 2389/2425/3274/2671/47/108/340): D- and z-Values in Ham. *J. Food Prot.* 59:588–591.

4. Cheng, T., R. Li, X. Kou, and S. Wang. 2017. Influence of controlled atmosphere on thermal inactivation of *Escherichia coli* ATCC 25922 in almond powder. *Food Microbiol.* 64:186–194.

5. Cheng, T., and S. Wang. 2018. Influence of storage temperature/time and atmosphere on survival and thermal inactivation of *Escherichia coli* ATCC 25922 inoculated to almond powder. *Food Control* 86:350–358.

6. Chung, H.-J., S. L. Birla, and J. Tang. 2008. Performance evaluation of aluminum test cell designed for determining the heat resistance of bacterial spores in foods. *LWT - Food Sci. Technol.* 41:1351–1359.

7. Chung, H.-J., S. Wang, and J. Tang. 2007. Influence of Heat Transfer with Tube Methods on Measured Thermal Inactivation Parameters for Escherichia coli. *J. Food Prot.* 70:851–859.

8. Condón, S., M. J. Arrizubieta, and F. J. Sala. 1993. Microbial heat resistance determinations by the multipoint system with the thermoresistometer TR-SC Improvement of this methodology. *J. Microbiol. Methods* 18:357–366.

9. Condon, S., P. Lopez, R. Oria, and F. J. Sala. 1989. Thermal Death Determination: Design and Evaluation of a Thermoresistometer. *J. Food Sci.* 54:451–457.

10. Conesa, R., S. Andreu, P. s. Fernández, A. Esnoz, and A. Palop. 2009. Nonisothermal heat resistance determinations with the thermoresistometer Mastia. *J. Appl. Microbiol.* 107:506–513.

11. Enache, E., A. Kataoka, D. G. Black, L. Weddig, M. Hayman, and K. Bjornsdottir-Butler. 2013. Heat Resistance of Histamine-Producing Bacteria in Irradiated Tuna Loins. *J. Food Prot.* 76:1608–1614.

12. Foster, A. M., L. P. Ketteringham, G. L. Purnell, A. Kondjoyan, M. Havet, and J. A. Evans. 2006. New apparatus to provide repeatable surface temperature–time treatments on inoculated food samples. *J. Food Eng.* 76:19–26.

13. Foster, A. M., L. P. Ketteringham, M. J. Swain, A. Kondjoyan, M. Havet, O. Rouaud, and J. A. Evans. 2006. Design and development of apparatus to provide repeatable surface temperature–time treatments on inoculated food samples. *J. Food Eng.* 76:7–18.

14. Gaze, J. E., A. R. Boyd, and H. L. Shaw. 2006. Heat inactivation of *Listeria monocytogenes* Scott A on potato surfaces. *J. Food Eng.* 76:27–31.

15. Hassani, M., S. Condón, and R. Pagán. 2007. Predicting Microbial Heat Inactivation under Nonisothermal Treatments. *J. Food Prot.* 70:1457–1467.

16. Hildebrandt, I. M., B. P. Marks, V. K. Juneja, M. Osoria, N. O. Hall, and E. T. Ryser. 2016. Cross-Laboratory Comparative Study of the Impact of Experimental and Regression Methodologies on *Salmonella* Thermal Inactivation Parameters in Ground Beef. *J. Food Prot.* 79:1097–1106.

17. Hildebrandt, I. M., B. P. Marks, E. T. Ryser, R. Villa-Rojas, J. Tang, F. J. Garces-Vega, and S. E. Buchholz. 2016. Effects of Inoculation Procedures on Variability and Repeatability of *Salmonella* Thermal Resistance in Wheat Flour. *J. Food Prot.* 79:1833–1839.

18. Jackson, T. C., M. D. Hardin, and G. R. Acuff. 1996. Heat Resistance of *Escherichia coli* O157:H7 in a Nutrient Medium and in Ground Beef Patties as Influenced by Storage and Holding Temperatures. *J. Food Prot.* 59:230–237.

19. Jin, T., H. Zhang, G. Boyd, and J. Tang. 2008. Thermal resistance of *Salmonella* enteritidis and *Escherichia coli* K12 in liquid egg determined by thermal-death-time disks. *J. Food Eng.* 84:608–614.

20. Karyotis, D., P. N. Skandamis, and V. K. Juneja. 2017. Thermal inactivation of *Listeria monocytogenes* and *Salmonella* spp. in sous-vide processed marinated chicken breast. *Food Res. Int.* 100:894–898.

21. Kikoku, Y., N. Tagashira, and H. Nakano. 2008. Heat Resistance of Fungi Isolated from Frozen Blueberries. *J. Food Prot.* 71:2030–2035.

22. Kou, X., R. Li, L. Hou, Z. Huang, B. Ling, and S. Wang. 2016. Performance of a Heating Block System Designed for Studying the Heat Resistance of Bacteria in Foods. *Sci. Rep.* 6:30758.

23. Lewis, R. J., A. Baldwin, T. O'Neill, H. A. Alloush, S. M. Nelson, T. Dowman, and V. Salisbury. 2006. Use of *Salmonella enterica* serovar Typhimurium DT104 expressing lux genes to assess, in real time and in situ, heat inactivation and recovery on a range of contaminated food surfaces. *J. Food Eng.* 76:41–48.

24. Lewis, R. J., K. Robertson, H. M. Alloush, T. Dowman, and V. Salisbury. 2006. Use of bioluminescence to evaluate the effects of rapid cooling on recovery of *Salmonella enterica* serovar Typhimurium DT104 after heat treatment. *J. Food Eng.* 76:49–52.

25. Li, L., J. Cepeda, J. Subbiah, G. Froning, V. K. Juneja, and H. Thippareddi. 2017. Dynamic predictive model for growth of *Salmonella* spp. in scrambled egg mix. *Food Microbiol.* 64:39–46.

26. MatWeb. 2019. Overview of materials for PVC, Foam Grade.

27. Mazzotta, A. S. 2001. Heat Resistance of *Listeria monocytogenes* in Vegetables: Evaluation of Blanching Processes. *J. Food Prot.* 64:385–387.

28. Mazzotta, A. S. 2001. Thermal Inactivation of Stationary-Phase and Salt-Adapted *Listeria monocytogenes* during Postprocess Pasteurization of Surimi-Based Imitation Crab Meat. *J. Food Prot.* 64:483–485.

29. McCann, M. S., J. J. Sheridan, D. A. McDowell, and I. S. Blair. 2006. Effects of steam pasteurisation on *Salmonella* Typhimurium DT104 and *Escherichia coli* O157:H7 surface inoculated onto beef, pork and chicken. *J. Food Eng.* 76:32–40.

30. McMaster-Carr. 2019. Flexible Rubber Foam Pipe Insulation Sheet.

31. Mulak, V., R. Tailliez, P. Eb, and P. Becel. 1995. Heat Resistance of Bacteria Isolated From Preparations Based on Seafood Products. *J. Food Prot.* 58:49–53.

32. Palop, A., J. Raso, S. Condón, and F. J. Sala. 1996. Heat Resistance of *Bacillus subtilis* and *Bacillus coagulans*: Effect of Sporulation Temperature in Foods With Various Acidulants. *J. Food Prot.* 59:487–492.

33. Peña-Meléndez, M., J. J. Perry, and A. E. Yousef. 2014. Changes in Thermal Resistance of Three *Salmonella* Serovars in Response to Osmotic Shock and Adaptation at Water Activities Reduced by Different Humectants. *J. Food Prot.* 77:914–918.

34. Perry, J. J., and A. E. Yousef. 2013. Factors Affecting Thermal Resistance of *Salmonella enterica* Serovar Enteritidis ODA 99-30581-13 in Shell Egg Contents and Use of Heat-Ozone Combinations for Egg Pasteurization. *J. Food Prot.* 76:213–219.

35. Redondo-Solano, M., D. E. Burson, and H. Thippareddi. 2016. Thermal Resistance of *Clostridium difficile* Spores in Peptone Water and Pork Meat. *J. Food Prot.* 79:1468–1474.

36. Sala, F. J., P. Ibarz, A. Palop, J. Raso, and S. Condon. 1995. Sporulation Temperature and Heat Resistance of *Bacillus subtilis* at Different pH Values. *J. Food Prot.* 58:239–243.

37. Schuman, J. D., B. W. Sheldon, and P. M. Foegeding. 1997. Thermal Resistance of *Aeromonas hydrophila* in Liquid Whole Egg. *J. Food Prot.* 60:231–236.

38. Shearer, A. E. H., A. S. Mazzotta, R. Chuyate, and D. E. Gombas. 2002. Heat Resistance of Juice Spoilage Microorganisms. *J. Food Prot.* 65:1271–1275.

39. Smith, D. F., I. M. Hildebrandt, K. E. Casulli, K. D. Dolan, and B. P. Marks. 2016. Modeling the Effect of Temperature and Water Activity on the Thermal Resistance of *Salmonella* Enteritidis PT 30 in Wheat Flour. *J. Food Prot.* 79:2058–2065.

40. Smith, D. F., and B. P. Marks. 2015. Effect of Rapid Product Desiccation or Hydration on Thermal Resistance of *Salmonella enterica* Serovar Enteritidis PT 30 in Wheat Flour. *J. Food Prot.* 78:281–286.

41. Splittstoesser, D. F., M. R. Mclellan, and J. J. Churey. 1996. Heat Resistance of *Escherichia coli* O157:H7 in Apple Juice. *J. Food Prot.* 59:226–229.

42. Syamaladevi, R. M., J. Tang, R. Villa-Rojas, S. Sablani, B. Carter, and G. Campbell. 2016. Influence of Water Activity on Thermal Resistance of Microorganisms in Low-Moisture Foods: A Review. *Compr. Rev. Food Sci. Food Saf.* 15:353–370.

43. Tournas, V., and R. W. Traxler. 1994. Heat Resistance of a *Neosartorya fischeri* Strain Isolated From Pineapple Juice Frozen Concentrate. *J. Food Prot.* 57:814–816.

44. Zhang, L., X. Kou, S. Zhang, T. Cheng, and S. Wang. 2018. Effect of water activity and heating rate on *Staphylococcus aureus* heat resistance in walnut shells. *Int. J. Food Microbiol.* 266:282–288.

45. Zhang, S., L. Zhang, R. Lan, X. Zhou, X. Kou, and S. Wang. 2018. Thermal inactivation of *Aspergillus flavus* in peanut kernels as influenced by temperature, water activity and heating rate. *Food Microbiol.* 76:237–244.

46. COMSOL, 2019. COMSOL Multiphysics® 5.4. COMSOL AB, Stockholm, Sweden.

47. Liptak, B. G. 2018. Instrument Engineers' Handbook, Volume Two: Process Control and Optimization. CRC Press.

Table 2.1. Design files for the TDT Sandwich.

Design file name	File type	Open source license	Location of the file
Printed circuit board design files	Electronics	GNU General Public License (GPL) 3.0	https://doi.org/10.17605/OSF.IO/WGYXP
Arduino code	Software	GNU General Public License (GPL) 3.0	https://doi.org/10.17605/OSF.IO/FE62V
Computer program	Software	GNU General Public License (GPL) 3.0	https://doi.org/10.17605/OSF.IO/EDPKU
Finite element model (unsolved)	COMSOL Multiphysics ® file	GNU General Public License (GPL) 3.0	https://doi.org/10.17605/OSF.IO/5NZEP

Table 2.2. Bill of materials for components of the TDT Sandwich printed circuit board.

Designator	Component	Quantity	Cost per unit (USD)	Total cost (USD)	Source of materials
PCB	Printed circuit boards (Pack of 10)	0.1	$5.00	$0.50	Send PCB design files from **Table 2.1** to a PCB manufacturer (e.g. https://jlcpcb.com/)
S1	Flat Head Screws, M2 x 0.4 mm Thread, 12 mm Long (pack of 100)	0.03	$5.60	$0.17	https://www.mcmaster.com/91420A006
S2	Hex Nut, Low-Strength, M2 x 0.4 mm Thread (pack of 100)	0.03	$1.57	$0.05	https://www.mcmaster.com/90591A111
BZ1	Buzzer, polarized	1	$1.12	$1.12	https://www.digikey.com/products/en?keywords=AI-1223-TWT-5V-5-R
C1 C3 C6 C8 C11 C13	Ceramic capacitor, 0.01 uF, 0603	6	$0.01	$0.07	https://www.arrow.com/en/products/c0603c103m5rac/kemet-corporation
C2 C4 C5 C7 C9 C10 C12 C14 C15 C16 C17 C18 C19 C20 C21 C22 C23 C24 C25 C26 C27	Ceramic capacitor, 0.1 uF, 0603	21	$0.01	$0.27	https://www.arrow.com/en/products/cl10b104ko8wpnc/samsung-electro-mechanics
D1 D2	LED, orange, R/A, 0805	2	$0.10	$0.21	https://www.arrow.com/en/products/ltst-s220kfkt/lite-on-technology
D3	LED, green, R/A, 0805	1	$0.12	$0.12	https://www.arrow.com/en/products/ltst-s220kgkt/lite-on-technology
D4	LED, red, R/A, 0805	1	$0.13	$0.13	https://www.arrow.com/en/products/ltst-s220krkt/lite-on-technology
D5	LED, amber, R/A, 0805	1	$0.61	$0.61	https://www.digikey.com/product-detail/en/osram-opto-semiconductors-inc/LA-A67F-AABB-24-1-30-R33-Z/475-3392-1-ND/7907989
F1	Fuse holder	1	$0.74	$0.74	https://www.arrow.com/en/products/64900001039/littelfuse
J8	Male headers, 16 pos, 2.54 mm	1	$0.55	$0.55	https://www.arrow.com/en/products/68021-

	pitch, R/A				216hlf/amphenol-fci
J7	Female headers, 15 pos, 2.54 mm pitch	2	$2.20	$4.39	https://www.arrow.com/en/products/1-535541-3/te-connectivity
J1 J2 J3	Thermocouple type-T miniature connector, PCB mount	3	$3.50	$10.50	https://evosensors.com/collections/miniature-pcb-flat-mounting/products/t1x-femx-con-fp-x-pccx
J4 J5	Connector, 01x02	2	$0.21	$0.42	https://www.arrow.com/en/products/39-30-1020/molex
J6	Power entry connector, IEC320-C6	1	$1.31	$1.31	https://www.digikey.com/product-detail/en/qualtek/771W-BX2-01/Q311-ND/417925
Q1 Q2 Q3 Q4	MOSFET, N-channel, 30V, 3.4A	4	$0.26	$1.03	https://www.arrow.com/en/products/irlml6346trpbf/infineon-technologies-ag
R1 R2 R3 R4 R5 R6	Resistor, 10 Ω, 0.1%, 0603	6	$0.09	$0.57	https://www.arrow.com/en/products/cpf0603b10re/te-connectivity
R13	Resistor, 100 Ω, 0.5 W, 1210	1	$0.09	$0.09	https://www.arrow.com/en/products/rc1210fr-07100rl/yageo
R7 R8	Resistor, 180 Ω, 0805	2	<$0.01	<$0.01	https://www.arrow.com/en/products/rmcf0805jt180r/stackpole-electronics
R21	Resistor, 1 kΩ, 0805	1	<$0.01	<$0.01	https://www.arrow.com/en/products/ac0805jr-071kl/yageo
R22	Resistor, 27 kΩ, 0805	1	<$0.01	<$0.01	https://www.arrow.com/en/products/rc0805fr-0727kl/yageo
R11 R12 R14 R15 R16 R17 R18 R19 R20 R23 R24 R25 R26	Resistor, 5.1 kΩ, 0805	13	<$0.01	$0.03	https://www.arrow.com/en/products/rc0805jr-075k1l/yageo
R9 R10	Resistor, 510 Ω, 0805	2	<$0.01	<$0.01	https://www.arrow.com/en/products/rmcf0805jt270r/stackpole-electronics
RN1	Resistor network, 8 elements, isolated, 2.2 kΩ	1	$0.17	$0.17	https://www.arrow.com/en/products/exb-2hv222jv/panasonic
RN2	Resistor network, 8 elements, isolated, 22 kΩ	1	$0.17	$0.17	https://www.arrow.com/en/products/exb-2hv223jv/panasonic
RN3	Resistor network, 8 elements, isolated, 510 Ω	1	$1.35	$1.35	https://www.arrow.com/en/products/vssr1603511guf/vishay

U4 U5	Voltage level translator, 8 bits, bidirectional	2	$0.66	$1.32	https://www.digikey.com/product-detail/en/nexperia-usa-inc/74LVC4245APW112/1727-2878-ND/763190
U6 U7	Solid state relay, zero crossing	2	$4.02	$8.04	https://www.arrow.com/en/products/cpc1966y/ixys
U13	LED 7-segment display, green, 10 pin, R/A	1	$2.36	$2.36	https://www.arrow.com/en/products/ldd-f302ni-ra/lumex
U1 U2 U3	Thermocouple converter	3	$4.85	$14.55	https://www.digikey.com/product-detail/en/maxim-integrated/MAX31856MUD/MAX31856MUD-ND/5050138
U9	Shift register, 8-Bit, parallel to serial	1	$0.30	$0.30	https://www.arrow.com/en/products/mc74hc589adtr2g/on-semiconductor
U8 U11 U12	Shift register, 8-Bit, serial/parallel to serial	3	$0.25	$0.75	https://www.arrow.com/en/products/74hc595pw118/nexperia
U10	CMOS timer	1	$0.32	$0.32	https://www.arrow.com/en/products/ne555pw/texas-instruments

Table 2.3. Bill of materials for other components of the TDT Sandwich.

Designator	Component	Quantity	Cost per unit (USD)	Total cost (USD)	Source of materials
CB1	Enclosure, ABS, gray, 5.12"L X 3.94"W	1	$4.30	$4.30	https://www.digikey.com/products/en?keywords=RM2015S
CB2	Arduino Nano V3.0 with USB cable	0.33	$12.35	$4.12	https://www.amazon.com/gp/product/B07KC9C6H5/
CB3	Fuse, 250 V, 2.5 A, fast-blow	1	$0.25	$0.25	https://www.arrow.com/en/products/021702.5mxp/littelfuse
CB4	USB-A to mini USB-B cable, 80 cm (Pack of 20)	0.05	$7.99	$0.40	https://www.ebay.com/itm/20x-5pin-Mini-B-To-A-USB-2-0-Cable-Cord-For-PC-Laptop-MP3-MP4-Digital-Camera-US/352454570522
CB5	Power cord, NEMA 5-15P to IEC 320-C15, 6 ft (Pack of 20)	0.05	$22.99	$1.15	https://www.ebay.com/itm/20-PACK-6FT-3-Prong-Mickey-Mouse-Power-Cord-Cable-for-Laptop-PC-Printer-Adapter/282413831612
CB6	Jumper, 2 positions	8	$0.32	$2.54	https://www.digikey.com/product-detail/en/880584-4/A122487-ND/1131873/?itemSeq=283547149
T1	PFA-insulated thermocouple, type T, 40" long, 40 AWG, stripped leads	0.6	$77.90	$46.74	https://www.omega.com/en-us/wire-sensor/5tc/p/5TC-TT-T-40-36
T2	Miniature thermocouple connector, type T, male (pack of 50)	0.06	$160.43	$9.63	https://www.omega.com/pptst/SMPW-CC.html
T3	Silicone wire grommet (pack of 50)	0.06	$2.87	$0.17	https://www.omega.com/pptst/SMPW-CC.html
T4	Silicone clamp grommet (pack of 50)	0.06	$2.90	$0.17	https://www.omega.com/pptst/SMPW-CC.html
A1	Aluminum 3003 Sheet, 0.032" Thick, 4" x 10" (pack of 6)	0.21	$10.25	$2.15	https://www.grainger.com/product/GRAINGER-APPROVED-Aluminum-Sheet-Stock-5MWN1

A2	Adhesive Transfer Tape, 4" X 20 yd, 2.30 mil Thick	0.02	$66.95	$1.12	https://www.grainger.com/product/15D108
H1	Polyimide etched-foil heater, 120 mm x 120 mm, 120 V, 144 W, 1 W/cm^2, uniform etched foil pattern, no adhesive, 300 mm lead wire sealed to corner of heater with silicone	2	$15.00	$30.00	Custom-order from a manufacturer: https://jymydq.en.alibaba.com/. Contact the manufacturer and provide them with the specifications as shown on the left.
H2	Expandable Polyester Sleeving, Red, 1/8" ID, 100' Long	0.02	$16.01	$0.21	https://www.mcmaster.com/9284k11
H3	Heat-Shrink Tubing, Red, 25' Long, 0.19" ID Before Shrinking	0.02	$15.56	$0.31	https://www.mcmaster.com/7856k74
H4	Plug contacts, Female 18-24 AWG	4	$0.06	$0.25	https://www.arrow.com/en/products/39-00-0038/molex
H5	Plug, 01x02	2	$0.09	$0.18	https://www.arrow.com/en/products/39-01-2020/molex
H6	Polyimide tape, Silicone Adhesive, 4" Wide, 15 Feet Long, 0.0025" Overall Thickness	0.04	$45.03	$2.00	https://www.mcmaster.com/7648A717
H7	Silicone Foam Strip with Adhesive, 3/4" Wide, 1/16" Thick, 30' Long	0.09	$68.48	$6.09	https://www.mcmaster.com/8645k12
B1	Polypropylene Box, 6" x 6" x 2"	1	$3.49	$3.49	https://www.flambeaucases.com/6-x-6-box.aspx
B2	Polyurethane Foam Mounting Tape, Open-Cell, 1/4" Thick, 1" Wide, 54' Long	0.04	$87.35	$3.24	https://www.mcmaster.com/7626A132
B3	Buna-N/PVC Foam Insulation Sheet, 4' x 36" x 1"	0.04	$54.64	$2.28	https://www.mcmaster.com/9349K4

Table 2.4. Bill of materials for consumables and specialized tools used during the construction process.

Designator	Component	Quantity	Cost per unit (USD)	Total cost (USD)	Source of materials
Z1	Printed circuit board stencil	1	$13.28	$13.28	https://jlcpcb.com/
Z2	Crimping tool	1	$22.99	$22.99	https://www.amazon.com/gp/product/B00YGLKBSK/
Z3	Paper trimmer	1	$25.19	$25.19	https://www.amazon.com/gp/product/B016LDV41S/
Z4	Bastard Cut Mill File	1	$2.99	$2.99	https://www.menards.com/main/tools/hand-tools/files/tool-shop-reg-6-bastard-cut-mill-file/2446555/p-1444428087759-c-1550852385008.htm
Z5	Instant bonding adhesive, 0.5 oz	1	$4.43	$4.43	https://www.mcmaster.com/5551T72
Z6	Leaded solder paste, 63/37 No Clean, 17.6 oz	1	$59.95	$59.95	https://www.amazon.com/gp/product/B071D7SM1C/

Table 2.5. Bill of materials for consumables used during operation of the TDT Sandwich.

Designator	Component	Quantity	Cost per unit (USD)	Total cost (USD)	Source of materials
P1	Mylar pouches, 3" x 3", PAKVF4W (Case of 5000)	1	$255.00	$255.00	https://www.impakcorporation.com/flexible_packaging/mylar-bag/minipouches/03MFW03TN

Table 2.6. Material properties used in the heat transfer model.

Model parameter/material property	**Aluminum**	**Buna-N/PVC insulation foam**
Density, ρ (kg m^{-3})	2700(*46*)	72.08(*30*)
Specific heat capacity, c_p (J kg^{-1} K^{-1})	900(*46*)	1515(*26*)*
Thermal conductivity, k (W m^{-1} K^{-1})	201(*46*)	0.011(*30*)

* No data available from manufacturer. Since the insulation material contains PVC foam, the c_p value was approximated as the average of a range of c_p values of PVC foam.

Numbers in brackets are the references from which the values were cited from.

Table 2.7. Characteristics of the TDT Sandwich system measured with 12 TDT Sandwich units. Values are displayed as mean (standard deviation). The reader is referred to the text for explanation of the symbols.

Sample amount (g)	Target temperature (°C)	Heating rate (°C/min)	t_{CUT} (s)	T_u^{tCUT} (°C)	T_u^{tss} (°C)	T_o^{tss} (°C)
0	70	25	138.6 (2.6)	-0.27 (0.15)	-0.17 (0.11)	0.00 (0.10)
		50	93.9 (2.8)	-0.30 (0.10)	-0.15 (0.08)	-0.02 (0.15)
		max	57.8 (4.5)	-0.4 (0.16)	-0.19 (0.08)	0.06 (0.12)
	90	25	187.4 (1.8)	-0.32 (0.19)	-0.20 (0.10)	0.03 (0.1)
		50	117.3 (3.2)	-0.42 (0.17)	-0.17 (0.09)	0.07 (0.09)
		max	61.8 (3.5)	-0.57 (0.22)	-0.23 (0.09)	0.03 (0.1)
	110	25	232.6 (1.8)	-0.33 (0.14)	-0.19 (0.11)	0.00 (0.09)
		50	140.7 (1.9)	-0.47 (0.12)	-0.23 (0.09)	0.06 (0.09)
		max	70.0 (5.1)	-0.71 (0.35)	-0.32 (0.10)	0.08 (0.16)
2	70	25	139.8 (2.4)	-0.27 (0.14)	-0.13 (0.12)	0.04 (0.22)
		50	93.6 (1.9)	-0.27 (0.19)	-0.17 (0.12)	-0.01 (0.07)
		max	55.1 (5.4)	-0.37 (0.23)	-0.18 (0.15)	0.01 (0.11)
	90	25	189.4 (4.0)	-0.38 (0.19)	-0.17 (0.14)	0.05 (0.13)
		50	118.1 (1.6)	-0.51 (0.20)	-0.23 (0.11)	0.05 (0.10)
		max	59.3 (4.9)	-0.63 (0.45)	-0.23 (0.12)	0.13 (0.13)
	110	25	237.1 (2.1)	-0.38 (0.18)	-0.19 (0.12)	0.00 (0.07)
		50	141.3 (2.5)	-0.50 (0.23)	-0.23 (0.12)	-0.01 (0.10)
		max	68.0 (2.4)	-0.96 (0.52)	-0.32 (0.15)	0.21 (0.23)
4	70	25	141.8 (2.4)	-0.45 (0.18)	-0.19 (0.13)	0.01 (0.14)
		50	96.9 (2.7)	-0.49 (0.15)	-0.17 (0.12)	-0.02 (0.10)
		max	52.9 (6.5)	-0.84 (0.48)	-0.21 (0.16)	0.30 (0.39)
	90	25	190.1 (2.7)	-0.53 (0.17)	-0.23 (0.13)	-0.02 (0.08)
		50	122.3 (2.6)	-0.66 (0.16)	-0.23 (0.16)	0.05 (0.17)
		max	66.7 (6.8)	-1.33 (0.43)	-0.32 (0.14)	0.48 (0.34)
	110	25	238.6 (2.8)	-0.62 (0.17)	-0.20 (0.13)	-0.01 (0.07)
		50	145.1 (2.2)	-0.78 (0.21)	-0.32 (0.14)	0.02 (0.09)
		max	73.9 (3.1)	-1.63 (0.54)	-0.30 (0.17)	0.88 (0.44)

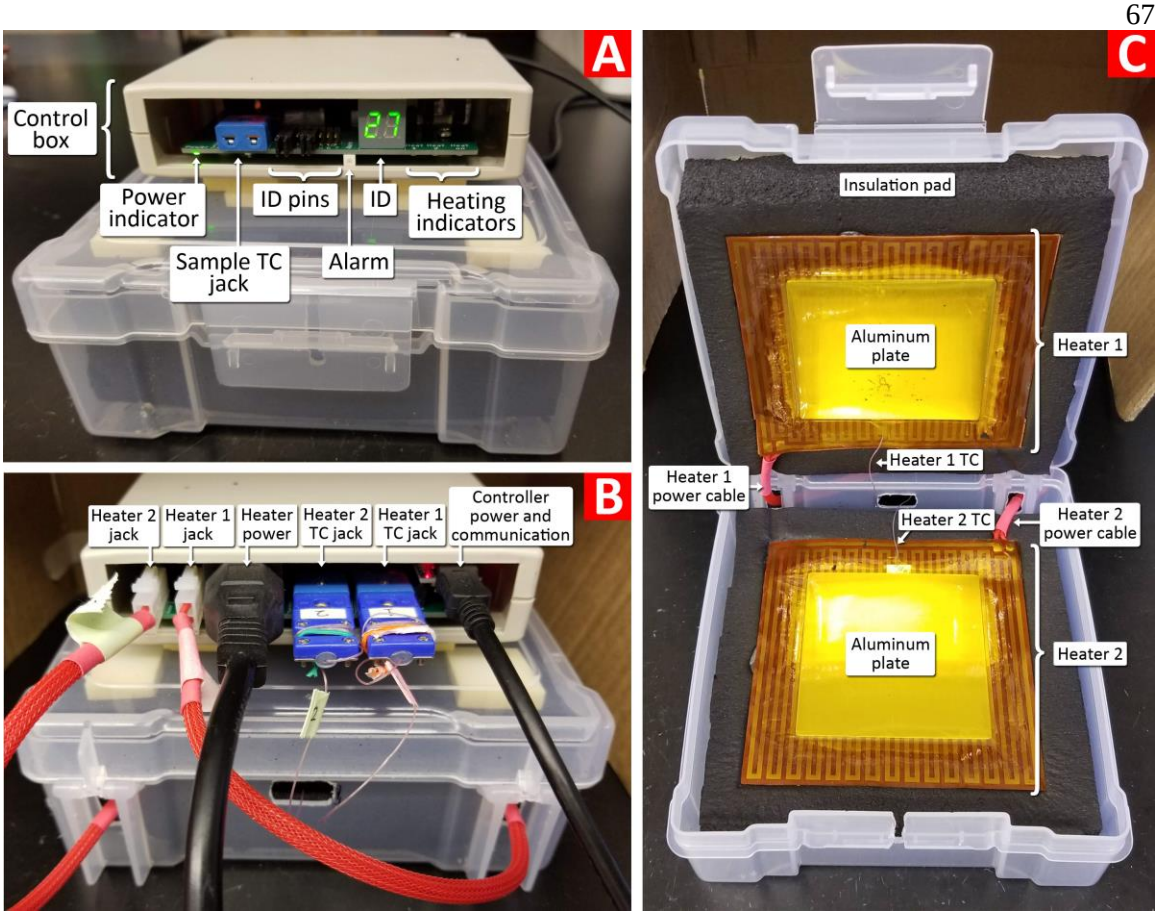

Figure 2.1. Annotated views of the TDT Sandwich from the (A) front, (B) back, and (C) inside. Abbreviations used: TC = thermocouple, ID = identification.

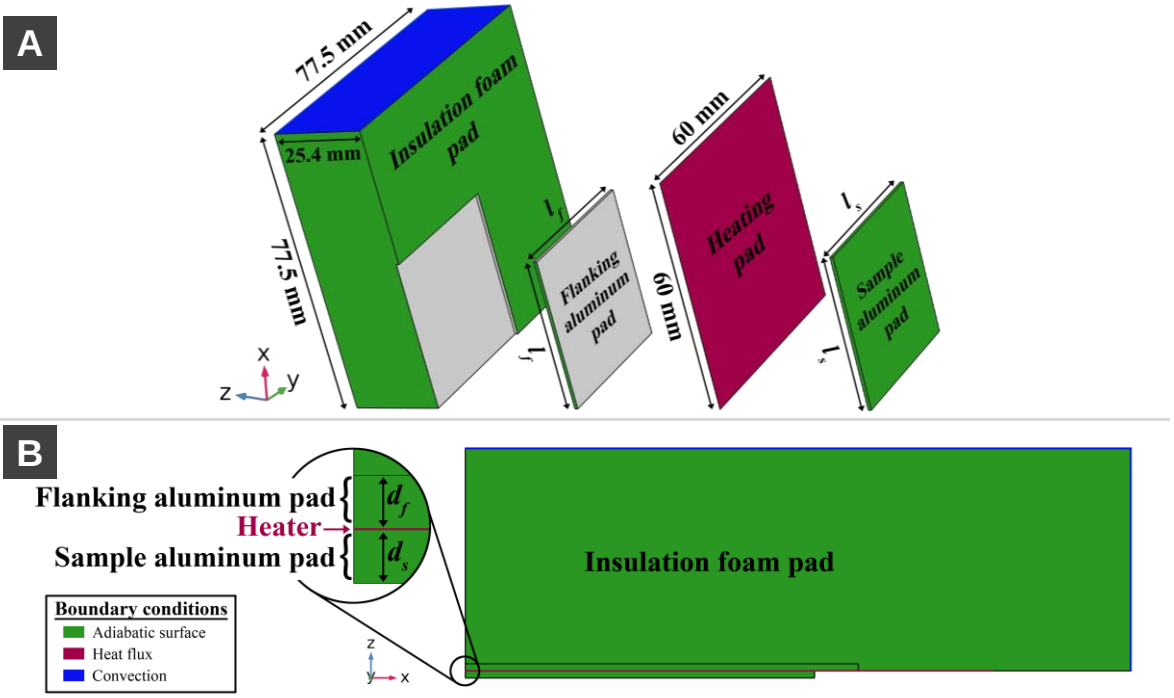

Figure 2.2. Geometry, dimensions, and boundary conditions of the heat transfer model viewed from (a) an exploded diagram and (b) projection on the z-x plane.

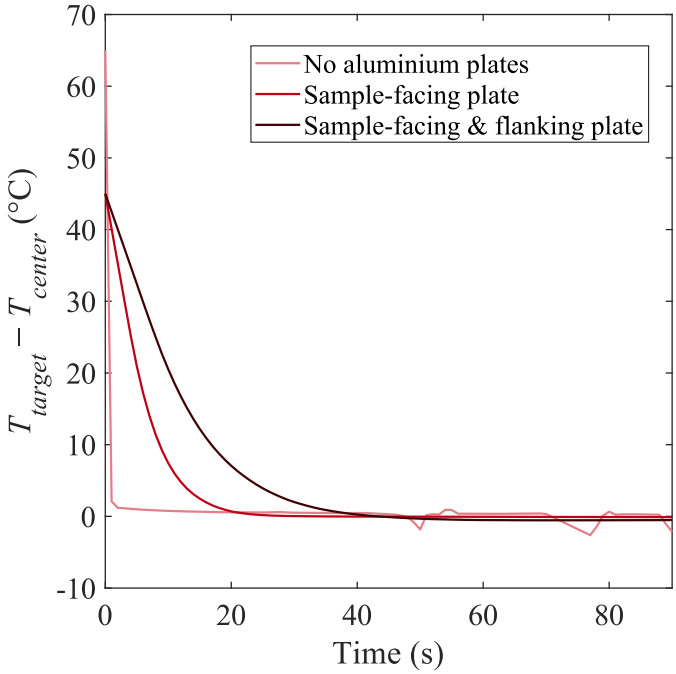

Figure 2.3. Difference between the target temperature, $\boldsymbol{T_{target}}$ and the temperature at the center of the sample-facing aluminum plate (or center of the heater if the plate is absent), $\boldsymbol{T_{center}}$ during a simulated 90 s heating process for three configurations of the TDT Sandwich.

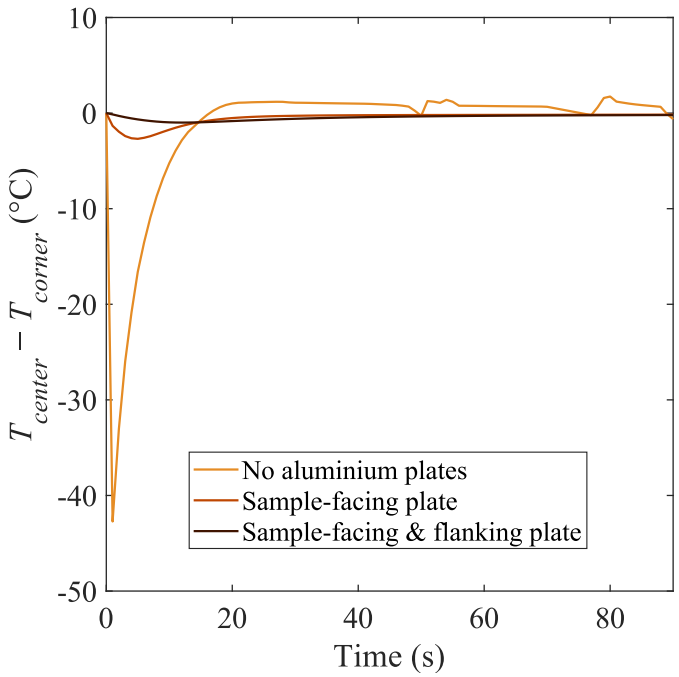

Figure 2.4. Difference between the temperature at the center of the sample-facing aluminum plate (or center of the heater if the plate is absent), $\boldsymbol{T_{center}}$ and the location of the corner of an imaginary sample pouch, $\boldsymbol{T_{corner}}$ during a simulated 90 s heating process for three configurations of the TDT Sandwich.

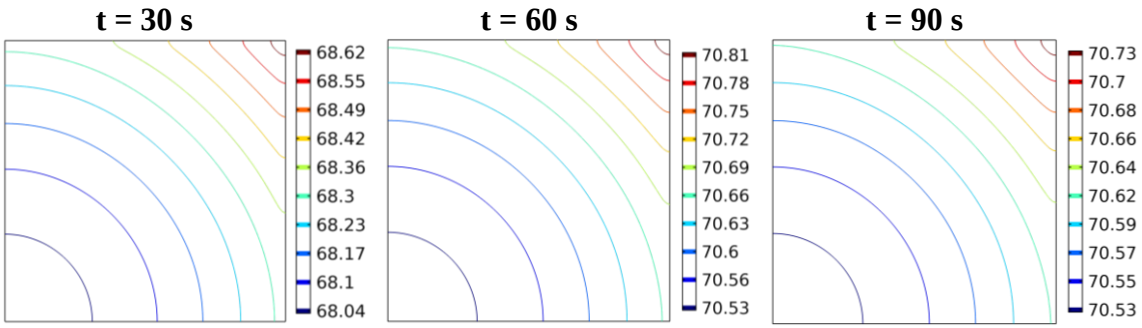

Figure 2.5. Temperature contour plots on a quadrant of the sample-facing aluminum plate at select timepoints during a simulated 90 s heating process for a TDT Sandwich configured for heaters with both sample-facing and flanking aluminum plates.

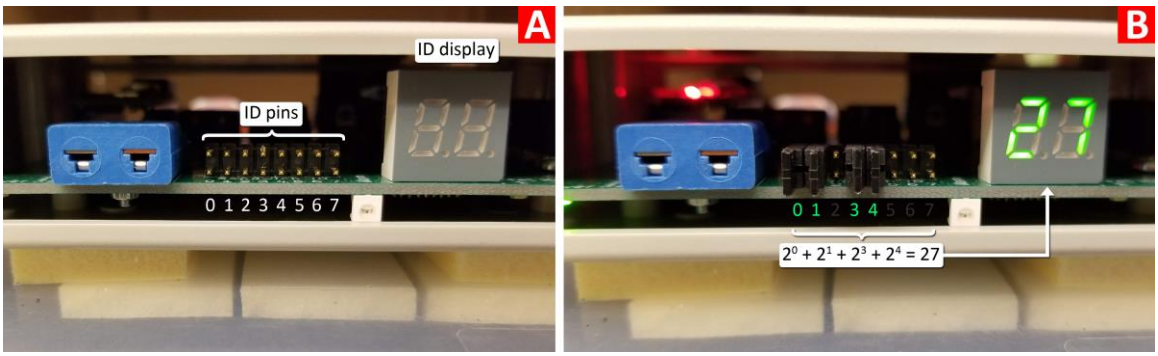

Figure 2.6. Pictorial guide for setting the ID of a TDT Sandwich: (A) The pins and display for the ID; (B) An example pin configuration for a sandwich with ID 27.

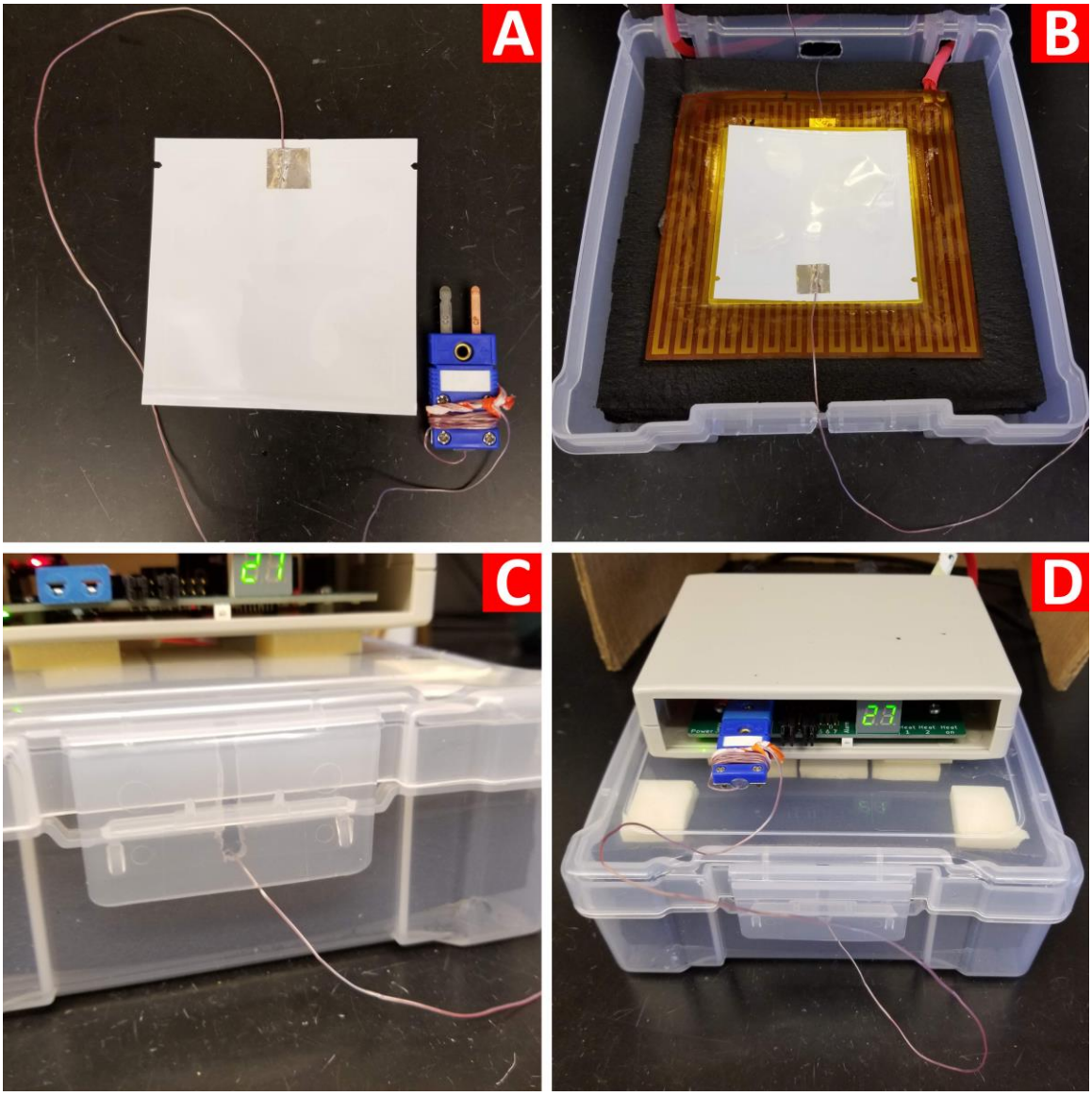

Figure 2.7. Preparation of a TDT Sandwich for operation: (A) Packing sample into a pouch, sealing, and (optional) inserting a thermocouple, (B) placing the packed sample on the bottom heating pad and (optional) routing the sample thermocouple out through the front slot hole, (C) Snapping the front clip shut, and (D, optional) plugging the sample thermocouple plug into the jack at the front of the control **box.**

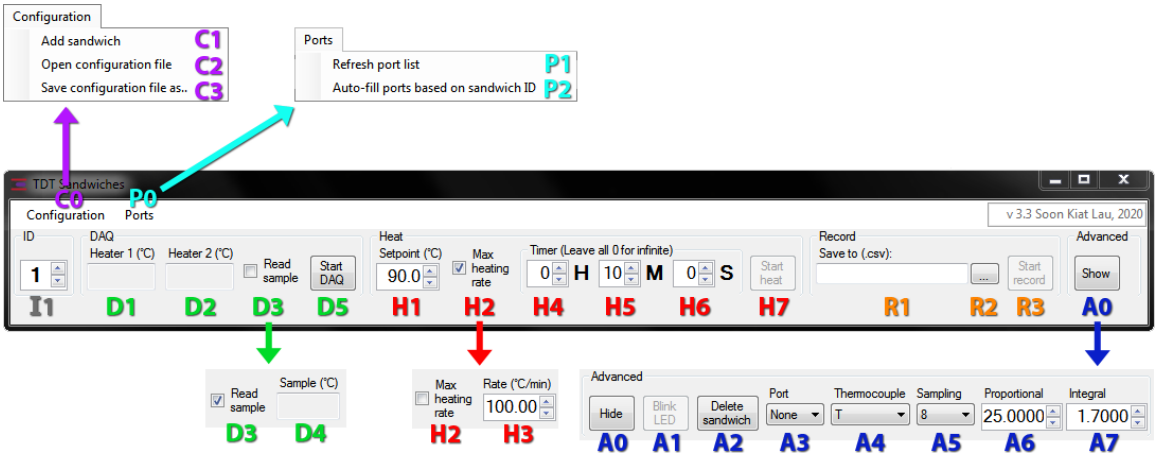

Figure 2.8. Annotated view of the TDT Sandwich computer program, with expanded menus, for a single virtual TDT Sandwich. The labels are used in the text.

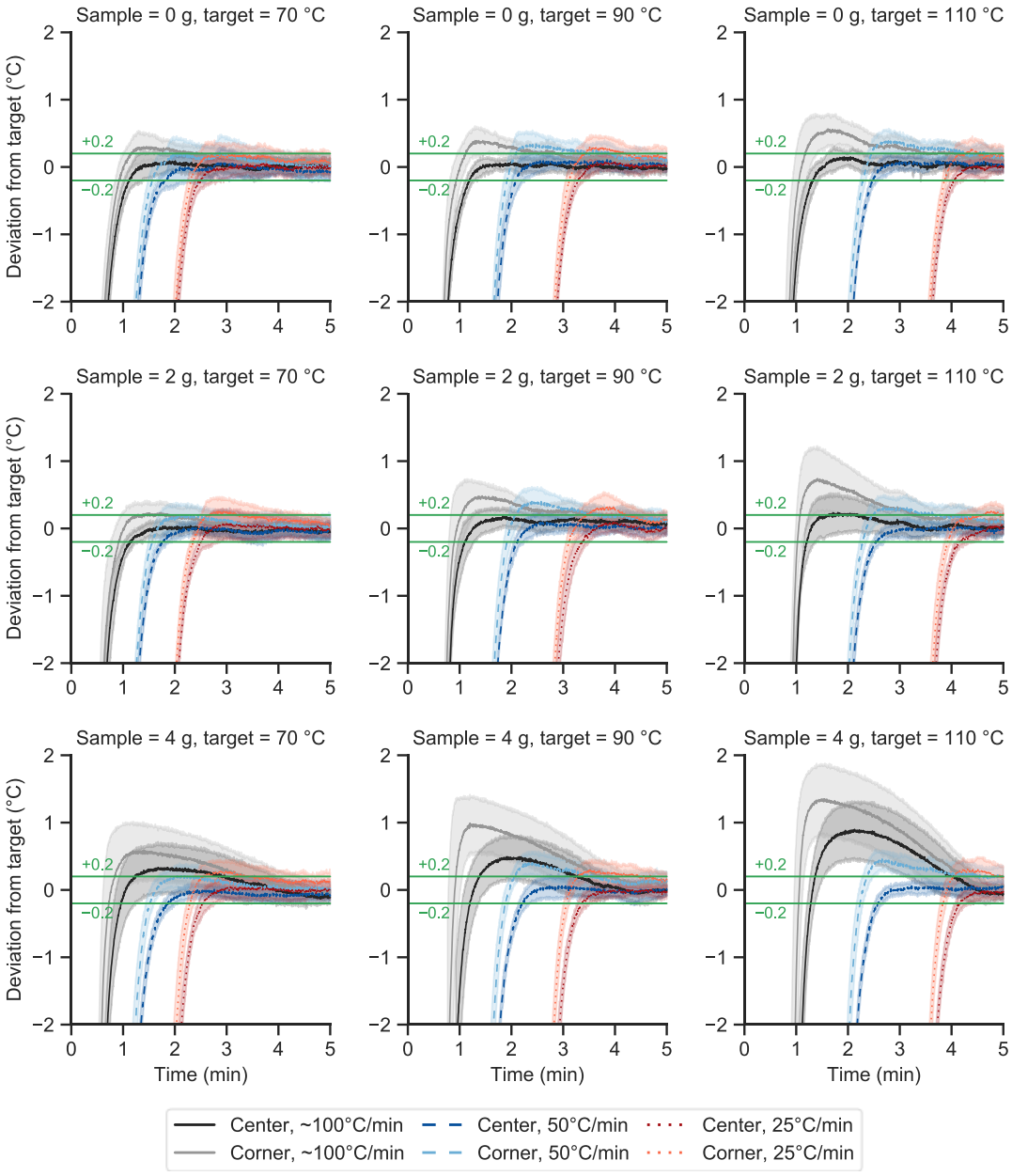

Figure 2.9. Deviation of the center and corner temperatures of whole milk powder samples from the target temperature measured with various whole milk powder sample sizes (rows), target temperature (columns), and heating rates (line styles). Plotted lines are means of 12 TDT Sandwiches and are shrouded by one standard deviation. Green lines represent a ±0.2 °C boundary.

Chapter 3: HumidOSH: A Self-Contained Environmental Chamber with Controls for Relative Humidity and Fan Speed

3.1. Introduction

Relative humidity (RH) is defined as the ratio of two quantities: the vapor pressure of water present in air and the saturation vapor pressure of water in air. In other words, it is a measure of how much moisture is present in air relative to the maximum amount of moisture that can be held by the air in vapor form. RH can affect samples in various manners, either directly or indirectly. Electrostatic discharge has been shown to be affected by RH and it is thus necessary to control RH when fabricating sensitive electronic devices (*8*). When most biological samples are placed in an environment with a fixed RH for a sufficient time, the vapor pressure of water in the sample will eventually equilibrate to that of the air around the sample. This equilibrium RH of the sample is defined as water activity and is expressed as a decimal quantity.

Water activity, a_w is a measure of the availability of water, and thus it affects the rate of any reactions that are directly or indirectly affected by the presence of water. As such, the a_w in a biological sample such as food can affect changes in its physical, biological, and chemical qualities. The glass transition temperatures of food powders are affected by a_w and the maintenance of low a_w is vital for ensuring flowability and non-aggregation of food powders (*1*, *4*, *5*). Water activity is a crucial parameter in controlling the proliferation of microorganisms in foods and even affects the thermal resistance of microorganisms in low-moisture foods (*14*, *15*). Chemical reactions in foods such as

autoxidation of lipids, degradation of anthocyanins, Maillard browning reaction, and most enzymatic activities are also affected in varying degrees by a_w (*12*). As such, the control of a_w, and hence RH, is indispensable in research on biological samples.

The control of RH has traditionally been achieved with the use of saturated binary salt solutions made of pure water and non-volatile salts such as lithium chloride or sodium chloride. These solutions will either absorb or desorb water vapor to maintain the RH of a closed environment to be equal to the equilibrium RH or a_w of the saturated salt solution (*3*). Ease of preparation and maintenance makes this method attractive for simple RH control, but the fixed equilibrium RH of the solutions means that multiple salt solutions must be prepared to achieve a range of RH. The advent of small, affordable, and reliable RH sensors has paved the way to programmable electronic RH-controlled chambers. These commercially available chambers control RH through a combination of electronic RH sensors, control loops, and a variety of methods to generate or remove humidity such as steam generators and condensers. Due to the high cost of these systems, a few custom RH control systems have been constructed such as a system that dries air with silica gel beads and bubbles air through water to add moisture (*13*), an open source humidity controller which mixes dry nitrogen gas with water-saturated nitrogen gas (*2*), Agenator: an open source humidity control system for dry aging of meat (*6*), and Polar Bear: an open source environmental chamber which controls temperature in addition to RH (*10*). The construction of such custom RH control systems can be motivated by cost and the desire to customize the systems according to research needs.

The ability to condition samples in an RH-controlled environment is invaluable to researchers from various fields. However, the high costs of commercially available equipment can make it difficult to condition large amounts of samples. Although custom alternatives exist, complete build instructions are either unavailable or the systems are missing desirable features such as easy manipulation of samples and a self-contained design. These needs, along with the many advantages of open source scientific equipment (*7, 9*), eventually culminated in the HumidOSH: a self-contained environmental chamber with controls for RH and fan speed. This work describes the design, construction, operation, and performance of the HumidOSH along with a case study on food samples.

3.2. Hardware Description

The HumidOSH (**Fig. 3.1**) is a large yet portable chamber with a user-friendly interface for adjusting the inside RH and fan rotational speed to create a controlled environment for samples. The RH sensor utilizes the SHT85 digital humidity sensor (Sensirion AG, Staefa ZH, Switzerland) which is specified to have an RH accuracy of 1.5 % (*11*). The system is capable of adjusting RH to within the range of 3 to 97 % and maintaining it within 0.2% of the target. The specified range of achievable RH is a conservative estimate; in actual usage, most HumidOSH units were able to exceed the limits of the range without issues. Although the RH sensor also acquires temperature readings, this data is not displayed during operation but can be acquired through the optional computer program. The system also includes a fan inside the chamber for circulating air and improving moisture transfer with the sample. The rotational speed of the fan can be adjusted between 1,200 to 7,500 RPM and will be maintained within 100

RPM of the target. A higher fan rotational speed results in higher average air velocity in the chamber, thus accelerating the equilibration of the sample with the surrounding air. Other features of the system include:

- Glove sleeves with replaceable hand gloves for handling samples inside the chamber.
- Sample door for adding/removing objects to/from the chamber during operation.
- Ceiling LED lights for illuminating the work area inside the chamber.
- Visual indicators for system operation status.
- Two-point calibration for the RH sensor.
- Refillable cartridges for humidifying or dehumidifying the air.
- Power extension cord for operating electronic devices inside the chamber.
- Self-contained system: every part of the system is either housed within or connected to the chamber, allowing for easy relocation of the system.
- Autoclavable aluminum trays and stainless steel tray rack for holding samples.
- HumidOSH units can be stacked on top of each other and are also appropriately sized for placement in commercially available shelves.
- Optional USB connection to a laptop or computer for recording real-time RH, temperature, and fan rotational speed readings.

A single HumidOSH unit costs about a tenth or less of leading commercial humidity-controlled chambers. Excluding the custom printed circuit boards, the HumidOSH is purposely designed to be built from commercially available components to reduce the time and expertise needed to build the system. The system is easy to clean and utilizes

disposables (*e.g.* gloves, silica gel beads) that can be replaced at affordable costs. The system does not have a temperature control system and is thus incapable of directly controlling the temperature of samples. The HumidOSH can be used for various applications such as:

- Adjusting the a_w or moisture content of samples.
- Performing accelerated shelf life studies in a high RH environment.
- Storage of moisture-sensitive samples.

3.3. Design Files

Table 3.1 lists the files needed for constructing or operating HumidOSH units and an optional computer program that can be used during operation of HumidOSH units. The printed circuit board (PCB) design files consist of both the control box PCB and the RH sensor PCB. There are many companies that can manufacture these PCBs when given the PCB design files. The laser cutting files are used with a laser cutter to cut holes on the control box for mounting various electronics on it, though the cutting can be done manually if no laser cutter is available. The Arduino code will be uploaded to the Arduino Nano microcontroller in the control box. The optional computer program is a Windows executable file for recording live readings from HumidOSH units. The design files are stored in online repositories (linked in **Table 3.1**) that contain "Wikis" explaining the use of the files and how to download them.

3.4. Bill of Materials

The materials required for constructing one HumidOSH system are listed in **Tables 3.2** to **3.4**. Consumables used during the construction and operation of the HumidOSH are given in **Table 3.5**. In **Table 3.6**, specialized tools that are used in the construction process are listed. Although these tools are not absolutely necessary to construct HumidOSH systems, they will make the construction process more efficient. Some items are sold in bulk but only a few quantities are needed; these are denoted by decimal quantities in the tables.

3.5. Build Instructions

Instructions on constructing the HumidOSH can be found at https://dx.doi.org/10.17504/protocols.io.6a5hag6. The designators used in the build instructions are defined in the bills of materials (**Tables 3.2** to **3.6**).

3.6. Operation Instructions

3.6.1. Basic Operation

Before operating the HumidOSH, the “wet” and “dry” columns must be filled sufficiently. These columns are located on the left side of the chamber. The wet column contains hydrated water beads made of water-absorbing polymers that slowly release moisture into the air to humidify the air. The dry column contains silica gel beads which absorb moisture from the air to dehumidify it. To fill the wet column, it is necessary to hydrate the wet beads (X5 from **Table 3.5**) with water at a mass ratio of 1:200 overnight. Approximately 5 g of water beads is sufficient to fill up one wet column. Excess water

should be removed before transferring the water beads into the wet column. To add the water beads into the wet column, first unscrew and remove the wet column housing from the HumidOSH unit (**Fig. 3.2(A)**). Then, remove the cap and plastic filter piece from the cartridge. Pour the hydrated water beads into the cartridge until it is about 4/5 full (**Fig. 3.2(B)**). Reinstall the plastic filter piece and cap and insert the assembled cartridge back into the column housing. Ensure that the gasket on the cap of the inner plastic column is well-seated before screwing the wet column back onto the HumidOSH unit (**Fig. 3.2(C)**). The procedure for filling the dry column is similar to that of the wet column but uses silica gel beads (X3 and X4 from **Table 3.5**) instead of water beads. Although both X3 and X4 will dehumidify the air, X4 is able to change color from orange to blue as the beads become saturated with water which is a useful visual indicator as to when to change the beads. However, X4 is more expensive than X3, therefore it is recommended to mix X4 with X3 at a mass ratio of approximately 1:10 to reduce costs while preserving the visual indicator feature.

Operation of the HumidOSH begins by preparing the samples that will be placed into the chamber. Distribute the samples among a maximum of six aluminum trays (T2 from **Table 3.4**) and slide them into the tray rack. Position the tray rack at the center of the chamber and plug the cables of the RH sensor and fan into the appropriate ports on the wall of the chamber (**Fig. 3.3(A)**). Connect the LED lights on the lid to the power cable on the wall and close the lid over the chamber (**Fig. 3.3(B)**). Fasten the latches along the walls of the chamber to the strike plates on the lid. If desired, add a small

amount of talcum powder (X1 from **Table 3.5**) to the inside of the gloves to lubricate the insides.

With the samples in the chamber and the lid secured, all that is left is to set the target RH and fan rotational speed. First, ensure that the power supply adapter for the control box is plugged into an electrical outlet. Once the control box has performed its boot up sequence, it will display the readings screen (**Fig. 3.4(A)**) which shows the readings for RH and fan rotational speed, and the status of the control system for both. At this point, the statuses should be "IDLE", indicating that the control systems are not running. RH readings are obtained and displayed every second while the system is powered but the fan rotational speed readings will only appear if the fan control system is activated. Otherwise, "N/A" will be displayed for the fan rotational speed reading. Pressing the black button once will change the screen to the adjustment of target RH screen (**Fig. 3.4(B)**). Here, the current target for RH is displayed. At the bottom of the screen, the user is prompted for the new target RH. To set the new target, simply key in the desired target with the keypad, keeping in mind that the given value should have only one decimal place and be in the range of 0.0 to 100.0 %, inclusive. If it is not desired to change the target RH, do not key in any value or clear any entered values using the backspace key. Press the black button to save the new target or, if the new target was left blank, keep the old target and move to the next screen. The next screen is for setting the target fan rotational speed (**Fig. 3.4(C)**) and is mostly similar to the one for RH. When keying in the new target, it should be an integer (*i.e.* no decimals) and be between 1,200 to 7,500 RPM, inclusive. Press the black button to change the screen to the RH sensor

calibration screen (**Fig. 3.4(D)**) which is not required for typical operation and will be described in **Section 3.6.3**. Pressing the black button will return the screen back to the readings screen. At this point, pressing the green button will start the control system for RH, which is indicated by the green button lighting up and flashing arrows beside the RH reading on the screen (**Fig. 3.4(F)**). Pressing the blue button will initiate a similar sequence of events for the fan control system. At anytime during operation, the targets for RH and fan rotational speed can be changed without stopping the control systems by scrolling to the appropriate screens with the black button and keying in new targets. The control systems will automatically adjust to the new targets once the new targets have been saved. To stop any of the control systems, simply press the appropriate button (green or blue) and hold for four seconds. A message will be displayed on the screen to show the remaining time to hold the button before the control system is turned off.

At any time during operation of the HumidOSH, samples in the chamber can be manipulated with the gloves at the front of the chamber. Before manipulating samples, it is recommended to turn on the LED lights in the chamber by flipping the switch at the front of the control box (**Fig. 3.4(A)**). In addition, the sample door on the left side of the chamber can be opened to transfer objects/samples in and out of the chamber. Manipulation of samples with the gloves changes the pressure inside the chamber which causes external air to seep in through tiny leaks. The same happens when the sample door is opened. Experience with using the HumidOSH demonstrated that these activities can cause a temporary change in RH as much as 4 % depending on the difference in RH between the inside and outside of the chamber. If electrical devices such as heat sealers,

weighing scales, or vortexes are to be used inside the chamber, they can be plugged into the extension cord attached to the left wall of the chamber.

3.6.2. Maintenance

During the course of using the HumidOSH, a few maintenance activities are necessary to keep it at top performance. The interior of the chamber should be cleaned periodically to remove spilled samples and prevent contamination of future samples. Before any cleaning is done, it is extremely important to remove the RH sensor and place it away from the chamber to prevent contaminating the sensor with the cleaning chemicals. In addition, power to the control box and extension cord should be disconnected. The tray rack should be removed from the chamber to be cleaned separately. The insides of the chamber can then be sprayed with a cleaning solution such as 70% ethanol and wiped down with paper towels. The tray rack and aluminum trays can be autoclaved if necessary or cleaned with the same cleaning solution. The fan on the tray rack should be removed before autoclaving is performed. The hand gloves attached to the glove sleeves can either be cleaned or replaced with a new pair. Once everything has been cleaned, place everything except the RH sensor back into the chamber, leave the lid open, and turn on the fan in the chamber to dry up the insides of the chamber. Once the insides are dry, reinstall the RH sensor.

Over time, the contents of the wet and dry columns of the system will need to be replaced, especially if it is desirable to adjust the RH to extreme values. The wet beads will shrink in size after prolonged usage and can either be soaked in water to rehydrate them or be replaced with a new batch of wet beads. If the silica gel beads in the dry

column have mostly turned from orange to blue in color, they can either be regenerated by heating at 120°C for about 2 hours or be replaced with new silica gel beads.

The RH sensor is sensitive to contamination and will show some inaccuracies over long periods of usage. Although this can be addressed by **Section 3.6.3**, it is also possible to simply replace the sensor by following step 79 of the build instructions in **Section 3.5**.

3.6.3. Calibration of Relative Humidity Sensor

Over time, the readings of the RH sensor may drift to inaccurate values. This drifting can be compensated with the two-point calibration included with HumidOSH. This calibration is a "soft" calibration; it merely applies scaling and offset to readings from the sensor. In addition, the calibration parameters are stored within the control box of HumidOSH and not the sensor, so the calibration values are not carried over when transferring the sensor to another HumidOSH system. To access the calibration protocol, press the black button on the control box until the calibration screen is shown (**Fig. 3.4(D)**). Here, the user can calibrate one of the two points or clear the saved calibrations. Based on the instructions on the screen, press either key "1" or "2" on the keypad to begin calibrating one of the points (**Fig. 3.4(E)**). Place the RH sensor in an airtight container that contains a reference standard for RH calibration. For example, saturated salt solutions with known equilibrium RH such as sodium chloride and lithium chloride can be used (*3*). Preparation of these solutions involve dissolving as much of the salt as possible in hot pure water until no more salt can be dissolved, then letting the solution cool down. If an airtight container is not available, simply pour some saturated salt

solution into a beaker, place the RH sensor in the container without touching the solution, and then seal the opening of the beaker to the RH sensor cable with Parafilm or a flexible plastic film. It is extremely important that the RH sensor does not come into direct contact with the salt solution as that may damage the sensor. Allow the air in the container to equilibrate with the salt solution for at least 10 minutes. The raw RH reading displayed on the screen (**Fig. 3.4(E)**) should also stabilize during this time. Once the raw RH reading is stable, key in the reference RH reading *i.e.* the known equilibrium RH of the saturated salt solution. Press the black button to save this calibration point. Repeat the calibration procedure for the second point with another saturated salt solution and the calibration procedure is complete. If a new RH sensor is installed into the HumidOSH system and the saved calibrations are no longer needed, erase the saved calibrations by scrolling to the calibration screen (**Fig. 3.4(D)**) and then press key "3" followed by "5," as shown by the instructions on the screen.

3.6.4. Computer Program

An optional computer program is available for recording readings from HumidOSH systems. In order to use the program, the microcontroller inside the control box must be connected to a computer or laptop with a USB cable. Multiple instances of the program can be opened to acquire readings from multiple HumidOSH systems. In this section, the colored labels in **Fig. 3.5** will be used to refer to the various sections of the program.

I1 is a dropdown list of all the open communication ports of the computer or laptop. The communication ports can be used by various devices such as USB devices.

The port that is connected to the HumidOSH system needs to be selected here. Some guesswork may be required here, so select a port from the list and press **D6** to attempt communication. If an error appears, select the next port and repeat. Sometimes, the first communication attempt to the HumidOSH system may fail, so it may be necessary to try twice. Once the communication attempt is successful, **D1** displays the RH reading, **D2** the temperature, **D3** the fan rotational speed, **D4** the target RH of the control system, and **D5** the target fan rotational speed of the control system. Pressing **D6** again while the readings are being acquired will end communications with the HumidOSH system. To record the readings, press **R2** to open a dialog box for choosing the location and file name for storing the readings; the path to the file will appear in **R1** when the selection is confirmed. Press **R3** to begin recording the data or to stop recording. All recorded data are stored in Comma Separated Value (CSV) files which can be opened with spreadsheet software such as Microsoft Excel or text editors.

3.7. Validation and Characterization

To test the ability of the HumidOSH to maintain a stable RH, samples of whole milk powder (28.5% milkfat, Land O'Lakes, Inc., St. Paul, MN) were placed in HumidOSH units set to target RH of either 5 % or 80 % and 5,000 RPM for target fan rotational speed. For the 80 % target RH, the whole milk powder samples were used as is, with a native a_w of 0.2030 ± 0.0033 a_w. As for the 5 % target RH, the a_w of the samples were first adjusted to a higher a_w through the addition of deionized water and then mixed using a kitchen mixer (KSM8990OB, KitchenAid, Benton Harbor, MI) with a wire whip attachment (W10361360, KitchenAid, Benton Harbor, MI) for 15 minutes at speed 4. The

hydrated milk powder was then left in sealed plastic bags at room temperature overnight to allow the mixture to equilibrate to 0.4291 ± 0.0044 a_w. When inserting the whole milk powder samples into the HumidOSH units, 500 g of whole milk powder were distributed across two aluminum trays per HumidOSH system and placed at the third and sixth positions from the top of the tray rack. Five HumidOSH systems were used for each target RH. The computer program described in **Section 3.6.4** was used to record readings from all the HumidOSH systems. Every day, two random samples were taken out from each HumidOSH system and measured for a_w with a water activity meter (4TE, METER Group, Pullman, WA). The validation study was performed continuously for 6 days.

The RH readings and a_w measurements of the validation study are shown in **Fig. 3.6**. When the HumidOSH units were set to 80 % target RH, the RH rose rapidly from approximately 25 % to 50 % within the first few hours of operation and then slowly rose to 80 % over the next two days. This behavior in RH increase is likely due to a large difference in vapor pressure between the air and the water beads in the wet column of the HumidOSH units at the beginning of the study which subsequently decreased as the RH of the air increased. The reverse of this trend was observed when drying the air to a target RH of 5 %, though the initial decrease was not as rapid. In addition, there is a noticeable spike in RH readings for all the HumidOSH units that occurred every day around the same time; these RH disturbances were caused by extraction of samples from the HumidOSH units for a_w measurements. It should be noted that the time of RH disturbances and a_w readings do not coincide exactly in **Fig. 3.6** because the RH readings are plotted in real-time format while the a_w measurements are plotted in daily format.

Upon achieving the target RH, all the HumidOSH units were able to maintain the RH within a tight tolerance (within 0.2 % of the target RH), as evident by the small standard deviations.

In general, the a_w of the whole milk powder samples lagged behind the RH during the first few days because of the time needed for vapor pressure equilibration between the sample and the air inside the HumidOSH units. The a_w readings stabilized after the third day and remained relatively constant for the remainder of the study. However, some of the stabilized a_w readings, especially when the target RH was 80 %, deviated from the target RH. This deviation is likely due to inaccuracies of the RH sensor in some of the HumidOSH units which led to inaccurate control of the RH and subsequently inaccurate a_w in the samples after equilibration. The largest deviation was 0.06 a_w or, equivalently, 6 % RH which is larger than the 1.5 % accuracy tolerance given by the manufacturer of the RH sensors used in HumidOSH. The deterioration in accuracy of the sensors can be explained by prolonged use of the HumidOSH units; all the HumidOSH units used in the validation studies had been used to condition various food samples for almost a year before the validation studies were performed. Therefore, it is recommended to either calibrate the sensors every few months (**Section 3.6.3**), replace the sensors periodically (**Section 3.6.2**), or simply apply an offset to the target RH to account for the sensor drift.

3.8. Acknowledgements

This material is based upon work that is supported by the National Institute of Food and Agriculture, U.S. Department of Agriculture, under award number 2015-68003-23415 and with partial support from the Nebraska Agricultural Experiment Station with funding

from the Hatch Act (Accession Number 1006859) through the USDA National Institute of Food and Agriculture. Much appreciation is directed to Rajendra Panth, Tushar Verma, and Han Yu for their help in the construction of multiple HumidOSH units. Many thanks to The Nebraska Innovation Studio for allowing use of their prototyping facilities.

3.9. References

1. Chang, K. S., D. W. Kim, S. S. Kim, and M. Y. Jung. 1998. Bulk flow properties of model food powder at different water activity. *Int. J. Food Prop.* 1:45–55.
2. Gaponenko, I., L. Musy, S. C. Muller, and P. Paruch. 2019. Open source standalone relative humidity controller for laboratory applications. *Eng. Res. Express* 1:025042.
3. Greenspan, L. 1977. Humidity Fixed-Points of Binary Saturated Aqueous-Solutions. *J. Res. Natl. Bur. Stand. Sect. -Phys. Chem.* 81:89–96.
4. Juarez-Enriquez, E., G. I. Olivas, E. Ortega-Rivas, P. B. Zamudio-Flores, S. Perez-Vega, and D. R. Sepulveda. 2019. Water activity, not moisture content, explains the influence of water on powder flowability. *LWT* 100:35–39.
5. Juarez-Enriquez, E., G. I. Olivas, P. B. Zamudio-Flores, E. Ortega-Rivas, S. Perez-Vega, and D. R. Sepulveda. 2017. Effect of water content on the flowability of hygroscopic powders. *J. Food Eng.* 205:12–17.
6. Lau, S. K., F. A. Ribeiro, J. Subbiah, and C. R. Calkins. 2019. Agenator: An open source computer-controlled dry aging system for beef. *HardwareX* 6:e00086.
7. Oberloier, S., and J. M. Pearce. 2018. General Design Procedure for Free and Open-Source Hardware for Scientific Equipment. *Designs* 2:2.

8. Paasi, J., S. Nurmi, R. Vuorinen, S. Strengell, and P. Maijala. 2001. Performance of ESD protective materials at low relative humidity. *J. Electrost.* 51–52:429–434.
9. Pearce, J. M. 2012. Building Research Equipment with Free, Open-Source Hardware. *Science* 337:1303–1304.
10. Pearce, J. M. 2014. Chapter 4 - Open-Source Microcontrollers for Science: How to Use, Design Automated Equipment With and Troubleshoot, p. 59–93. *In* J.M. Pearce (ed.), Open-Source Lab. Elsevier, Boston.
11. Sensirion. 2018. Datasheet SHT 85 Humidity and Temperature Sensor.
12. Singh, R. P., and D. R. Heldman. 2008. Introduction to Food Engineering, Fourth Edition, 4th ed. Academic Press, Amsterdam ; Boston.
13. Smith, D. F., and B. P. Marks. 2015. Effect of Rapid Product Desiccation or Hydration on Thermal Resistance of *Salmonella enterica* Serovar Enteritidis PT 30 in Wheat Flour. *J. Food Prot.* 78:281–286.
14. Sperber, W. H. 1983. Influence of Water Activity on Foodborne Bacteria — A Review. *J. Food Prot.* 46:142–150.
15. Syamaladevi, R. M., J. Tang, R. Villa-Rojas, S. Sablani, B. Carter, and G. Campbell. 2016. Influence of Water Activity on Thermal Resistance of Microorganisms in Low-Moisture Foods: A Review. *Compr. Rev. Food Sci. Food Saf.* 15:353–370.

Table 3.1. Design files for the HumidOSH.

Design file name	File type	Open source license	Location of the file
Printed circuit board design files	Electronics	GNU General Public License (GPL) 3.0	https://dx.doi.org/10.17605/OSF.IO/579FQ
Laser cutting files for control box	CAD	GNU General Public License (GPL) 3.0	https://dx.doi.org/10.17605/OSF.IO/QG5F6
Arduino code	Software	GNU General Public License (GPL) 3.0	https://dx.doi.org/10.17605/OSF.IO/M8WEK
Computer program	Software	GNU General Public License (GPL) 3.0	https://dx.doi.org/10.17605/OSF.IO/DGMQS

Table 3.2. Bill of materials for components of the control box printed circuit board.

Designator	Component	Quantity	Cost per unit (USD)	Total cost (USD)	Source of materials
PCB	Printed circuit boards (Pack of 10)	0.1	$5.00	$0.50	Send PCB design files from **Table 3.1** to a PCB manufacturer (e.g. https://jlcpcb.com/)
C1 C2 C3 C6	Unpolarized capacitor, 0.1 µF, 0603	4	0.0352	$0.14	https://www.arrow.com/en/products/cl10b104kb8nnnc/samsung-electro-mechanics
C4 C5 C7	Unpolarized capacitor, 10 µF, 0603	3	0.456	$1.37	https://www.arrow.com/en/products/grm188r61c106ma73d/murata-manufacturing
D1 D2 D3	Schottky Diode, 30V, 1A	3	0.3	$0.90	https://www.arrow.com/en/products/pmeg3010egwx/nexperia
J6	RJ-45 jack, R/A	1	0.7402	$0.74	https://www.arrow.com/en/products/rjhse5080/amphenol
J12	Female header, 15 positions, 2.54 mm pitch	2	1.38	$2.76	https://www.digikey.com/products/en?keywords=SAM1213-15-ND
J7	Mini-DIN 6 Receptacle, R/A	1	1.73	$1.73	https://www.arrow.com/en/products/md-60sm/cui-inc
J11	DC barrel jack, 2.1 x 5.5 mm	1	0.5276	$0.53	https://www.arrow.com/en/products/pj-102a/cui-inc
J9 J10	Header, R/A, 2 positions, white	2	0.4654	$0.93	https://www.arrow.com/en/products/0039301020/molex
J8	Header, R/A, 2 positions, black	1	0.59	$0.59	https://www.digikey.com/products/en?keywords=50-36-2457

J4	Shrouded header, straight, 4 positions	1	0.8204	$0.82	https://www.arrow.com/en/products/5-103908-3/te-connectivity
J5	Shrouded header, straight, 9 positions	1	2.26	$2.26	https://www.digikey.com/product-detail/en/te-connectivity-amp-connectors/5-103908-8/A33905-ND/1122468
J1 J14	Shrouded header, 2 positions	2	0.45	$0.90	https://www.arrow.com/en/products/292207-2/te-connectivity
J2 J3	Shrouded header, 4 positions	2	1.1	$2.20	https://www.arrow.com/en/products/292207-4/te-connectivity
J13	DC barrel jack, 1.35 x 3.5 mm	1	0.76	$0.76	https://www.arrow.com/en/products/pj-007/cui-inc
Q1 Q2 Q3 Q4 Q5 Q6	MOSFET, N-channel, 30 V, 3.4 A	6	0.399	$2.39	https://www.arrow.com/en/products/irlml6346trpbf/infineon-technologies-ag
R5 R8	Resistor, 120 Ω, 0.1%, 0603	2	0.3515	$0.70	https://www.arrow.com/en/products/rt0603brd07120rl/yageo
R4 R6 R7 R9 R10 R15 R17 R19	Resistor, 604 Ω, 0603	8	0.0017	$0.01	https://www.arrow.com/en/products/rc0603fr-07604rl/yageo
R1 R2 R22 R23	Resistor, 1.5 kΩ, 0603	4	0.0013	$0.01	https://www.arrow.com/en/products/rc0603jr-071k5l/yageo
R20 R21	Resistor, 2.2 kΩ, 0603	2	0.0017	$0.00	https://www.arrow.com/en/products/rc0603fr-132k2l/yageo
R11 R14 R16 R18	Resistor, 5.1 kΩ, 0603	4	0.0017	$0.01	https://www.arrow.com/en/products/rc0603fr-075k1l/yageo
R12 R13	Resistor, 10 kΩ, 0603	2	0.0018	$0.00	https://www.arrow.com/en/products/rc0603fr-0710kl/yageo

R3	Resistor, 3.3 MΩ, 0603	1	0.0017	$0.00	https://www.arrow.com/en/products/rc0603fr-073m3l/yageo
U2	PWM Fan Controller	1	0.9195	$0.92	https://www.arrow.com/en/products/emc2301-1-aczl-tr/microchip-technology
U3	Linear Regulator, 5 V to 3.3 V, 1A	1	0.5197	$0.52	https://www.arrow.com/en/products/mc7805bdtg/on-semiconductor
U1	I2C Buffer	1	2.802	$2.80	https://www.arrow.com/en/products/pca9615dpj/nxp-semiconductors

Table 3.3. Bill of materials for components of the relative humidity sensor printed circuit board.

Designator	Component	Quantity	Cost per unit (USD)	Total cost (USD)	Source of materials
PCB	Printed circuit boards (Pack of 10)	0.1	$5.00	$0.50	Send PCB design files from **Table 3.1** to a PCB manufacturer (e.g. https://jlcpcb.com/)
C1 C2	Unpolarized capacitor, 0.1 uF, 0603	2	0.0352	$0.07	https://www.arrow.com/en/products/cl10b104kb8nnnc/samsung-electro-mechanics
J1	RJ-45 jack, straight	1	0.7517	$0.75	https://www.arrow.com/en/products/0955032881/molex
R2 R3	Resistor, 1.5 kohm, 0603	2	0.0013	$0.00	https://www.arrow.com/en/products/rc0603jr-071k5l/yageo
R4 R5	Resistor, 120 ohm, 0.1%, 0603	2	0.3515	$0.70	https://www.arrow.com/en/products/rt0603brd07120rl/yageo
R1	Resistor, 3.3 Mohm, 0603	1	0.0017	$0.00	https://www.arrow.com/en/products/rc0603fr-073m3l/yageo
U1	I2C Buffer	1	2.802	$2.80	https://www.arrow.com/en/products/pca9615dpj/nxp-semiconductors
J2	Female header, 4 positions, 2.54 mm pitch	1	1.38	$1.38	https://www.digikey.com/product-detail/en/SSW-115-01-T-S/SAM1213-15-ND/1112290

Table 3.4. Bill of materials for physical components of the HumidOSH.

Designator	Component	Quantity	Cost per unit (USD)	Total cost (USD)	Source of materials
L.L1	12V LED Strip Light, SMD 2835, 16.4ft	0.13	$7.99	$1.06	https://www.amazon.com/gp/product/B00HSF65MC/
L.L2	LED Strip to DC Female Plug Connector (Pack of 10)	0.1	$9.99	$1.00	https://www.amazon.com/gp/product/B01DM7F8O0/
L1	Clear epoxy resin mix, 1 gal kit	0.2	$62.97	$12.59	https://www.amazon.com/gp/product/B01LYK2NAG/
L2	Silicone seal with adhesive backing, red, 10 ft	0.8	$20.50	$16.40	https://www.mcmaster.com/1129a994-1129A94
L3	Draw latch, 2-5/16" Long x 15/16" Wide (pack of 10)	1	$10.57	$10.57	https://www.mcmaster.com/1590a13
L4	Truss Screws, #5-40, 1/4" long (pack of 100)	0.2	$6.12	$1.22	https://www.mcmaster.com/91770A124
L5	Locknuts, #5-40 (pack of 100)	0.2	$5.54	$1.11	https://www.mcmaster.com/90633a006
L6	Cable ties, 0.09" width, 0.04" thick, 3" long (pack of 100)	0.01	$5.52	$0.06	https://www.mcmaster.com/7130K101
L7	Cable tie mount (pack of 50)	0.02	$10.01	$0.20	https://www.mcmaster.com/7566k62
C1	Storage Box, 132 qt	1	$38.99	$38.99	https://www.irisusainc.com/clear-box-with-buckles-132-qt-cb-130-clear
C2	Duct Flange, Galvanized Steel, Size 5	2	$9.22	$18.44	https://www.mcmaster.com/1758K14
C3	Truss Screws, 1/4"-20, 5/8" long (pack of 100)	0.14	$8.17	$1.14	https://www.mcmaster.com/90271A539
C4	Flat washers, 1/4" (pack of 100)	0.14	$3.37	$0.47	https://www.mcmaster.com/92141A029
C5	Locknuts, 1/4"-20 (pack of 100)	0.14	$4.39	$0.61	https://www.mcmaster.com/95615A120
C6	Deck Plate Kit, 6"	1	$15.98	$15.98	https://www.amazon.com/gp/product/B011J5JJ60/
C7, A4	Truss Screws, #10-24, 1/2" long (pack of 100)	0.1	$5.22	$0.52	https://www.mcmaster.com/90272A242
C8, A3	Flat Washers, #10 (pack of 100)	0.2	$2.33	$0.47	https://www.mcmaster.com/92141a011
C9, A7	Locknuts, #10-24 (pack of 100)	0.1	$3.31	$0.33	https://www.mcmaster.com/90631A011
C10	Unthreaded spacers, 3/8" OD, 7/8" Long, for	0.2	$12.59	$2.52	https://www.mcmaster.com/94639A410

	Number 6 Screw Size (pack of 100)				
C11	Locknuts, #6-32 (pack of 100)	0.2	$2.91	$0.58	https://www.mcmaster.com/90633A007
C12	Truss Screws, #6-32, 1-1/4" long (pack of 100)	0.2	$7.56	$1.51	https://www.mcmaster.com/91770A155
C13, T.F5	Flat Washers, #6 (pack of 100)	0.22	$1.17	$0.26	https://www.mcmaster.com/92141a008
C14	Cable Gland - Waterproof RJ-45	1	$9.94	$9.94	https://www.arrow.com/en/products/827/adafruit-industries
C15	RJ 45 cable, 1 ft Long (pack of 10)	0.1	$15.99	$1.60	https://www.amazon.com/gp/product/B00K2E4X2U/
C16	Mini DIN-6 bulkhead connector, female-female	1	$5.23	$5.23	https://www.wallcoinc.com/Calrad_35_498_BH_6_Bulk_Head_Chrome_plated_6_Pin_p/wal22-35-498-bh-6.htm
C17	Mini DIN-6 cable, male-male, 2 m	1	$3.23	$3.23	https://www.arrow.com/en/products/ak678-2/assmann-wsw-components-inc
C18	Hose Barb Thru-Panel Elbow Adapter, 1/4" x 1/4", natural nylon	3	$2.45	$7.35	https://www.kempcospec.com/ProductDetails.asp?ProductCode=KITPL4-4-4NN
C19	Submersible Cord Grip, 0.18"-0.39" Cord OD, M16 Knockout Size	1	$4.03	$4.03	https://www.mcmaster.com/7310K32
C20	Extension cord, 10 ft, 0.38" OD	1	$16.94	$16.94	https://www.mcmaster.com/5776K24
C21	Plug, NEMA 5-15	1	$7.80	$7.80	https://www.mcmaster.com/7216K51
C22	Submersible Cord Grip, 0.14"-0.32" Cord OD, PG-9 Knockout Size	1	$3.33	$3.33	https://www.mcmaster.com/7310K12
C.L1	DC Power Pigtail Cable, 2.1mm x 5.5mm Barrel Plug, 50 cm long (pack of 10)	0.1	$7.99	$0.80	https://www.amazon.com/gp/product/B01GPL8MVG/
C.L2	Power Barrel Connector Plug 1.35mm ID, 3.50mm OD	1	$1.14	$1.14	https://www.arrow.com/en/products/pp3-002d/cui-inc
A1	Triple Bracket for Standard 10” Canisters (U Style)	1	$9.99	$9.99	https://www.bulkreefsupply.com/triple-bracket-for-standard-10-ro-canisters-u-style-bulk-reef-supply.html
A2	Truss Screws, #10-24, 3/4" long (pack of 100)	0.1	$4.44	$0.44	https://www.mcmaster.com/90271A245
A5	12 VDC vacuum diaphragm pump	1	$10.24	$10.24	https://www.ebay.com/itm/DC12V-65-120kpa-5L-min-Micro-Vacuum-Pump-Negative-Pressure-Suction-Pump-Holder/322354285216
A6	Rubber Washers, #10 (pack of 100)	0.06	$10.33	$0.62	https://www.mcmaster.com/90133A017

A8	Zinc-Plated Steel Corner Bracket, 2" x 2" x 5/8"	2	$0.92	$1.84	https://www.mcmaster.com/1556a54
A9	Screws, #8-32, 3/8" long (pack of 100)	0.06	$3.44	$0.21	https://www.mcmaster.com/90275A192
A10	Flat Washers, #8 (pack of 100)	0.06	$2.00	$0.12	https://www.mcmaster.com/92141A009
A11	Locknuts, #8-32 (pack of 100)	0.06	$3.16	$0.19	https://www.mcmaster.com/90631A009
A12	Power Supply, 12V DC 2A, 5.5mm - 2.1mm (Pack of 5)	0.2	$34.99	$7.00	https://www.amazon.com/dp/B07HNR28KK/
A13	Tube Clamps, 1/4" to 5/16" ID (pack of 20)	0.1	$9.68	$0.97	https://www.mcmaster.com/9579K62
A.C1	10" Reverse Osmosis Canister 1⁄4" Ports	2	$16.99	$33.98	https://www.bulkreefsupply.com/reverse-osmosis-canisters.html
A.C2	10" BRS Reactor Refillable Cartridge - Hard Shell	2	$9.99	$19.98	https://www.bulkreefsupply.com/10-brs-reactor-refillable-cartridge-hard-shell.html
A.C3, A.S2	Elbow Adapter, 1/4" Tube ID x 1/4" NPT	0.8	$9.58	$7.66	https://www.mcmaster.com/5463K489
A.S1	Solenoid Valve, 12 VDC, 1/4" NPT, N/C	2	$11.99	$23.98	https://www.ebay.com/itm/1-4-NPT-12V-DC-Electric-Solenoid-Valve-12-Volt-DC-NC-RO-Air-Water-BBTF/290723310425?hash=item43b075ab59:g:bpcAAOSwx2VZgfdz
A.S3, A.P3	Plug contacts, 22-28 AWG, crimp	6	$0.08	$0.48	https://www.arrow.com/en/products/0039000046/molex
A.S4	Plug, 2 positions	2	$0.31	$0.62	https://www.arrow.com/en/products/0039012020/molex
A.P1	2 Conductor Wire, 50' Long	0.01	$9.95	$0.10	https://www.amazon.com/gp/product/B01CSWPJRG/
A.P2	Insulated Quick-Disconnect Terminals, Single Crimp Female, 22-18 Gauge, 0.187" Wide x 0.02" Thick Tab (Pack of 100)	0.02	$15.62	$0.31	https://www.mcmaster.com/7060K15
A.P4	Plug, 2 positions, black	1	$0.33	$0.33	https://www.digikey.com/products/en?keywords=39-01-3025
A.T1	PVC Clear Tubing, 1/4" ID, 3/8" OD (sold in ft)	4	$0.28	$1.12	https://www.mcmaster.com/5233k56
A.T2	Wye, 1/4" Tube ID	0.1	$17.50	$1.75	https://www.mcmaster.com/5463k723
A.T3	Check Valve, 1/4" ID, Polypropylene	2	$0.75	$1.50	https://www.usplastic.com/catalog/item.aspx?itemid=32233
A.T4	HEPA Air Filter (1/4" In-line)	2	$3.99	$7.98	https://www.austinhomebrew.com/HEPA-Air-Filter-14-In-line_p_4588.html

A.B1	Plastic case, 8.5" x 5.1" x 2" (pack of 10)	0.1	$16.99	$1.70	https://www.amazon.com/IRIS-Medium-Modular-Supply-Case/dp/B00FZVPWTI
A.B2	Threaded Hex Standoff, Nylon, #6-32, 1/4" Hex Size, 1/4" Long	8	$0.28	$2.24	https://www.mcmaster.com/92745a340
A.B3	Nylon Hex Nut, #6-32 (Pack of 100)	0.04	$6.37	$0.25	https://www.mcmaster.com/94812a300
A.B4	Arduino Nano V3.0 with USB cable	0.33	$12.35	$4.12	https://www.amazon.com/WYPH-ATmega328P-Microcontroller-Development-Pre-soldered/dp/B07KC9C6H5/
A.B5	Push Button, Black, N/O, SPST, Momentary Contact, Panel Mount	1	$1.07	$1.07	https://www.arrow.com/en/products/1505/adafruit-industries
A.B6	Switch, Rocker, SPST, 10A, 125V	1	$1.02	$1.02	https://www.arrow.com/en/products/srb22a2dbbnn/zf-electronics
A.B7	Cable assembly, 2 positions	2	$0.53	$1.05	https://www.arrow.com/en/products/2058943-1/te-connectivity
A.B8	Push Button, Green, Illuminated, N/O, SPST, Momentary Contact, Panel Mount	1	$1.72	$1.72	https://www.arrow.com/en/products/1440/adafruit-industries
A.B9	Push Button, Blue, Illuminated, N/O, SPST, Momentary Contact, Panel Mount	1	$1.95	$1.95	https://www.arrow.com/en/products/1477/adafruit-industries
A.B10	Cable assembly, 4 positions	2	$1.10	$2.20	https://www.arrow.com/en/products/2058943-3/te-connectivity
A.B11	20x4 LCD, Black on RGB, 3.3V	1	$25.00	$25.00	https://www.digikey.com/products/en?keywords=LCD-14074
A.B12	Shrouded header, straight, 4 positions	1	$0.82	$0.82	https://www.arrow.com/en/products/5-103908-3/te-connectivity
A.B13	Flat Flex Cable Assembly, 4 Position, 8.00" Long	1	$4.34	$4.34	https://www.digikey.com/product-detail/en/A9CCG-0408F/A9CCG-0408F-ND/470254/?itemSeq=299521541
A.B14	Keypad, 12 Button	1	$3.95	$3.95	https://www.arrow.com/en/products/com-14662/sparkfun-electronics
A.B15	Shrouded header, straight, 9 positions	1	$1.92	$1.92	https://www.digikey.com/product-detail/en/te-connectivity-amp-connectors/5-103635-8/A33875-ND/1122439
A.B16	Flat Flex Cable Assembly, 9 Position, 8.00" Long	1	$5.39	$5.39	https://www.digikey.com/product-detail/en/te-connectivity-amp-connectors/A9CCG-0908F/A9CCG-0908F-ND/470278

A.B17	Screws, #2-56, 1/4" long (pack of 100)	0.08	$4.75	$0.38	https://www.mcmaster.com/90272A081
A.B18	Flat Washers, #2 (pack of 100)	0.16	$1.40	$0.22	https://www.mcmaster.com/92141A003
A.B19	Unthreaded spacers, 3/16" OD, 3/16" Long, for Number 2 Screw Size (pack of 100)	0.04	$9.24	$0.37	https://www.mcmaster.com/94639a703
A.B20	Locknuts, #2-56 (pack of 100)	0.08	$3.51	$0.28	https://www.mcmaster.com/90631A003
G1	Nitrile gloves, large	1	$9.95	$9.95	https://www.grainger.com/product/SHOWA-Chemical-Resistant-Glove-4JF22
G2	Push Fit Glove System	1	$13.95	$13.95	https://www.feldfire.com/Lakeland-Push-Fit-Glove-System_p_7777.html
G3	Nitrile cleanroom gloves, medium	1	$3.18	$3.18	https://www.mcmaster.com/5221T6
G4	Quick-release Clamps, 2" to 6" ID (pack of 10)	0.2	$15.41	$3.08	https://www.mcmaster.com/5322K22
T1	Tray rack	1	$75.27	$75.27	https://www.supplyclinic.com/items/multi-mod-rack-6-place-zirc-21z105
T2	Aluminum Quarter Sheet Pan	1	$3.29	$3.29	https://www.webstaurantstore.com/bakers-mark-quarter-size-19-gauge-wire-in-rim-aluminum-bun-sheet-pan-13-x-9-1-2/407BUNQRTR.html
T3	Boss Head Clamp	1	$7.50	$7.50	https://www.fishersci.com/shop/products/premium-boss-head/s13919
T4	RJ 45 cable, 3 ft Long (pack of 10)	0.1	$17.99	$1.80	https://www.amazon.com/gp/product/B00K2E4QZE/
T.F1	Fan, 12 VDC	1	$10.88	$10.88	https://www.arrow.com/en/products/9ga0512p7g001/sanyo-denki
T.F2	Mini DIN-6 plug	1	$1.45	$1.45	https://www.arrow.com/en/products/md-60/cui-inc
T.F3	Screws, #6-32, 3" long (pack of 100)	0.01	$7.43	$0.07	https://www.mcmaster.com/90276A163
T.F4	Locknuts, #6-32 (pack of 100)	0.01	$2.72	$0.03	https://www.mcmaster.com/90631A007
T.F6	Heat-Shrink Tubing, 25' Long, 0.06" ID Before Shrinking	0.02	$10.68	$0.21	https://www.mcmaster.com/7856K716
T.F7	Heat-Shrink Tubing, 4' Long, 0.25" ID Before Shrinking	0.06	$3.09	$0.19	https://www.mcmaster.com/7856k45
T.R1	Relative humidity and temperature sensor	1	29.22	$29.22	https://www.digikey.com/products/en?keywords=sht85

T.R2	Female header, 4 positions, R/A, 2.54 mm pitch	1	0.73	$0.73	https://www.digikey.com/product-detail/en/851-87-004-20-001101/1212-1347-ND/3757597

Table 3.5. Bill of materials for consumables used during the construction and operation of the HumidOSH.

Designator	Component	Cost per unit (USD)	Source of materials
X1	Talc powder	$7.29	https://www.amazon.com/gp/product/B005U4A9KW/
X2	Silicone sealant	$17.23	https://www.mcmaster.com/74955A54
X3	Non-indicating Silica Gel Beads, 2-4 mm diameter, 55 lb drum	$99.40	https://www.impakcorporation.com/desiccants/bulk_desiccant/639AG55
X4	Indicating Silica Gel Beads, 2-4 mm diameter, 5 lb can	$28.50	https://www.impakcorporation.com/desiccants/bulk_desiccant/640SGO05
X5	Water beads	$6.99	https://www.amazon.com/gp/product/B06XZNMMKC/

Table 3.6. Bill of materials for specialized tools used during the construction of the HumidOSH.

Designator	Component	Cost per unit (USD)	Source of materials
Z1	Crimping tool	$22.99	https://www.amazon.com/gp/product/B00YGLKBSK/
Z2	Drill bit set for plastic	$64.72	https://www.mcmaster.com/27465A94
Z3	Tap, 10-24 Thread Size	$5.22	https://www.mcmaster.com/2522A739
Z4	Tap wrench	$7.65	https://www.mcmaster.com/25605a63
Z5	2"-12" Round Hole Cutter	$26.69	https://www.menards.com/main/heating-cooling/ductwork/ductwork-tools-installation/masterforce-reg-2-12-round-hole-cutter/thht-1448/p-1488180037069-c-6833.htm

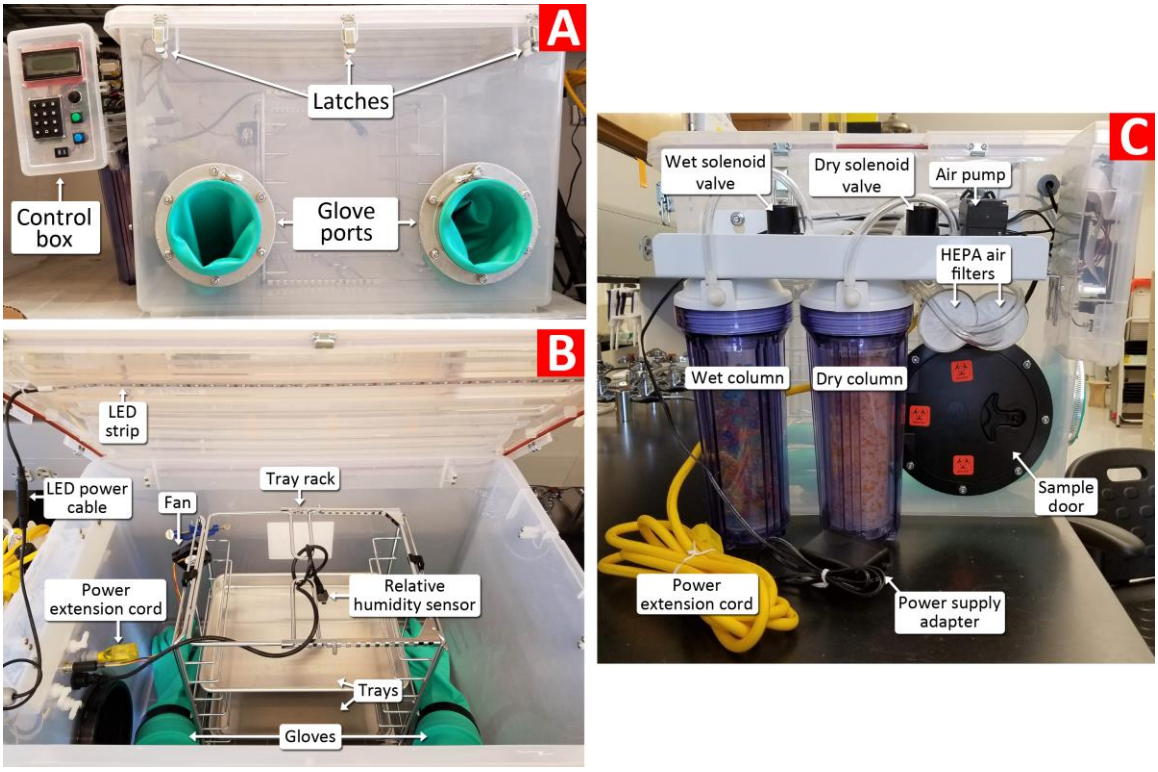

Figure 3.1. Annotated views of the HumidOSH from the (A) front, (B) inside, and (C) left side.

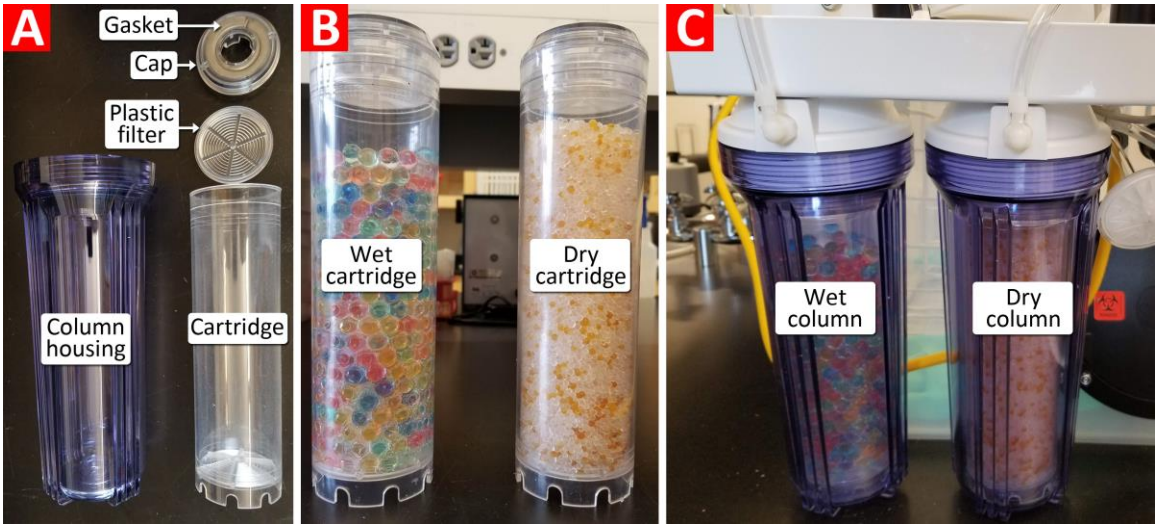

Figure 3.2. Steps for preparing the wet and dry columns: (A) Anatomy of a wet/dry column, (B) filled wet and dry columns, and (C) installed wet and dry columns.

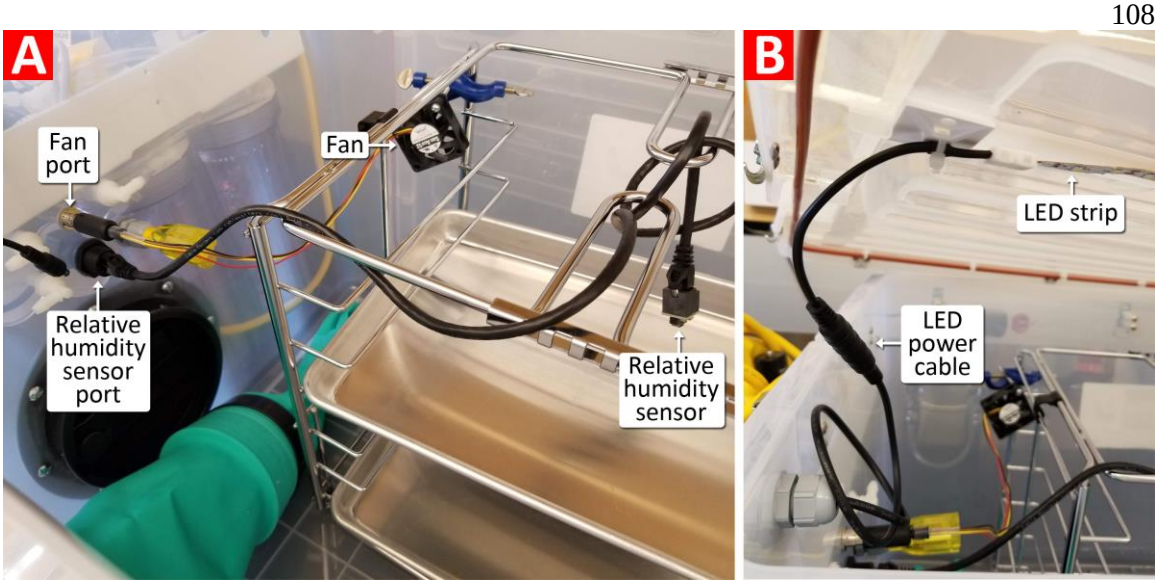

Figure 3.3. Preparing the parts inside the HumidOSH for operation: (A) Placing the tray rack inside the chamber and plugging the relative humidity sensor and fan into their respective ports on the wall, and (B) connecting power to the ceiling LED strip.

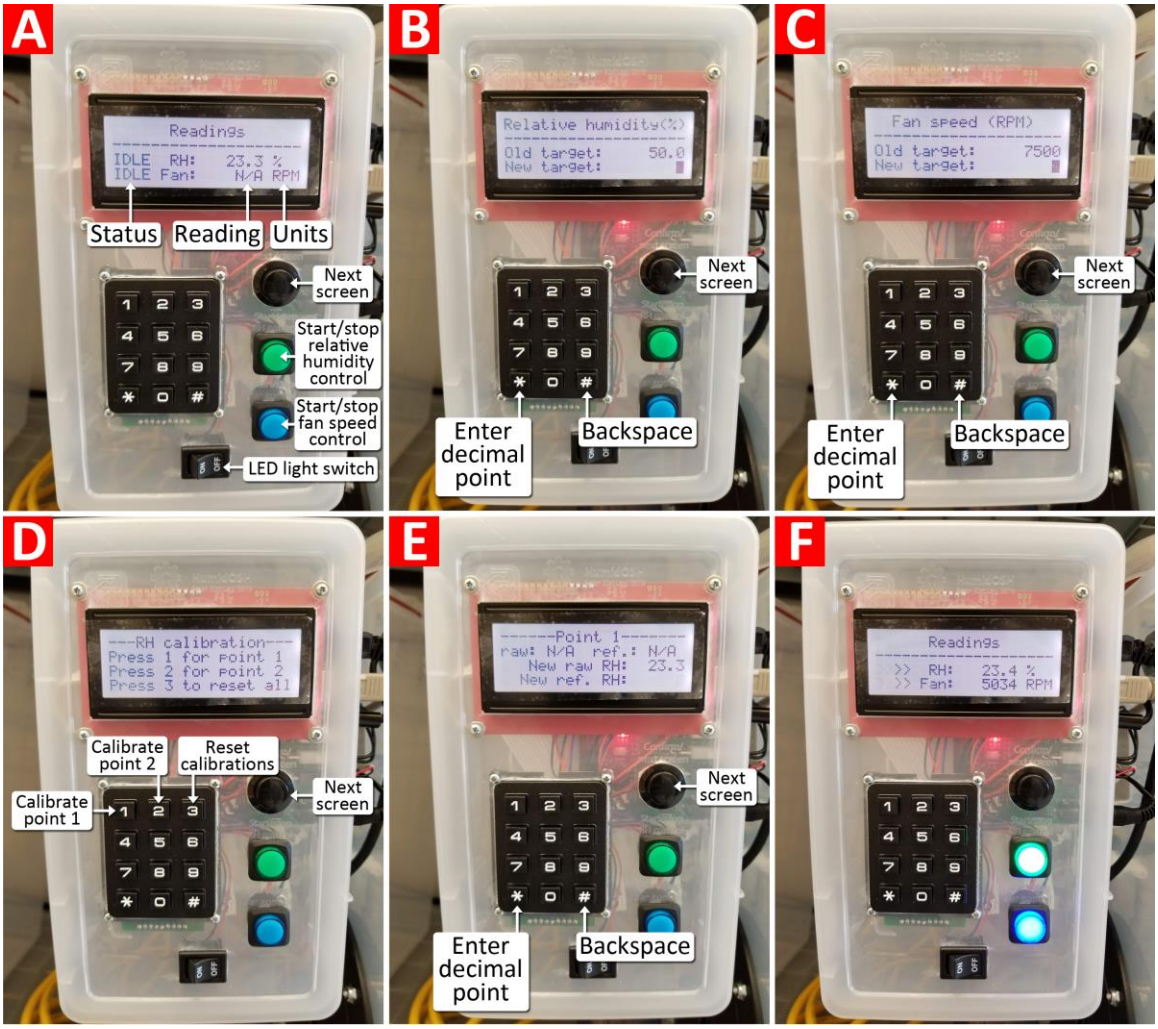

Figure 3.4. Annotated views of the menu screens displayed by the control box and the relevant buttons for each screen: (A) Readings screen without any environmental controls active, (B) adjustment of the target relative humidity, (C) adjustment of the target fan rotational speed, (D) two-point calibration menu for the relative humidity sensor, (E) calibration of point 1 for the relative humidity sensor (point 2 has a similar screen), and (F) readings screen with both environmental controls active.

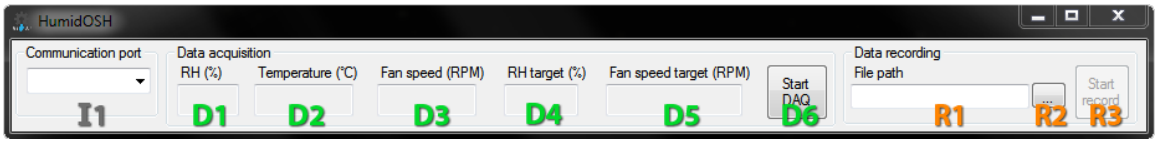

Figure 3.5. Annotated view of the optional computer program.

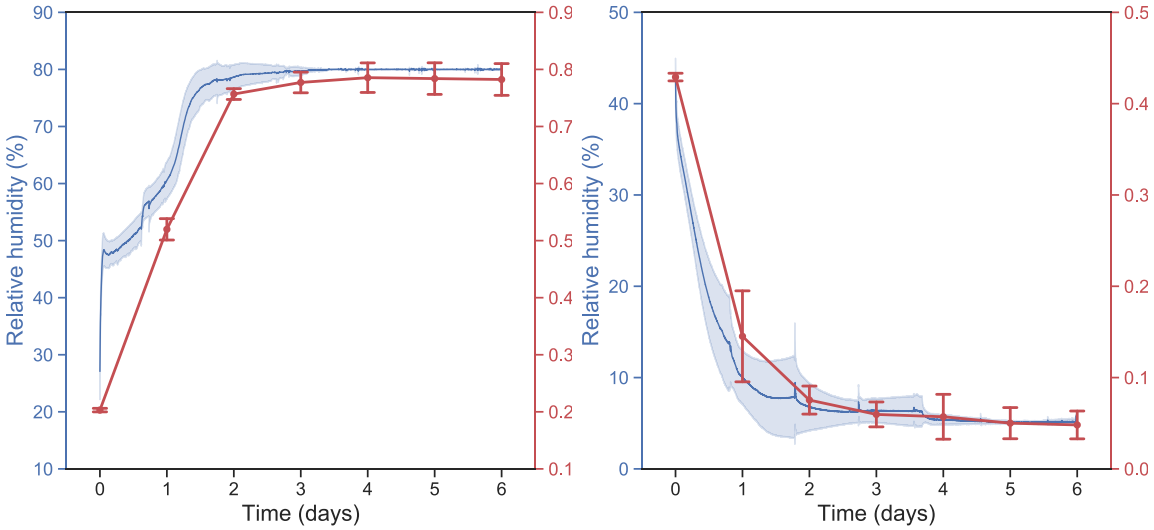

(a) Target relative humidity = 80 % (b) Target relative humidity = 5 %

Figure 3.6. Real-time mean relative humidity readings and daily mean water activity measurements of whole milk powder samples in HumidOSH units operating with target relative humidity of (a) 80 % and (b) 5 %. The shaded envelope of the relative humidity plot and error bars of the water activity plot represent one standard deviation. Linear interpolation is performed between each water activity data point.

Chapter 4: A Comparison of Methods for Determining Thermal Inactivation Kinetics: A Case Study on *Salmonella* in Whole Milk Powder

4.1. Introduction

The preventive control requirements set forth by the Food Safety Modernization Act in the US has sparked many efforts to characterize the lethality of existing and novel pasteurization and sterilization processes. In the realm of thermal processes, the characterization workflow usually involves subjecting food products inoculated with pathogens of concern to a few isothermal inactivation studies. Subsequently, the collected data is modeled by one or more models for predicting the effectiveness (or ineffectiveness) of thermal processes.

Considering that food products come in all shapes, forms, and sizes, it is of no surprise then that there exists a wealth of methodologies for performing isothermal inactivation studies. Traditionally, isothermal inactivation studies are performed with the use of a water or oil bath to maintain isothermal conditions. Before soaking the inoculated food samples into the bath, they are first packaged in a variety of vessels such as thin capillary tubes (*2*, *40*, *50*, *52*, *55*), test tubes (*1*, *7*, *27*, *57*), small vials (*23*, *44*), bags or pouches (*13*, *21*, *26*, *33*, *35*, *36*, *37*, *47*), reusable vessels such as the thermal death time (TDT) disk (*6*, *21*, *22*, *25*, *53*, *54*), or, if the food itself has a natural physical barrier, without any packaging (*45*). Although the water or oil bath is sufficient for most isothermal inactivation studies, it comes with its own issues and limitations such as liquid

spillage and lack of control over heating rate. As such, a few custom equipment have been developed as more efficient or flexible alternatives such as the thermoresistometer (*8*, *9*, *10*, *20*, *42*, *48*), the BUGDEATH apparatus (*14*, *15*, *17*, *31*, *32*, *38*), a custom heating block system (*3*, *4*, *29*, *65*, *66*), and the TDT Sandwich.

The abundance of methodologies for isothermal inactivation studies provide researchers with more flexibility but also comes with a price—increased experimental noise. The noise could originate from various sources such as differences in heat transfer characteristics due to the material or size of the vessels (*1*, *7*) or variations in experimental methodologies (*21*). The consequences of such experimental noises are wide-ranging. Hildebrandt et al. (*21*) conducted a cross-laboratory thermal inactivation study with mostly similar methodologies between two laboratories and noted that despite having very similar methodologies, the combined uncertainty from various sources such as the definition of come-up time, model regression procedure, and type of vessel still contributed to observable differences in thermal resistance values and model parameters. The use of test tubes for determining thermal resistance of *Listeria monocytogenes* in milk was shown to result in extraordinarily high thermal resistance values which was presumed to be due to splashing and condensation on the cap of the tube that was cooler than the submerged glass tube (*12*). The choice of methodologies for performing isothermal inactivation studies must thus not only focus on the microbiological aspects of the study, but also consider engineering issues such heat transfer physics.

When developing a new methodology or system for determining thermal inactivation kinetics, the aforementioned issues should be addressed via a comparison

study with existing methods to ensure consistency in results. The TDT Sandwich in **Chapter 2** was developed to be a more efficient alternative to traditional methods but has yet to be compared thoroughly to existing methods. Therefore, the objective of this study was to compare three thermal treatment methods (TDT disks in water bath, pouches in water bath, and TDT Sandwich) on the thermal inactivation kinetics of *Salmonella* in whole milk powder (WMP), fitted to both the log-linear and Weibull models.

4.2. Materials and Methods

4.2.1. Inoculum

The *Salmonella* strains along with the inoculum preparation procedure used in this study follow those described by Verma et al. and Wei et al. (*59*, *62*). In summary, *Salmonella enterica* serovars Agona 447967, Mbandaka 698538, Montevideo 488275, Reading Moff 180418, and Tennessee K4643 were grown in tryptic soy broth (211825, Becton, Dickinson and Company, Sparks, MD) supplemented with 0.6 % (w/w) yeast extract (212720, Becton, Dickinson and Company, Sparks, MD) at 37 °C for 24 ± 2 hr, transferred to tryptic soy agar (236920, Becton, Dickinson and Company, Franklin Lakes, NJ) supplemented with 0.6 % (w/w) yeast extract (212720, Becton, Dickinson and Company, Sparks, MD) and incubated overnight at 37 °C for 24 ± 2 hr to produce lawns, harvested with 3 mL of 0.1 % (w/w) buffered peptone water (218103, Becton, Dickinson and Company, Sparks, MD), and finally mixed in equal proportions to produce a *Salmonella* cocktail. All prepared inoculum contained ca. 10.5 $\log_{10}$ (CFU/mL) and were used to inoculate samples within 2 hours of preparation.

4.2.2. Inoculation

Every step in the inoculation procedure was performed in a biosafety cabinet. Three production lots of Grade A pasteurized WMP (28.5% milkfat, Land O'Lakes, Inc., St. Paul, MN) with background microflora of less than 100 CFU/g were used in this study. For each production lot, 400 ± 0.1 g samples were obtained and divided into two 200 g batches in resealable 1-gallon plastic bags. A 10 mL aliquot of the previously prepared *Salmonella* cocktail inoculum was transferred to a sterile 15 mL centrifuge tube (339650, Thermo Fisher Scientific, Rochester, NY), closed, and vortexed for 30 s. Subsequently, the cap of the centrifuge tube was removed and replaced with a finger-operated spray head (ps20-410-natural, Midwest Bottles LLC, Garrison, KY). The custom spray device was then inserted into one of the 1-gallon bag containing WMP and the sample was spray-inoculated. The spray-inoculation was repeated with another 10 mL of inoculum for a final concentration of 20 g of inoculum per 200 g of WMP. The contents were then mixed by hand for 5 min to manually detach and reincorporate clumps that were stuck to the inner lining of the bags. Subsequently, the contents were transferred into another plastic sample bag (B01195, Nasco, Fort Atkinson, WI) which was sealed using the built-in foldable tabs. The bag was then placed in a paddle mixer (9000471, Neutec Group Inc, Farmingdale, NY) and mixed for 15 minutes. The inoculation procedure was repeated for the other 1-gallon bag of WMP to obtain a final total mass of 400 g of WMP inoculated at a 1:10 mass ratio. The inoculated samples were divided between two sterile aluminum trays and placed into HumidOSH (**Chapter 3**) units set to a target relative humidity of 20 % and target fan rotational speed of 5,000

RPM to recondition the inoculated samples back to their native water activity of 0.20 a_w at 25 °C. Based on preliminary homogeneity and stability data of *Salmonella*-inoculated WMP, moisture equilibration of the inoculated samples was performed for a minimum of two days before the samples were used in subsequent experiments within two weeks. All sample packing activities for the isothermal inactivation studies were performed inside the environmental chambers to ensure minimal change in the water activity of the samples during the packing process.

4.2.3. Enumeration of *Salmonella*

The *Salmonella* survivors of the thermal treatments were enumerated by serially diluting samples in 0.1 % (w/w) buffered peptone water at a 1:10 ratio per dilution level and spread plating 100 µL of the appropriate dilution onto mTSA media (*22*, *34*, *62*). The mTSA media consists of tryptic soy agar (236920, Becton, Dickinson and Company, Franklin Lakes, NJ) supplemented with 0.6 % (w/w) yeast extract (212720, Becton, Dickinson and Company, Sparks, MD), 0.05 % (w/w) ammonium iron(III) citrate (F5879-500G, Sigma Aldrich, St. Louis, MO), and 0.03 % (w/w) sodium thiosulfate pentahydrate (S445-500, Fisher Scientific, Fair Lawn, NJ). Inoculated plates were incubated at 37 °C for 24 ± 2 hr. Colonies with black centers were counted as *Salmonella*.

4.2.4. Moisture content and water activity

Before each thermal inactivation study was performed, moisture content and water activity measurements were performed on the inoculated WMP samples. Moisture content measurements were performed with approximately 4 g of samples in duplicates with a halogen moisture analyzer (HG53-P, Mettler Toledo, Greifensee, Switzerland) set

to 105°C and time setting “5”. Water activity of samples at room temperature (25 °C) were measured in duplicates using a water activity meter (4TE, METER Group, Pullman, WA).

4.2.5. Thermal treatment

The WMP samples were subjected to three methods for the isothermal inactivation studies: thermal death time (TDT) disks (*6*, *25*) in water bath, TDT Sandwich, and pouches in water bath. All three methods were performed at target temperatures of 75, 80, and 85 °C. However, since the samples were initially at room temperature, there was a time delay before the samples equilibrated to the target treatment temperature. This time delay is henceforth referred to as come-up time (CUT): the average time taken to reach within 0.5 °C of the target treatment temperature plus twice the standard deviation. For each thermal treatment, the CUT was measured for all three target temperatures before the actual isothermal inactivation studies were performed. The procedures for CUT measurement and isothermal inactivation studies for each thermal treatment method are described in subsequent sections. The time at which CUT was achieved is defined as time zero and signifies the start of the isothermal inactivation experiment. Since the first author was directly involved in the design and development of the TDT Sandwich, the first author’s operational knowledge of the TDT Sandwich may introduce experimental biases. Therefore, the thermal treatments were primarily performed by co-authors who were newly trained on all three thermal treatment methods for both the CUT measurements and isothermal inactivation studies.

4.2.6. TDT disks in water bath

The TDT disk consists of an aluminum screw cap and an aluminum base with a cavity. For each TDT disk, approximately 0.8 g of WMP sample were compacted into the cavity of the base and the cap was screwed on to seal onto the base with an O-ring (9396K104, McMaster-Carr, Elmhurst, IL). CUT measurements were performed with 15 normal TDT disks and three TDT disks with built-in type T thermocouples, all of which were filled with non-inoculated WMP. The TDT disks were hung on six aluminum rods using steel wire with three TDT disks per rod as illustrated in **Fig. 4.1**. Temperature measurements were recorded with a datalogger (USB-TC, Measurement Computing Corporation, Norton, MA) when all 18 TDT disks were submerged into the water bath. The CUT measurements were repeated three times.

For a given treatment temperature and WMP production lot combination in the isothermal inactivation study, a total of 18 TDT disks without thermocouples (six timepoints, three replicates) were filled with approximately 0.8 g of inoculated WMP and submerged simultaneously into a water bath (NESLAB RTE 17, Thermo Fisher Scientific, Newington, NH) pre-heated to the target temperature to begin the thermal treatment. At each timepoint, one aluminum rod was pulled out to get three TDT disks which were immediately cooled in an ice slurry bath for at least one minute before they were enumerated for *Salmonella* survivors. The extra replicate for the TDT disks as compared to the other two methods is to compensate for occasional leaks in a few TDT disks which were discarded and not included in the final data set.

4.2.7. TDT Sandwich

The TDT Sandwich is a clamshell-like device that applies dry heat to samples with two resistive heating elements. Before using the TDT Sandwich, WMP samples were packed into heat-sealable 7.62 cm x 7.62 cm aluminized pouches (03MFW03TN, IMPAK Corporation, Los Angeles, CA) in quantities of approximately 2 g. When using the TDT Sandwich, each sample is treated by a single TDT Sandwich unit that is independent of other TDT Sandwich units. The CUT at each treatment temperature was measured in triplicates with a different TDT Sandwich unit per replicate by inserting a type T thermocouple (5TC-TT-T-40-36, Omega Engineering Inc., Norwalk, CT) to the inside center of a pouch through a hole created with a pushpin at one of the edges of the pouch. The heating rates of the TDT Sandwiches were decreased to 20.0, 17.5, and 17.0 °C/min for treatment temperatures of 75, 80, and 85 °C, respectively, to match the slower CUT of the TDT disks in order to avoid introducing discrepancies in inactivation kinetics due to different heating rates (*1*, *30*, *66*). These heating rates were chosen based on preliminary trials.

For a given treatment temperature and WMP production lot combination in the isothermal inactivation study, a total of 12 pouches without thermocouples (six timepoints, two sub-samples) were prepared. Before each study was performed, the placement of pouches in TDT Sandwich units was randomized with a random list generator. The TDT Sandwiches were operated at heating rates of 20.0, 17.5, and 17.0 °C/min for treatment temperatures of 75, 80, and 85 °C as previously determined from the CUT studies. When the heating timer for a TDT Sandwich had expired, the pouch

inside it was immediately transferred into an ice slurry bath for at least one minute before its contents were enumerated for *Salmonella* survivors.

4.2.8. Pouches in water bath

This treatment is a hybrid of the TDT disk and TDT Sandwich. Samples were packed in similar quantities and pouches as the TDT Sandwich and submerged into the same water bath as the TDT disks. The pouches were attached with paper clips onto custom-built scaffolds made from steel wire (**Fig. 4.2(a)**) and submerged simultaneously into the water bath to begin the CUT measurements or isothermal inactivation studies. Six scaffolds were used to accommodate a total of 12 pouches (six timepoints, two sub-samples) for each temperature-production lot combination in the isothermal inactivation study. During the CUT measurements, pouches with thermocouples were placed at specific locations as shown in **Fig. 4.2(b)**. In order to prevent water leakage during the CUT measurements, the type T thermocouple (5TC-TT-T-40-36, Omega Engineering Inc., Norwalk, CT) was sealed to the open edge of the pouch with adhesive (7628A62, McMaster-Carr, Elmhurst, IL) before applying heat to seal the entire edge. CUT measurements were repeated three times. During the isothermal inactivation experiments, no thermocouples were inserted into the pouches. One wireframe scaffold was pulled out at each timepoint to get two pouches which were immediately cooled in an ice slurry bath for at least one minute before they were enumerated for *Salmonella* survivors.

4.2.9. Thermal inactivation models

The *Salmonella* inactivation data were fitted to primary log-linear or Weibull models with a secondary Bigelow (z-value) model for the effect of temperature (*43*, *58*). The primary log-linear model directly predicts inactivation of *Salmonella* over time:

$$\log_{10}\left(\frac{N}{N_0}\right) = -\frac{t}{D_T} \tag{4.1}$$

where N is the number of survivors at time t (CFU/g), N_0 is the number of survivors at time zero of the thermal treatment *i.e.* immediately after achieving CUT (CFU/g), t is the instantaneous time of the thermal treatment (s), and D_T is the decimal reduction time or D-value at temperature T (s). The secondary Bigelow model for temperature is:

$$\log_{10}\left(\frac{D_T}{D_{ref}}\right) = -\frac{T - T_{ref}}{z} \tag{4.2}$$

where D_{ref} is the D-value at reference temperature T_{ref} (s), T is the instantaneous temperature of the thermal treatment (°C), and z is the z-value (°C). By substituting Equation 4.2 into Equation 4.1, the consolidated log-linear model is thus:

$$\log_{10}\left(\frac{N}{N_0}\right) = -\frac{t}{D_{ref} \cdot 10^{\left(\frac{T_{ref}-T}{z}\right)}} \tag{4.3}$$

The microbial inactivation data will be fitted to this consolidated model, also known as a 1-step regression. The 1-step regression has been shown to better at fitting data and estimating the parameters in comparison to 2-step regression (*21*, *24*). The 2-step regression, in this study, would have involved fitting temperature at each temperature to Equation 4.1 before fitting the individual D_T at each temperature to Equation 4.2.

The corresponding primary, secondary, and consolidated models for the Weibull model are as follows (*58*):

$$\log_{10}\left(\frac{N}{N_0}\right) = -\frac{1}{\ln(10)}\left(\frac{t}{\alpha_T}\right)^{\beta} \tag{4.4}$$

$$\log_{10}\left(\frac{\alpha_T}{\alpha_{ref}}\right) = -\frac{T - T_{ref}}{z} \tag{4.5}$$

$$\log_{10}\left(\frac{N}{N_0}\right) = -\frac{1}{\ln(10)}\left(\frac{t}{\alpha_{ref} \cdot 10^{\left(\frac{T_{ref}-T}{z}\right)}}\right)^{\beta} \tag{4.6}$$

where α_T is the scale factor at temperature T (s), β is the shape factor, and α_{ref} is the scale factor at reference temperature T_{ref} (s). In the context of inactivating microorganisms in food products, α usually has a log-linear dependence on temperature while β remains constant (*58*); the form of Equation 4.5 aims to emulate this. Equation 4.4 is sometimes simplified to the following form:

$$\log_{10}\left(\frac{N}{N_0}\right) = -\left(\frac{t}{\delta_T}\right)^{\beta} \tag{4.7}$$

where $\delta_T = \sqrt[\beta]{\ln(10)} \cdot \alpha_T$. The appeal of this simplified equation is due to its brevity and its similarity to Equation 4.1—both equations are equivalent when $\beta = 1$, at which point the physical meaning of δ_T can be likened to the decimal reduction time, D_T. However, the dependency of δ_T on β could introduce a few complications such as introducing variations from β into that δ_T and interdependency of variables during the curve-fitting process. Therefore, the expanded form (Equation 4.6) is used in all subsequent analyses in this study. A fixed value of 80 °C was assumed for T_{ref} based on the range of

treatment temperatures in this study; D_{ref} and α_{ref} will thus henceforth be written as $D_{80°C}$ and $\alpha_{80°C}$, respectively. The experimental data for each thermal treatment method-lot combination were fitted to Equations 4.4 and 4.6 using the Levenberg–Marquardt algorithm for non-linear least squares regression as implemented in the curve_fit function of the Python SciPy library with a maximum of 200 iterations and convergence tolerance of 10^{-8} (*61*).

4.2.10. Normality of model parameters

In order to evaluate the differences between the three thermal treatment methods, it is desirable to perform statistical tests for significant differences. Most of these tests, however, implicitly assume that the population from which the sample comes from is normally distributed. While most model parameters in the field of biology have been shown to be normally distributed, there have also been cases which strongly suggest a lognormal distribution, thus necessitating a logarithmic transformation of the data before performing the statistical analyses (*5*, *19*). It is thus necessary to verify if the parameters of Equations 4.4 and 4.6 are normally distributed.

The normality of the model parameters were tested by generating the distribution of the parameters through Monte Carlo simulations (*5*). The simulations were performed with both Equations 4.4 and 4.6 as the models. The mean and standard deviation for survivors at each temperature-timepoint combination were calculated across all lots and thermal treatment methods to obtain an array of inputs for the model. The errors for log-transformed survivor values were assume to be normally distributed, which has been shown to be true in other cases (*28*). Random values were then picked from the normal

distributions to obtain 5 replicates of survivors per temperature-timepoint combination. Equations 4.4 and 4.6 were then fitted to the entire dataset as described previously. This process was iterated for 400 times to obtain a distribution of model parameters. The Shapiro-Wilk test is used in combination with measures of skewness, kurtosis, manual evaluation of the mean and median values, and visual inspection of histograms to determine the normality or lognormality of the model parameters. The Shapiro-Wilk test for normality has been shown to be more robust and has higher power under various situations in comparison to other tests such as the Kolmogorov-Smirnov and Anderson-Darling tests (*18*, *46*, *64*). Skewness and kurtosis values that are closer to zero indicate a better fit to the normal distribution (*5*, *19*). The Shapiro-Wilk test, skewness, and kurtosis values were calculated using the Python SciPy library (*61*).

4.2.11. Convergence of model parameters

The Levenberg–Marquardt algorithm used in the curve fitting process aims to find the minimum for the least squares differences, but the algorithm may converge to one of many local minima instead of the global minimum (*41*). This, in turn, could result in abnormal model parameters. In order to verify that the fitted model parameters were not affected by the presence of local minima during the regression process, the regression of both Equations 4.4 and 4.6 for each of the three thermal treatment methods were repeated 10,000 times with random initial guesses for the model parameters. The initial guesses for $D_{80°C}$ and z for the log-linear model were constrained within the ranges of [3, 15) min and [3, 15) °C, respectively, while the initial guesses for $\alpha_{80°C}$, z, and β for the Weibull model were constrained within the ranges of [3, 15) min, [3, 15) °C, and [0.7, 1.3),

respectively. These ranges were chosen based on expected behavior of the inactivation models such as positive values for all the parameters and reasonable expectations of the model parameters based on visual inspection of the experimental data. Any fitting attempts that resulted in zero or negative values were discarded. The curve fitting was performed using the same function, maximum iterations, and convergence tolerance as described previously.

4.2.12. Statistical analysis between methods

The statistical significance of differences between the methods were analyzed using Tukey's honestly significant difference (HSD) test as implemented in the Python statsmodels library to account for family-wise error rates when comparing multiple pairs of data (*51*). Since one of the assumptions of the Tukey HSD test is normal distribution of the samples, the tests were performed only after verification that the model parameters are normally distributed. Tukey HSD was performed on the model parameters for both the log-linear and Weibull models between the three thermal treatment methods.

The CUT of an isothermal inactivation experiment could inactivate a portion of the target microorganism population before isothermal conditions can be achieved. A higher starting population is usually desirable to generate enough datapoints before the lower limit of detection is reached. Therefore, the differences between the *Salmonella* population before thermal treatment, $\log_{10} N_c$ and immediately after CUT, $\log_{10} N_0$ for all three thermal treatment methods were also analyzed with Tukey HSD.

4.2.13. Global models

In addition to fitting the log-linear and Weibull models to each thermal treatment method, both models were also globally fitted across all methods. The suitability of the models were evaluated by calculating their root mean square error (RMSE) and corrected Akaike's Information Criterion (AIC_c). AIC_c is preferred over its uncorrected counterpart for its improved accuracy for small sample sizes (*39*). Lower RMSE and AIC_c values generally indicate that a particular model is a better fit for the data. The relative probability that a model ("model 1") is better than the other ("model 2") can be calculated using the AIC_c values (*39*):

$$Probability = \frac{e^{\left(\frac{AIC_{c,2}-AIC_{c,1}}{2}\right)}}{1+e^{\left(\frac{AIC_{c,2}-AIC_{c,1}}{2}\right)}} \quad (4.8)$$

where $AIC_{c,1}$ and $AIC_{c,2}$ are the AIC_c values for "model 1" and "model 2," respectively.

4.3. Results and Discussion

The raw data generated and analyzed in this study may be downloaded from https://doi.org/10.17605/OSF.IO/JZ63G.

The CUT for WMP using all three thermal treatment methods are shown in **Table 4.1**. It should be noted that the heating rates of the TDT Sandwich were reduced in order to match the CUT of the TDT disks in water bath. Due to these adjustments, the pouches in water bath had the fastest CUT across all temperatures. The variability in the time needed to reach within 0.5 °C of the target temperature for the methods using a water bath were an order of magnitude higher than those of the TDT Sandwich. These variations could be caused by spatial variability of temperature and fluid velocity in the

water bath based on the proximity of the samples to the inlet or outlet of the water pump (**Fig. 4.1** and **4.2**). The small variability of the TDT Sandwich indicate a high degree of consistency among individual TDT Sandwich units.

The normality test results generated by Monte Carlo simulations for the log-linear and Weibull model parameters for the WMP data in this study are summarized in **Table 4.2**. The probability values were calculated using the Shapiro-Wilk test which tests against the null hypothesis that the sample data comes from a normal distribution. Assuming significance at probabilities less than 0.05, $\alpha_{80°C}$ is not distributed normally in the log scale while z for the Weibull model is not normally distributed in the natural scale. As for the other parameters, the lognormal transformation improves the normality of the data as seen by the generally lower skew and kurtosis values. Manual evaluation of the mean and median, however, suggest that all the model parameters are well-approximated by normal distributions, with or without logarithmic transformations. This inference is further supported by the probability density histograms of the model parameters that are very well-approximated by the normal distribution curve (**Fig. 4.3** and **4.4**). The normal and lognormal distribution curves also mostly overlap in all cases. Although the statistical results should not be ignored, visual evaluation of the data overwhelmingly supports a normal distribution, and any deviation from a normal distribution appears to be minimal. This dilemma is in fact due to the "consistency" property of goodness-of-fit tests such as the Shapiro-Wilk test which, if the sample size is large enough, produces statistically significant differences from the normal distribution even though the differences are small (*19*). Therefore, statistical tests for normality

should also be accompanied by manual evaluation of the data (*e.g.* mean and median) and visualization of the data distribution. In the case of the WMP data in this study, further statistical analyses will be performed on the model parameters by considering the model parameters to be normally distributed.

The model parameters for the log-linear model are compared across the three thermal treatment methods in **Table 4.3**. In terms of magnitude, $D_{80°C}$ was highest for the TDT Sandwich, closely followed by the pouch and TDT disk in water bath. This order was reversed for z. Tukey HSD tests for each model parameters indicates no significant between every pair of thermal treatment method. Similarly, there were no significant differences among the thermal treatment methods for the Weibull model parameters (**Table 4.4**). These results suggest that all three methods are comparable and interchangeable. It is important to note that the TDT Sandwich consistently exhibited lower or comparable standard deviations for the model parameters, suggesting more repeatable results with this method. The fitted models are plotted against the inactivation data in **Fig. 4.5**. The similarity in model parameters between all three methods is apparent in the close proximity and similar curvatures of the curves.

Table 4.5 summarizes the destruction of *Salmonella* during CUT of all three thermal treatment methods. As the treatment temperature increased, more *Salmonella* were inactivated during the CUT phase. The CUT values in **Table 4.1** at each temperature suggest that the higher inactivation were caused by the longer CUT which exposed the population to high temperatures for a longer period of time before time zero was achieved. Tukey HSD tests did not detect significant differences among the methods

at each treatment temperature. However, in terms of average magnitude, the TDT Sandwich had less inactivation during the CUT than the other two methods especially in comparison to the pouch method at 85 °C (calculated p-value: 0.052). It should again be noted that the TDT Sandwich units were operated at slower heating rates to match the CUT of the TDT disks; operation at its maximum heating rate (~100 °C/min) would result in smaller CUT and possibly less inactivation.

Due to statistically insignificant differences among the three methods, the inactivation data for all three methods were combined and fitted to the log-linear and Weibull models. The resulting model parameters are listed in **Table 4.6**. The Weibull model had lower RMSE and AIC_c values than the log-linear model, indicating a better fit to the WMP data than the log-linear model. In fact, the probability likelihood that the Weibull model is more correct than the log-linear model was calculated to be > 0.99. Visual inspection of the models on the combined dataset (**Fig. 4.6**) also shows that the Weibull model fits the trend of the data across all three methods better than the log-linear model. In particular, the Weibull model was able to capture the "tailing off" effect at the later periods of the thermal treatment. On the other hand, the log-linear appeared to overestimate the inactivation especially at the 100 min timepoint of the 75 °C thermal treatment. Wei et. al (*63*) measured the thermal resistance of *Salmonella* in WMP at various water activities and reported the D-value at 80 °C and z-value for WMP equilibrated to 0.20 a_w to be 12.12 min and 17.68 °C, respectively. The choice between the Weibull and log-linear models is not straightforward and is dependent on the food matrix and microorganism (*58*). In the realm of low-moisture foods, the Weibull model

had better performance for some microorganisms and food products: nine Shiga toxin-producing *Escherichia coli* strains in model foods for confectionary, seasoning, chicken meat powder and pet food (*11*); *E. coli* O121 in wheat flour (*56*); *Enterococcus faecium* in wheat flour (*34*); *Salmonella* Typhimurium, Tennessee, Agona and Montevideo in whey protein powder (*49*); *Salmonella* Enteritidis PT 30 in almond kernels (*60*). On the other hand, the traditional log-linear model was sufficient for certain bacteria-food combinations: *Salmonella* Enteritidis PT 30 in wheat flour (*53*); *Salmonella* Enteritidis PT 30 in almonds (*16*); *Salmonella* Enteritidis in wheat flour (*34*). Due to the simplicity of the log-linear model, it is preferable to the Weibull model if both models have comparable fitting performance to inactivation data. Therefore, it would be prudent to evaluate the fit of both models before deciding on one. In the case of the WMP data in this study, the Weibull model was shown to be a better fit.

In conclusion, the thermal inactivation kinetics of *Salmonella* in WMP are comparable when measured with TDT disks in water bath, pouches in water bath, and the TDT Sandwich. The TDT Sandwich exhibited some advantages over the other two methods such as smaller variations in CUT and fitted model parameters. The Weibull model fitted the thermal inactivation data better than the log-linear model in this study. The framework presented in this study could be extended to other microorganisms and food matrices to further evaluate the congruence between different thermal treatment methods.

4.4. Acknowledgements

This material is based upon work that is supported by the National Institute of Food and Agriculture, U.S. Department of Agriculture, under award number 2015-68003-23415 and with partial support from the Nebraska Agricultural Experiment Station with funding from the Hatch Act (Accession Number 1006859) through the USDA National Institute of Food and Agriculture.

4.5. References

1. Al-Holy, M., Z. Quinde, D. Guan, J. Tang, and B. Rasco. 2004. Thermal Inactivation of *Listeria innocua* in Salmon (*Oncorhynchus keta*) Caviar Using Conventional Glass and Novel Aluminum Thermal-Death-Time Tubes. *J. Food Prot.* 67:383–386.
2. Carlier, V., J. C. Augustin, and J. Rozier. 1996. Heat Resistance of *Listeria monocytogenes* (Phagovar 2389/2425/3274/2671/47/108/340): D- and z-Values in Ham. *J. Food Prot.* 59:588–591.
3. Cheng, T., R. Li, X. Kou, and S. Wang. 2017. Influence of controlled atmosphere on thermal inactivation of *Escherichia coli* ATCC 25922 in almond powder. *Food Microbiol.* 64:186–194.
4. Cheng, T., and S. Wang. 2018. Influence of storage temperature/time and atmosphere on survival and thermal inactivation of *Escherichia coli* ATCC 25922 inoculated to almond powder. *Food Control* 86:350–358.
5. Christopoulos, A. 1998. Assessing the distribution of parameters in models of ligand–receptor interaction: to log or not to log. *Trends Pharmacol. Sci.* 19:351–357.

6. Chung, H.-J., S. L. Birla, and J. Tang. 2008. Performance evaluation of aluminum test cell designed for determining the heat resistance of bacterial spores in foods. *LWT - Food Sci. Technol.* 41:1351–1359.
7. Chung, H.-J., S. Wang, and J. Tang. 2007. Influence of Heat Transfer with Tube Methods on Measured Thermal Inactivation Parameters for *Escherichia coli*. *J. Food Prot.* 70:851–859.
8. Condón, S., M. J. Arrizubieta, and F. J. Sala. 1993. Microbial heat resistance determinations by the multipoint system with the thermoresistometer TR-SC Improvement of this methodology. *J. Microbiol. Methods* 18:357–366.
9. Condon, S., P. Lopez, R. Oria, and F. J. Sala. 1989. Thermal Death Determination: Design and Evaluation of a Thermoresistometer. *J. Food Sci.* 54:451–457.
10. Conesa, R., S. Andreu, P. s. Fernández, A. Esnoz, and A. Palop. 2009. Nonisothermal heat resistance determinations with the thermoresistometer Mastia. *J. Appl. Microbiol.* 107:506–513.
11. Daryaei, H., W. Peñaloza, I. Hildebrandt, K. Krishnamurthy, P. Thiruvengadam, and J. Wan. 2018. Heat inactivation of Shiga toxin-producing *Escherichia coli* in a selection of low moisture foods. *Food Control* 85:48–56.
12. Donnelly, C. W., E. H. Briggs, and L. S. Donnelly. 1987. Comparison of Heat Resistance of *Listeria monocytogenes* in Milk as Determined by Two Methods. *J. Food Prot.* Allen Press 50:14–17.
13. Enache, E., A. Kataoka, D. G. Black, L. Weddig, M. Hayman, and K. Bjornsdottir-Butler. 2013. Heat Resistance of Histamine-Producing Bacteria in Irradiated Tuna Loins. *J. Food Prot.* 76:1608–1614.

14. Foster, A. M., L. P. Ketteringham, G. L. Purnell, A. Kondjoyan, M. Havet, and J. A. Evans. 2006. New apparatus to provide repeatable surface temperature–time treatments on inoculated food samples. *J. Food Eng.* 76:19–26.
15. Foster, A. M., L. P. Ketteringham, M. J. Swain, A. Kondjoyan, M. Havet, O. Rouaud, and J. A. Evans. 2006. Design and development of apparatus to provide repeatable surface temperature–time treatments on inoculated food samples. *J. Food Eng.* 76:7–18.
16. Garces-Vega, F. J., E. T. Ryser, and B. P. Marks. 2019. Relationships of Water Activity and Moisture Content to the Thermal Inactivation Kinetics of *Salmonella* in Low-Moisture Foods. *J. Food Prot.* Allen Press 82:963–970.
17. Gaze, J. E., A. R. Boyd, and H. L. Shaw. 2006. Heat inactivation of *Listeria monocytogenes* Scott A on potato surfaces. *J. Food Eng.* 76:27–31.
18. Ghasemi, A., and S. Zahediasl. 2012. Normality Tests for Statistical Analysis: A Guide for Non-Statisticians. *Int. J. Endocrinol. Metab.* 10:486–489.
19. Hancock, A. A., E. N. Bush, D. Stanisic, J. J. Kyncl, and C. T. Lin. 1988. Data normalization before statistical analysis: keeping the horse before the cart. *Trends Pharmacol. Sci.* Elsevier 9:29–32.
20. Hassani, M., S. Condón, and R. Pagán. 2007. Predicting Microbial Heat Inactivation under Nonisothermal Treatments. *J. Food Prot.* 70:1457–1467.
21. Hildebrandt, I. M., B. P. Marks, V. K. Juneja, M. Osoria, N. O. Hall, and E. T. Ryser. 2016. Cross-Laboratory Comparative Study of the Impact of Experimental and Regression Methodologies on *Salmonella* Thermal Inactivation Parameters in Ground Beef. *J. Food Prot.* 79:1097–1106.

22. Hildebrandt, I. M., B. P. Marks, E. T. Ryser, R. Villa-Rojas, J. Tang, F. J. Garces-Vega, and S. E. Buchholz. 2016. Effects of Inoculation Procedures on Variability and Repeatability of *Salmonella* Thermal Resistance in Wheat Flour. *J. Food Prot.* 79:1833–1839.

23. Jackson, T. C., M. D. Hardin, and G. R. Acuff. 1996. Heat Resistance of *Escherichia coli* O157:H7 in a Nutrient Medium and in Ground Beef Patties as Influenced by Storage and Holding Temperatures. *J. Food Prot.* 59:230–237.

24. Jewell, K. 2012. Comparison of 1-step and 2-step methods of fitting microbiological models. *Int. J. Food Microbiol.* 160:145–161.

25. Jin, T., H. Zhang, G. Boyd, and J. Tang. 2008. Thermal resistance of *Salmonella enteritidis* and *Escherichia coli* K12 in liquid egg determined by thermal-death-time disks. *J. Food Eng.* 84:608–614.

26. Karyotis, D., P. N. Skandamis, and V. K. Juneja. 2017. Thermal inactivation of *Listeria monocytogenes* and *Salmonella* spp. in sous-vide processed marinated chicken breast. *Food Res. Int.* 100:894–898.

27. Kikoku, Y., N. Tagashira, and H. Nakano. 2008. Heat Resistance of Fungi Isolated from Frozen Blueberries. *J. Food Prot.* 71:2030–2035.

28. Kilsby, D. C., K. W. Davies, P. J. McClure, C. Adair, and W. A. Anderson. 2000. Bacterial thermal death kinetics based on probability distributions: the heat destruction of *Clostridium botulinum* and *Salmonella* Bedford. *J. Food Prot.* 63:1197–1203.

29. Kou, X., R. Li, L. Hou, Z. Huang, B. Ling, and S. Wang. 2016. Performance of a Heating Block System Designed for Studying the Heat Resistance of Bacteria in Foods. *Sci. Rep.* 6:30758.

30. Kou, X., R. Li, L. Zhang, H. Ramaswamy, and S. Wang. 2019. Effect of heating rates on thermal destruction kinetics of *Escherichia coli* ATCC25922 in mashed potato and the associated changes in product color. *Food Control* 97:39–49.

31. Lewis, R. J., A. Baldwin, T. O'Neill, H. A. Alloush, S. M. Nelson, T. Dowman, and V. Salisbury. 2006. Use of *Salmonella enterica* serovar Typhimurium DT104 expressing lux genes to assess, in real time and in situ, heat inactivation and recovery on a range of contaminated food surfaces. *J. Food Eng.* 76:41–48.

32. Lewis, R. J., K. Robertson, H. M. Alloush, T. Dowman, and V. Salisbury. 2006. Use of bioluminescence to evaluate the effects of rapid cooling on recovery of *Salmonella enterica* serovar Typhimurium DT104 after heat treatment. *J. Food Eng.* 76:49–52.

33. Li, L., J. Cepeda, J. Subbiah, G. Froning, V. K. Juneja, and H. Thippareddi. 2017. Dynamic predictive model for growth of *Salmonella* spp. in scrambled egg mix. *Food Microbiol.* 64:39–46.

34. Liu, S., R. V. Rojas, P. Gray, M.-J. Zhu, and J. Tang. 2018. *Enterococcus faecium* as a *Salmonella* surrogate in the thermal processing of wheat flour: Influence of water activity at high temperatures. *Food Microbiol.* 74:92–99.

35. Ma, L., G. Zhang, P. Gerner-Smidt, V. Mantripragada, I. Ezeoke, and M. P. Doyle. 2009. Thermal Inactivation of *Salmonella* in Peanut Butter. *J. Food Prot.* 72:1596–1601.

36. Mazzotta, A. S. 2001. Heat Resistance of *Listeria monocytogenes* in Vegetables: Evaluation of Blanching Processes. *J. Food Prot.* 64:385–387.

37. Mazzotta, A. S. 2001. Thermal Inactivation of Stationary-Phase and Salt-Adapted *Listeria monocytogenes* during Postprocess Pasteurization of Surimi-Based Imitation Crab Meat. *J. Food Prot.* 64:483–485.

38. McCann, M. S., J. J. Sheridan, D. A. McDowell, and I. S. Blair. 2006. Effects of steam pasteurisation on *Salmonella* Typhimurium DT104 and *Escherichia coli* O157:H7 surface inoculated onto beef, pork and chicken. *J. Food Eng.* 76:32–40.

39. Motulsky, H., and A. Christopoulos. 2004. Fitting Models to Biological Data Using Linear and Nonlinear Regression: A Practical Guide to Curve Fitting1 edition. Oxford University Press, U.S.A., Oxford ; New York.

40. Mulak, V., R. Tailliez, P. Eb, and P. Becel. 1995. Heat Resistance of Bacteria Isolated From Preparations Based on Seafood Products. *J. Food Prot.* 58:49–53.

41. Nocedal, J., and S. Wright. 2006. Numerical Optimization, 2nd ed. Springer-Verlag, New York.

42. Palop, A., J. Raso, S. Condón, and F. J. Sala. 1996. Heat Resistance of *Bacillus subtilis* and *Bacillus coagulans*: Effect of Sporulation Temperature in Foods With Various Acidulants. *J. Food Prot.* 59:487–492.

43. Peleg, M. 2006. Advanced Quantitative Microbiology for Foods and Biosystems: Models for Predicting Growth and Inactivation1 edition. CRC Press, Boca Raton.

44. Peña-Meléndez, M., J. J. Perry, and A. E. Yousef. 2014. Changes in Thermal Resistance of Three *Salmonella* Serovars in Response to Osmotic Shock and

Adaptation at Water Activities Reduced by Different Humectants. *J. Food Prot.* 77:914–918.

45. Perry, J. J., and A. E. Yousef. 2013. Factors Affecting Thermal Resistance of *Salmonella enterica* Serovar Enteritidis ODA 99-30581-13 in Shell Egg Contents and Use of Heat-Ozone Combinations for Egg Pasteurization. *J. Food Prot.* 76:213–219.
46. Razali, N. M., and Y. B. Wah. 2011. Power comparisons of Shapiro-Wilk , Kolmogorov-Smirnov , Lilliefors and Anderson-Darling tests. *J. Stat. Model. Anal.* 2:21–33.
47. Redondo-Solano, M., D. E. Burson, and H. Thippareddi. 2016. Thermal Resistance of *Clostridium difficile* Spores in Peptone Water and Pork Meat. *J. Food Prot.* 79:1468–1474.
48. Sala, F. J., P. Ibarz, A. Palop, J. Raso, and S. Condon. 1995. Sporulation Temperature and Heat Resistance of *Bacillus subtilis* at Different pH Values. *J. Food Prot.* 58:239–243.
49. Santillana Farakos, S. M., J. F. Frank, and D. W. Schaffner. 2013. Modeling the influence of temperature, water activity and water mobility on the persistence of *Salmonella* in low-moisture foods. *Int. J. Food Microbiol.* 166:280–293.
50. Schuman, J. D., B. W. Sheldon, and P. M. Foegeding. 1997. Thermal Resistance of *Aeromonas hydrophila* in Liquid Whole Egg. *J. Food Prot.* 60:231–236.
51. Seabold, S., and J. Perktold. 2010. statsmodels: Econometric and statistical modeling with python, 9th Python in Science Conference.
52. Shearer, A. E. H., A. S. Mazzotta, R. Chuyate, and D. E. Gombas. 2002. Heat Resistance of Juice Spoilage Microorganisms. *J. Food Prot.* 65:1271–1275.

53. Smith, D. F., I. M. Hildebrandt, K. E. Casulli, K. D. Dolan, and B. P. Marks. 2016. Modeling the Effect of Temperature and Water Activity on the Thermal Resistance of *Salmonella* Enteritidis PT 30 in Wheat Flour. *J. Food Prot.* 79:2058–2065.

54. Smith, D. F., and B. P. Marks. 2015. Effect of Rapid Product Desiccation or Hydration on Thermal Resistance of *Salmonella enterica* Serovar Enteritidis PT 30 in Wheat Flour. *J. Food Prot.* 78:281–286.

55. Splittstoesser, D. F., M. R. Mclellan, and J. J. Churey. 1996. Heat Resistance of *Escherichia coli* O157:H7 in Apple Juice. *J. Food Prot.* 59:226–229.

56. Suehr, Q. J., N. M. Anderson, and S. E. Keller. 2019. Desiccation and Thermal Resistance of *Escherichia coli* O121 in Wheat Flour. *J. Food Prot.* 82:1308–1313.

57. Tournas, V., and R. W. Traxler. 1994. Heat Resistance of a *Neosartorya fischeri* Strain Isolated From Pineapple Juice Frozen Concentrate. *J. Food Prot.* 57:814–816.

58. van Boekel, M. A. J. S. 2002. On the use of the Weibull model to describe thermal inactivation of microbial vegetative cells. *Int. J. Food Microbiol.* 74:139–159.

59. Verma, T., X. Wei, S. K. Lau, A. Bianchini, K. M. Eskridge, and J. Subbiah. 2018. Evaluation of *Enterococcus faecium* NRRL B-2354 as a Surrogate for *Salmonella* During Extrusion of Low-Moisture Food. *J. Food Sci.* 83:1063–1072.

60. Villa-Rojas, R., J. Tang, S. Wang, M. Gao, D.-H. Kang, J.-H. Mah, P. Gray, M. E. Sosa-Morales, and A. López-Malo. 2013. Thermal Inactivation of *Salmonella* Enteritidis PT 30 in Almond Kernels as Influenced by Water Activity. *J. Food Prot.* 76:26–32.

61. Virtanen, P., R. Gommers, T. E. Oliphant, M. Haberland, T. Reddy, D. Cournapeau, E. Burovski, P. Peterson, W. Weckesser, J. Bright, S. J. van der Walt, M. Brett, J.

Wilson, K. J. Millman, N. Mayorov, A. R. J. Nelson, E. Jones, R. Kern, E. Larson, C. J. Carey, İ. Polat, Y. Feng, E. W. Moore, J. VanderPlas, D. Laxalde, J. Perktold, R. Cimrman, I. Henriksen, E. A. Quintero, C. R. Harris, A. M. Archibald, A. H. Ribeiro, F. Pedregosa, and P. van Mulbregt. 2020. SciPy 1.0: fundamental algorithms for scientific computing in Python. 3. *Nat. Methods*. Nature Publishing Group 17:261–272.

62. Wei, X., S. K. Lau, J. Stratton, S. Irmak, A. Bianchini, and J. Subbiah. 2018. Radio-Frequency Processing for Inactivation of *Salmonella enterica* and *Enterococcus faecium* NRRL B-2354 in Black Peppercorn. *J. Food Prot.* 81:1685–1695.
63. Wei, X., S. K. Lau, B.D. Chaves, M.-G.C. Danao, S. Agarwal, and J. Subbiah. 2020. Effect of water activity on the thermal inactivation kinetics of *Salmonella* in dairy powders. *J. Dairy Sci. Accepted.*
64. Yap, B. W., and C. H. Sim. 2011. Comparisons of various types of normality tests. *J. Stat. Comput. Simul.* Taylor & Francis 81:2141–2155.
65. Zhang, L., X. Kou, S. Zhang, T. Cheng, and S. Wang. 2018. Effect of water activity and heating rate on *Staphylococcus aureus* heat resistance in walnut shells. *Int. J. Food Microbiol.* 266:282–288.
66. Zhang, S., L. Zhang, R. Lan, X. Zhou, X. Kou, and S. Wang. 2018. Thermal inactivation of *Aspergillus flavus* in peanut kernels as influenced by temperature, water activity and heating rate. *Food Microbiol.* 76:237–244.

Table 4.1. Come-up time (CUT) data for the three thermal treatment methods at each treatment temperature.

Method	Temperature (°C)	Time to reach ±0.5 s of target temperature (s)	CUT (s)
TDT disk in water bath	75	127 ± 26	180
	80	144 ± 38	220
	85	151 ± 47	244
Pouch in water bath	75	50 ± 21	92
	80	84 ± 28	140
	85	116 ± 28	171
TDT Sandwich	75	184 ± 3	190
	80	225 ± 3	232
	85	243 ± 4	250

Where possible, values are shown as mean ± standard deviation. Heating rates of TDT Sandwich were purposely decreased to achieve similar CUT to that of the TDT disks.

Table 4.2. Normality tests for the log-linear (Equation 4.3) and Weibull (Equation 4.6) model parameters as predicted by Monte Carlo simulations with $\boldsymbol{T_{ref}} = 80°C$.

Model	Parameter	Transformation	Mean (min)	Median (min)	Skew	Kurtosis	Shapiro-Wilk probability
Log-linear	$D_{80°C}$	None	10.56	10.55	0.209	0.001	0.313
		Logarithmic	10.55	10.55	0.143	-0.034	0.628
	z	None	16.47	16.44	0.250	-0.051	0.058
		Logarithmic	16.46	16.44	0.132	-0.109	0.299
Weibull	$\alpha_{80°C}$	None	3.52	3.52	0.172	0.189	0.155
		Logarithmic	3.48	3.52	-0.248	-0.002	0.047
	z	None	16.83	16.78	0.429	0.184	0.001
		Logarithmic	16.81	16.78	0.283	0.026	0.051
	β	None	0.88	0.88	0.094	0.007	0.322
		Logarithmic	0.88	0.88	-0.090	-0.106	0.323

Mean and median values for lognormal distributions are expressed in their natural coordinates.

Table 4.3. Log-linear model (Equation 4.3) parameters for the three thermal treatment methods with $\boldsymbol{T_{ref}} = 80°C$.

Method	$D_{80°C}$ (min)	z (°C)
TDT disk in water bath	10.20 ± 1.28 [A]	16.63 ± 2.77 [A]
Pouch in water bath	10.87 ± 0.73 [A]	17.64 ± 2.55 [A]
TDT Sandwich	11.00 ± 0.51 [A]	15.72 ± 0.76 [A]

Values are reported as mean ± standard deviation. Within columns, values sharing a common letter are not significantly different ($\alpha = 0.05$).

Table 4.4. Weibull model (Equation 4.6) parameters for the three thermal treatment methods with $\boldsymbol{T_{ref}} = 80°C$.

Method	$\alpha_{80°C}$ (min)	z (°C)	β
TDT disk in water bath	3.69 ± 0.90 [A]	16.78 ± 2.94 [A]	0.91 ± 0.05 [A]
Pouch in water bath	3.57 ± 0.17 [A]	18.35 ± 3.12 [A]	0.88 ± 0.03 [A]
TDT Sandwich	3.32 ± 0.94 [A]	16.11 ± 0.58 [A]	0.84 ± 0.12 [A]

Values are reported as mean ± standard deviation. Within columns, values sharing a common letter are not significantly different ($\alpha = 0.05$).

Table 4.5. Comparison of the *Salmonella* survivors before thermal treatments, $\log_{10} N_c$ and at time zero, $\log_{10} N_0$.

Temperature (°C)	Method	$\log_{10} N_c$	$\log_{10} N_0$	$\log_{10}(N_c/N_0)$
75	TDT disk in water bath	7.12 ± 0.07	6.99 ± 0.22	0.12 ± 0.2 [A]
	Pouch in water bath	7.08 ± 0.27	7.08 ± 0.19	0.00 ± 0.09 [A]
	TDT Sandwich	6.97 ± 0.20	7.08 ± 0.20	-0.11 ± 0.06 [A]
80	TDT disk in water bath	6.86 ± 0.11	6.48 ± 0.18	0.38 ± 0.28 [A]
	Pouch in water bath	7.08 ± 0.11	6.93 ± 0.21	0.15 ± 0.14 [A]
	TDT Sandwich	7.01 ± 0.04	6.95 ± 0.16	0.06 ± 0.20 [A]
85	TDT disk in water bath	6.97 ± 0.18	6.20 ± 0.37	0.77 ± 0.52 [A]
	Pouch in water bath	7.19 ± 0.18	6.14 ± 0.27	1.06 ± 0.32 [A]
	TDT Sandwich	6.97 ± 0.21	6.82 ± 0.29	0.15 ± 0.16 [A]

Values are reported as mean ± standard deviation. Within a given temperature, values sharing a common letter are not significantly different (α = 0.05).

Table 4.6. Model parameter estimates for the log-linear (Equation 4.3) and Weibull (Equation 4.6) models globally fitted across all methods with $\boldsymbol{T_{ref}} = 80°C$.

Model	$D_{80°C}$ or $\alpha_{80°C}$ (min)	z (°C)	β	RMSE ($\log_{10}$ CFU/g)	AIC_c
Log-linear	10.62 (0.13)	16.51 (0.34)	-	0.377	-312
Weibull	3.46 (0.29)	16.90 (0.41)	0.87 (0.03)	0.362	-324

Values are reported as parameter estimate (standard error of estimate).

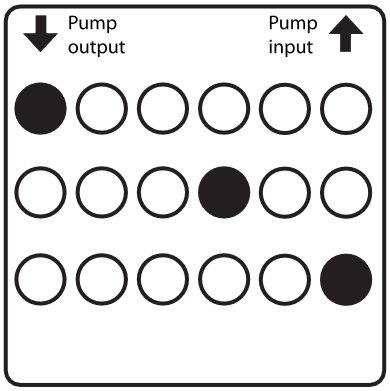

Figure 4.1. Location of TDT disks with thermocouples (filled circles) and without (empty circles) in the water bath during the CUT measurements. The same setup, without thermocouples, was used during the isothermal inactivation experiments.

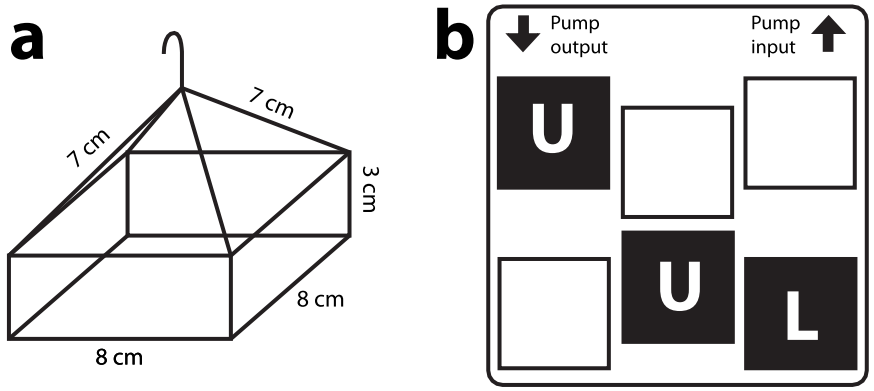

Figure 4.2. Dimensions of the scaffolds for the pouches (A) and their locations in the water bath during the CUT measurements (B). Filled squares represent scaffolds with one of two pouches containing a thermocouple, either at the upper (U) level or the lower (L) level. The same setup, without thermocouples, was used during the isothermal inactivation experiments.

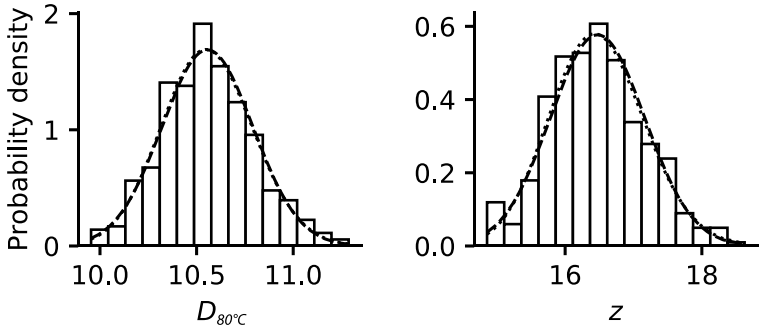

Figure 4.3. Probability density histogram overlaid with fitted normal distribution (dashed line) and lognormal distribution (dotted line) curves of the log-linear model parameters as predicted by Monte Carlo simulations.

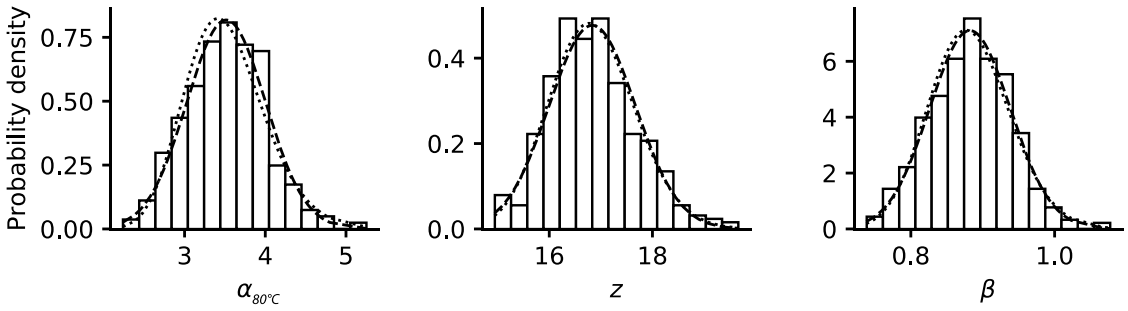

Figure 4.4. Probability density histogram overlaid with fitted normal distribution (dashed line) and lognormal distribution (dotted line) curves of the Weibull model parameters as predicted by Monte Carlo simulations.

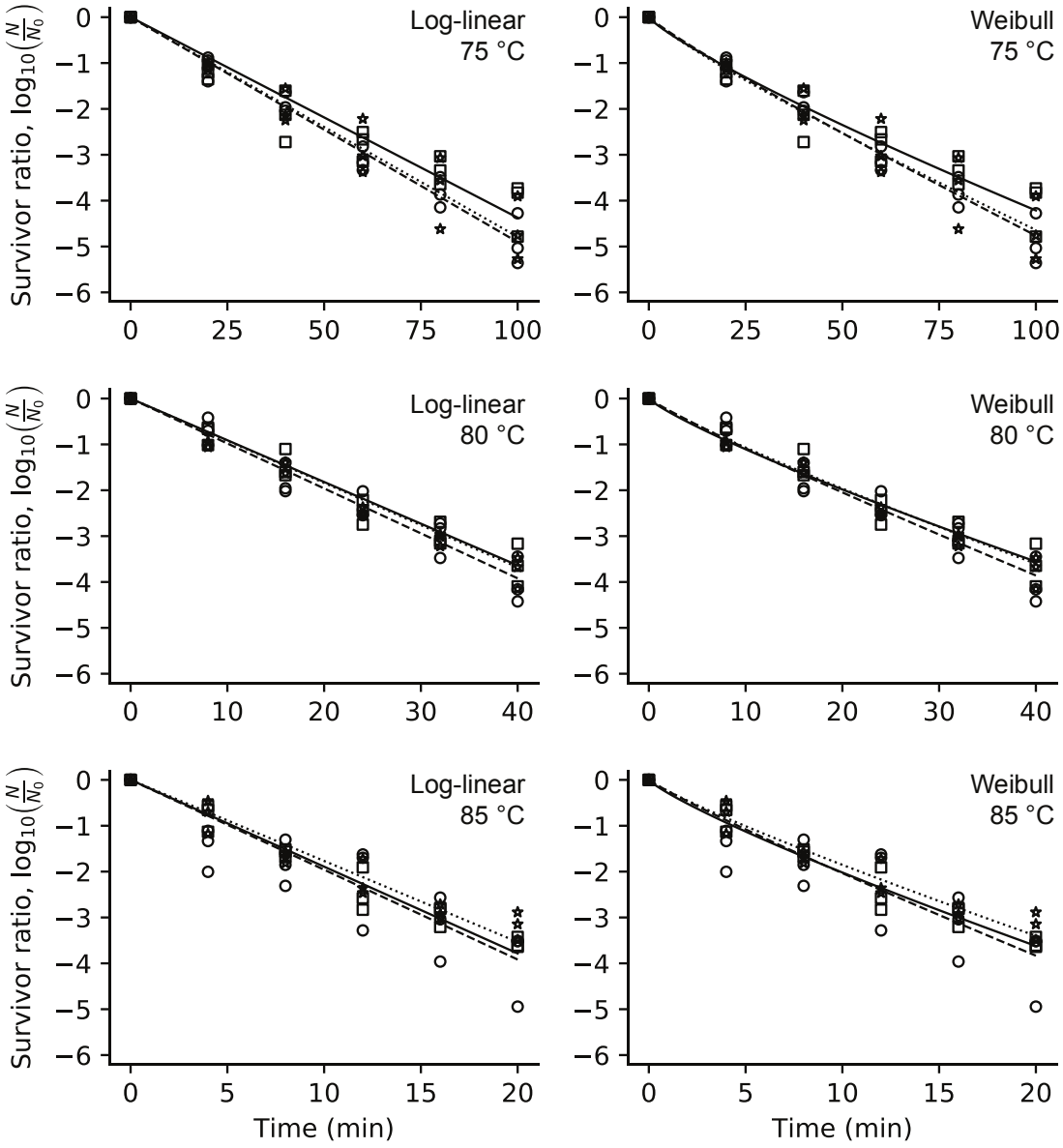

Figure 4.5. Experimental and predicted survival of *Salmonella* in whole milk powder determined with TDT disks in water bath (○, dashed lines), pouches in water bath (☆, dotted lines), and TDT Sandwich (□, solid lines) at each treatment temperature.

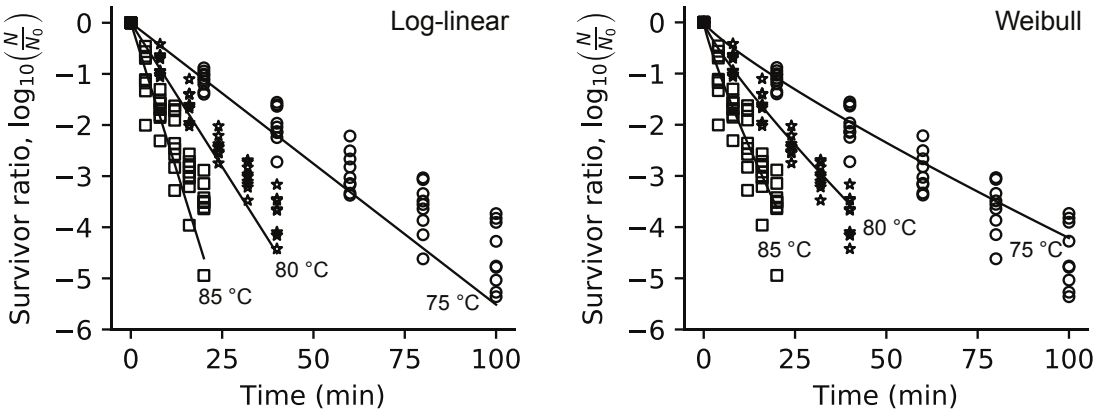

Figure 4.6. Global log-linear and Weibull models fitted to *Salmonella* inactivation data combined across all methods at 75 (○), 80 (☆), and 85 °C (□).

Chapter 5: Thermal Inactivation Kinetics of *Salmonella* and *Enterococcus faecium* NRRL-B2354 in whole chia seeds (*Salvia hispanica L.*)

5.1. Introduction

Consumption of chia seeds (*Salvia hispanica L.*) has recently gained popularity among health-conscious consumers due to health-promoting properties such as a high Omega-3 to Omega-6 fatty acids ratio, phenolic acids, flavonoids, high fiber content, and bioactive peptides (*1*, *6*, *28*, *32*). The seeds also have a unique property of forming a gel coating or mucilage when exposed to water (*3*). Due to its positive health and functional properties, there have been efforts to use chia seeds in food products in a variety of ways such as emulsions (*17*), gum replacements (*3*), or direct incorporation into bakery products (*29*, *34*).

As an agricultural product, there is a risk for chia seeds to be contaminated during the production process and cause foodborne illnesses when consumed raw. In addition, chia seeds are sometimes processed into other products by sprouting them, thus presenting another route for contamination. A multistate outbreak in the US between the years 2013 to 2014 was traced to multiple *Salmonella* serotypes in sprouted chia seed powder (*9*, *31*). Outbreak investigation revealed that the seeds used for producing the implicated product were not thermally treated by any means before sprouting (*9*). Laboratory sprouting simulation experiments show that *Salmonella* populations do not decrease when seeds are dried at room temperature (25 °C) and only showed a 5-log

reduction when dried at high temperatures (60 °C) (*18*). Also, *Salmonella* survives extremely well on dried chia seeds (*18*), with a mean time of 94 days depending on the serovars (*5*). As such, there is a dire need for an intervention technology that can reliably reduce *Salmonella* populations in chia seeds. Soaking chia seeds in peracetic acid solution for 1 hour was found to reduce *Salmonella* populations by more than 4 $\log_{10}$ CFU/g (*13*). High intensity pulsed light applied on a monolayer bed of chia seeds was able to achieve a 4-log reduction of *Salmonella* Typhimurium within 15 s (*25*). There are, however, no studies to date determining the thermal resistance of *Salmonella* in chia seeds. In addition, a suitable nonpathogenic surrogate for *Salmonella* should be determined to facilitate validation of scaled-up thermal pasteurization processes for chia seeds.

The objectives of this study were to determine the thermal inactivation kinetics of *Salmonella* in chia seeds, assess the suitability of *Enterococcus faecium* NRRL-B2354 as a surrogate for *Salmonella* in chia seeds for thermal processes, and evaluate the quality of the seeds after thermal treatment.

5.2. Materials and Methods

5.2.1. Food sample

Chia seed samples (Organic Chia Seeds, BetterBody Foods, Lindon, UT) were either purchased from online retailers or obtained directly from a supplier and stored at room temperature before use. The chia seeds were mixtures of black and white seeds. Samples from three independent production lots were procured for this study, henceforth referred to as lots 1, 2, and 3. All three lots had expiration dates within two months apart

from one another. The background microflora of the chia seeds were enumerated by initially diluting approximately 1.5 g of sample at a 1:30 (w/w) ratio with 0.1 % (w/w) buffered peptone water (BPW) (218103, Becton, Dickinson and Company, Sparks, MD) in a sampling bag with filter (B01348, Nasco, Fort Atkinson, WI) and stomaching the mixture with a paddle mixer (9000471, Neutec Group Inc, Farmingdale, NY) for 1 min. The dilution procedure is explained in **Section 5.2.5**. The diluted sample was then serially diluted and spread plated onto tryptic soy agar (236920, Becton, Dickinson and Company, Franklin Lakes, NJ) supplemented with 0.6 % (w/w) yeast extract (212720, Becton, Dickinson and Company, Sparks, MD). The inoculated plates were incubated at 37 °C for 24 ± 2 hours before they were enumerated by counting every colony on the plates.

5.2.2. Moisture content and water activity

The moisture contents of 7.5 ± 0.5 g samples were measured with a halogen moisture analyzer (HG53-P, Mettler Toledo, Greifensee, Switzerland) set to 105°C and time setting "5". Water activity values of samples at room temperature (25 °C) were measured using a water activity meter (4TE, METER Group, Pullman, WA).

5.2.3. Inoculum

The bacterial strains and inoculum preparation procedure described by Verma et al. and Wei et al. were used in this study (*35*, *37*). In particular, the *Salmonella enterica* serovars used were Agona 447967, Mbandaka 698538, Montevideo 488275, Reading Moff 180418, and Tennessee K4643 while the surrogate bacterium was *Enterococcus faecium* NRRL B-2354. Briefly, the bacterial strains were incubated separately in tryptic

soy broth (211825, Becton, Dickinson and Company, Sparks, MD) with 0.6 % (w/w) yeast extract at 37 °C for 24 ± 2 hr. Aliquots of 0.1 mL were then spread plated onto tryptic soy agar with 0.6 % (w/w) yeast extract and incubated overnight at 37 °C for 24 ± 2 h to produce lawns. The lawns were harvested by agitating them with 3 mL of 0.1 % (w/w) BPW and a sterile cell spreader. The harvested lawns of the five *Salmonella* serovars were mixed in equal proportions to produce a 5-strain *Salmonella* cocktail (*ca.* 10.6 $\log_{10}$ CFU/mL), while the harvested lawns of *E. faecium* (*ca.* 10.1 $\log_{10}$ CFU/mL) were used as is.

5.2.4. Inoculation

Chia seed samples were inoculated in 1 kg batches using 20 mL of either the 5-strain *Salmonella* cocktail or the *E. faecium* inoculum. The inoculation was performed in a biosafety cabinet by spreading the chia seeds flat in a large sampling bag (89085-580, VWR) and spraying the inoculum onto the bed of chia seeds using a custom spray device made of a sterile 15 mL centrifuge tube (339650, Thermo Fisher Scientific, Rochester, NY) and a finger-operated spray head (ps20-410-natural, Midwest Bottles LLC, Garrison, KY). The bag was subsequently folded, tied, and shaken by hand for 1 min. The contents were then emptied into the mixing bowl of a mixer (KSM8990OB, KitchenAid, Benton Harbor, MI) with a cover (W10687880, KitchenAid, Benton Harbor, MI) and a wire whip attachment (W10361360, KitchenAid, Benton Harbor, MI). The mixer was operated at speed 4 (*i.e.* “medium” speed) for 10 min. Upon mixing, the inoculated batch was distributed between two aluminum trays and placed into

HumidOSH units set to equilibrate the seeds to their mean native water activity of 0.53 with a fan speed of 4,000 RPM.

5.2.5. Dilution pretreatment before enumeration

When soaked in water or, in this study, BPW, chia seeds form a gel coating on their surfaces which can hold large amounts of liquid. During preliminary trials, it was found that diluting and stomaching chia seeds in a typical 1:10 (w/w) ratio with BPW resulted in insufficient liquid available to be pipetted for enumeration because most of the water was held by the gel coating of the chia seeds. In addition, it was possible that bacteria inoculated onto the chia seeds were trapped in or underneath the gel coating, thus reducing the number of bacteria cells in the pipetted liquid and less observed recovery. Therefore, it was necessary to determine an appropriate method for preparing the chia seeds for microbiological enumeration. The following three pretreatments were tested with approximately 2 g of inoculated chia seed samples diluted to a 1:30 (w/w) ratio with 0.1 % (w/w) BPW:

- Purée: A diluted seed sample purée was prepared using a small electrical coffee and spice grinder (BCG211OB, KitchenAid, Benton Harbor, MI). After addition of seeds and BPW into a grinder bowl, the grinder was pulsed five times, with each pulse consisting of one second of grinding followed by two seconds of rest. Subsequently, the mixture was allowed to sit for 2 min. Finally, the mixture was ground continuously for 1 min. Each purée was prepared with a separate grinder bowl that was disinfected with 70% ethanol. The pulsing and soaking steps were found through preliminary trials to be necessary to ensure that the seeds did not

clump together or remain whole by the end of the grinding process. Samples were pipetted directly from the grinder bowl for serial dilutions.

- None: Chia seeds were placed into a sampling bag with filter (B01348, Nasco, Fort Atkinson, WI) before being diluted with BPW. The mixture was immediately stomached for 1 min. By the end of the stomaching process, the seeds remained whole, though the formation of gel coating was very apparent. Liquid was pipetted out from each bag on the side of the filter sheet without any whole seeds or fragments.
- Soak 5 min: Similar to the "None" pretreatment, except the BPW-diluted seeds were allowed to sit for 5 min before the mixture was stomached. By the end of the stomaching process, the seeds and their gel coatings were still visibly intact.

The puréeing pretreatment is deemed to be the most robust pretreatment for further use in sample preparation because it disintegrated the seeds and gel coating, resulting in a homogenized mixture. Theoretically, any bacteria trapped in or underneath the gel coating will be released. The "None" pretreatment was considered as it is a straightforward way of preparing the samples and is commonly done for most microbiological studies, yet its low yield of liquid available for enumeration was problematic. The unrealized intent of the "Soak 5 min" pretreatment was to allow the gel coating of the seeds to absorb more water and to soften the gel coating leading to disintegration during stomaching. The calculations of bacterial recovery for the puréeing pretreatment were done slightly differently than the other two pretreatments by accounting for the homogenization and incorporation of the ground seeds into the liquid phase. The pretreatments were tested with samples inoculated to "high" (*ca.* 8 $\log_{10}$

CFU/g) and "low" (*ca.* 3 $\log_{10}$ CFU/g) levels to determine if the amount of bacteria present could affect the recovery. The former exactly follows the previously described inoculation procedure while the latter involves an additional step of serially diluting the inoculum five-fold with 0.1 % (w/w) BPW before it was sprayed onto the chia seeds. Five replicates were performed for each bacteria-pretreatment-inoculation level combination.

5.2.6. Enumeration of bacteria

Salmonella cells were enumerated by pretreating and diluting the chia seed samples using one of the previously described pretreatments. Except for the previously described experiments for determining the best dilution pretreatment, the "None" dilution pretreatment was used for all microbiological work. The extracted dilution liquid was then serially diluted with 0.1 % (w/w) BPW. Aliquots of 0.1 mL from appropriate dilutions were then spread plated onto mTSA media which contains tryptic soy agar, 0.6 % (w/w) yeast extract, 0.05 % (w/w) ammonium iron(III) citrate (F5879-500G, Sigma Aldrich, St. Louis, MO), and 0.03 % (w/w) sodium thiosulfate pentahydrate (S445-500, Fisher Scientific, Fair Lawn, NJ) (*11*, *21*, *37*). Inoculated plates were incubated at 37 °C for 24 ± 2 h before being enumerated for *Salmonella* by counting typical colonies with a black center.

The recovery of *E. faecium* follows the same procedure as *Salmonella* except that a differential media for *E. faecium* (eTSA) was used (*37*). The eTSA media consists of tryptic soy agar, 0.6 % (w/w) yeast extract, 0.05 % (w/w) ammonium iron(III) citrate, and

0.025 % (w/w) esculin hydrate (117830500, Acros Organics). Colonies with a black center were counted as *E. faecium*.

5.2.7. Stability and homogeneity of inoculation

After the inoculation process, the bacteria were exposed to a progressively drier environment as they equilibrated to 0.53 a_w which could result in some loss of bacteria. The stability and homogeneity of the inoculation during the water activity equilibration process was thus evaluated by taking five samples from the inoculated sample at random locations and enumerating them for *Salmonella* or *E. faecium*. The moisture content and water activity of two randomly collected samples were also measured. The enumerations and moisture measurements were performed daily up to the fourth day post-inoculation, after which all measurements were only performed on day 7, 18, and 30. The inoculated samples were used for isothermal inactivation studies within two weeks of inoculation; the measurements on day 18 and 30 were performed to investigate the long-term survival of the inoculated bacteria.

5.2.8. Isothermal inactivation

The isothermal inactivation experiments were conducted using TDT Sandwiches. Chia seed samples were packed into heat-sealable aluminized pouches (03MFW03TN, IMPAK Corporation, Los Angeles, CA) in quantities of 2.0 ± 0.5 g and heat-sealed inside the relative humidity-controlled chambers before they were subjected to thermal treatments. One pouch was placed at the center of each TDT Sandwich at room temperature. The TDT Sandwich units were then operated at their maximum heating rates (~100 °C/min) to achieve isothermal conditions at 80, 85, and 90 °C. Before beginning

the isothermal inactivation experiments, the come-up time (CUT) of the samples were measured in triplicates (one TDT sandwich per replicate) by a type T thermocouple (5TC-TT-T-40-36, Omega Engineering Inc., Norwalk, CT) placed at the inside center of pouches containing 2.0 ± 0.5 g of uninoculated chia seeds. The CUT in this study is defined as the mean time for the sample to reach within 0.5 °C of the target isothermal treatment temperature plus two standard deviations. The CUT for achieving 80, 85, and 90 °C were determined to be 1 min 20 s, 1 min 25 s, and 1 min 16 s, respectively.

The isothermal inactivation studies were carried out with 12 pouches (six timepoints, two replicates) per bacteria-lot-temperature combination. The pouches were randomly assigned among 12 TDT Sandwich units. The timepoint at which CUT was achieved was designated as time zero of the isothermal inactivation study. Lot 3 exhibited lower thermal resistances for both bacteria and was thus assigned different timepoints than the other two lots. Samples that completed their assigned thermal treatment durations were immediately transferred to an ice slurry bath and cooled for at least a minute before its contents were diluted and enumerated for *Salmonella* or *E. faecium* survivors.

5.2.9. Thermal inactivation models

The inactivation data for *Salmonella* and *E. faecium* were fitted to consolidated models consisting of a primary model (log-linear or Weibull) at each isothermal temperature and a secondary model (Bigelow *i.e.* z-value) that accounts for temperature-dependence of parameters in the primary model (*23*, *33*). This 1-step regression of fitting microbial inactivation data to a consolidated model has been shown to result in better

model fits and model parameter estimates compared to a 2-step regression *i.e.* fitting the primary and secondary models separately (*10*, *15*). The primary, secondary, and consolidated models for the primary log-linear model are as follows:

$$\log_{10}\left(\frac{N}{N_0}\right) = -\frac{t}{D_T} \tag{5.1}$$

$$\log_{10}\left(\frac{D_T}{D_{ref}}\right) = -\frac{T - T_{ref}}{z} \tag{5.2}$$

$$\log_{10}\left(\frac{N}{N_0}\right) = -\frac{t}{D_{ref} \cdot 10^{\left(\frac{T_{ref}-T}{z}\right)}} \tag{5.3}$$

where N is the *Salmonella* or *E. faecium* population at time t (CFU/g), N_0 is the corresponding populations at time zero of the isothermal study (CFU/g), t is the instantaneous time of the thermal treatment (s), D_T is the decimal reduction time *i.e.* D-value at temperature T (s), D_{ref} is the decimal reduction time at the reference temperature T_{ref} (s), T is the temperature of the thermal treatment (°C), and z is the z-value (°C).

The corresponding equations for the Weibull model are as follows (*33*):

$$\log_{10}\left(\frac{N}{N_0}\right) = -\frac{1}{\ln(10)}\left(\frac{t}{\alpha_T}\right)^{\beta} \tag{5.4}$$

$$\log_{10}\left(\frac{\alpha_T}{\alpha_{ref}}\right) = -\frac{T - T_{ref}}{z} \tag{5.5}$$

$$\log_{10}\left(\frac{N}{N_0}\right) = -\frac{1}{\ln(10)}\left(\frac{t}{\alpha_{ref} \cdot 10^{\left(\frac{T_{ref}-T}{z}\right)}}\right)^{\beta} \tag{5.6}$$

where α_T is the scale factor at temperature T (s), β is the shape factor, and α_{ref} is the scale factor at the reference temperature T_{ref} (s). In this consolidated model, β is assumed to be independent of temperature.

Since 85 °C is the midpoint of the range of temperatures investigated in this study, T_{ref} was fixed to 85 °C; D_{ref} and α_{ref} will henceforth be written as $D_{85°C}$ and $\alpha_{85°C}$, respectively. The curve fitting of Equations 4 and 6 to microbial inactivation data was performed using the curve_fit function of the Python SciPy library with the Levenberg–Marquardt algorithm set to a maximum of 200 iterations and convergence tolerance of 10^{-8} (*36*). The log-linear and Weibull models were compared by calculating their root mean square error (RMSE) and corrected Akaike's Information Criterion (AICc) values.

5.2.10. High temperature water activity

While collecting microbial inactivation data for the isothermal inactivation study, lot 3 had noticeably fewer survivors across all treatment conditions compared to the other two lots. Recently, it was shown that the thermal resistance of *Salmonella* in soy protein powder is influenced by the high temperatures encountered during a pasteurization process (*16*). Therefore, it was hypothesized that the lower thermal resistance in lot 3 may have been caused by a different water activity profile at the high temperatures encountered in this study. The water activity of the inoculated samples from all three lots were thus measured from 20 to 80 °C in 10 °C increments using a vapor sorption analyzer (METER Group, Pullman, WA) and a custom high temperature water activity

meter. The former was operated from 20 °C to its maximum operating temperature of 60 °C and was set to the “volatile” setting which uses the in-built capacitance sensor. The latter is a system adapted from the HumidOSH by stripping the system down to only its control box and relative humidity sensor. The Sensirion SHT85 relative humidity sensor used in the HumidOSH can operate between -40 and 105 °C; therefore, the custom system was used to measure the water activity of the samples from 50 to 80 °C. The overlap at 50 and 60 °C for both systems serves to compare and bridge the measurements acquired from both systems. The sensor was installed inside a machined clamshell-like stainless steel test cell that seals onto itself with a silicone O-ring. The test cell was placed inside a convection oven (Model 28, Precision Scientific Group, Chicago, IL) set to the target temperature and allowed to equilibrate for at least 45 min before measurements. Approximately 1 g of sample was then placed in a stainless steel cup and transferred into the test cell. Once the relative humidity and temperature readings inside the test cell have stabilized (~15 min), water activity readings were calculated as the relative humidity reading divided by 100. Before measurements at each temperature, the sensor was calibrated with saturated lithium chloride and sodium chloride solutions based on their temperature-dependent equilibrium relative humidity values (*7*). Three samples from each lot were measured at each temperature for both systems.

5.2.11. Lipid analyses

The Omega-3 fatty acid content in chia seeds primarily consists of α-linolenic acid (ALA). Since the chia seeds were exposed to high temperatures for prolonged periods of time during thermal pasteurization, it is a concern whether the ALA content is

preserved after the thermal treatment. Therefore, uninoculated chia seed samples were subjected to the same protocols for the isothermal inactivation studies at 80, 85, and 90 °C for durations of 70 min 25 s, 37 min 8 s, and 14 min 44 s, respectively. The thermal treatment durations were calculated to achieve approximately 4 log reduction of *Salmonella* based on a log-linear model of lot 1 which demonstrated the highest thermal resistance. In the context of this study, the treatment at 90 °C emulates a high-temperature-short-time treatment while the 80 °C treatment is the low-temperature-long-time counterpart. The treated samples, along with controls, were analyzed for peroxide value (PV), thiobarbituric acid reactive substances (TBARS), omega-3 fatty acids, and omega-6 fatty acids. PV and TBARS were measured using spectrophotometric methods described by Li et al. (*20*) and Guillén-Sans (*8*), respectively. Both omega-3 and omega-6 fatty acids were measured by performing a fatty acid content analysis according to the AOAC method 996.06 (*12*). Omega-3 fatty acid content was calculated as the sum of ALA (*all-cis*-9,12,15-octadecatrienoic acid) and eicosatrienoic acid (all-cis-11,14,17-eicosatetraenoic acid). Omega-6 fatty acid content was calculated as the sum of linoleic acid (*all-cis*-9,12-octadecadienoic acid), gamma-linolenic acid (*all-cis*-6,9,12-octadecatrienoic acid), eicosadienoic acid (*all-cis*-11,14-eicosadienoic acid), dihomo-gamma-linolenic acid (*all-cis*-8,11,14-eicosatrienoic acid), and docosadienoic acid (*all-cis*-13,16-docosadienoic acid).

5.2.12. Statistical analyses

For the study on dilution pretreatments, differences between pretreatments within each bacteria-inoculation level combination were analyzed using Tukey's honestly

significant difference (HSD) test with the Python statsmodels library to account for family-wise error rates during multiple comparisons (*27*). As for the quality analyses, each quality attribute was analyzed separately by first performing a two-way ANOVA with interaction between treatment and lot using the same Python statsmodels library. If the interaction term was not significant, the two-way ANOVA was repeated without the interaction term. If any of the main effects (treatment or lot) were found to be significant, Tukey HSD was used to analyze pairwise differences between the levels in that main effect. On the other hand, if the interaction term in the two-way ANOVA was significant, Tukey HSD was used to analyze pairwise differences between lots within individual treatments, and pairwise differences between treatments with lots within each treatment pooled.

5.3. Results and Discussion

The raw data generated and analyzed in this study may be downloaded from https://doi.org/10.17605/OSF.IO/BC84F.

The aerobic plate counts for lots 1, 2, and 3 were calculated to be 2.68 ± 0.05, 2.40 ± 0.33, and 2.13 ± 0.12 $\log_{10}$ CFU/g, respectively. The native moisture content and water activity of the chia seed samples, as measured in triplicates per lot, were 6.78 ± 0.04, 6.94 ± 0.09, and 7.14 ± 0.06 % (wet basis) and 0.521 ± 0.002, 0.529 ± 0.010, 0.535 ± 0.04 for lots 1, 2, and 3, respectively. The recovery of *Salmonella* and *E. faecium* from chia seeds using various pretreatments is listed in **Table 5.1**. There is a large gap (~5 $\log_{10}$ CFU/g) in the quantity of bacteria recovered between the low and high inoculation levels which is expected because the low inoculation level used an inoculum that was

diluted fivefold. Within each inoculation levels for *Salmonella*, the puréeing pretreatment consistently had a significant difference compared to the other two pretreatments. In terms of magnitude, however, the puréeing pretreatment had only slightly higher (~0.1 $\log_{10}$ CFU/g) recovery than the other two pretreatments. The significant statistical differences can be attributed to the small variations in the recovery values. As for *E. faecium*, there were insignificant differences between the pretreatments, both statistically and in magnitude. For both bacteria, the trends for recovery at both low and high inoculation levels are the same, indicating that all the pretreatments should perform similarly regardless of the amount of bacteria present in the sample. In this study, the puréeing pretreatment is considered the "gold standard" in pretreatments because it reliably disintegrates the gel coating of the chia seeds to release any bacteria potentially trapped within or underneath the gel coating. However, it also requires the most work and time because each sample needs a sterile grinding cup, thus necessitating either a workflow to continuously sterilize, clean, and re-sterilize grinding cups after each puréeing or having a large inventory of grinding cups. On the other hand, the absence of pretreatments (*i.e.* the "None" pretreatment) has advantages and disadvantages that are essentially opposite of that of the puréeing pretreatment. As the results show, the recovery of both *Salmonella* and *E. faecium* are practically the same regardless of pretreatment. Therefore, the presumed advantage of the puréeing pretreatment for recovering more bacteria is nullified. Thus, for the microbial enumeration of samples in other parts of this study, chia seed samples were diluted with BPW in the sampling bags with filter and directly stomached without any pretreatments. The difficulty of preparing chia seeds for microbial enumeration has been reported in the literature. Fong and Wang

(*5*) diluted their seeds tenfold and mixed the mixture by hand for 1 min to avoid formation of a gelatinous matrix. Keller et al. (*18*) increased the amount of diluent to dilute the seeds at a 1:20 ratio and also mixed the mixture by hand. On the other hand, Hylton et al. (*13*) used a lower dilution ratio (1:5) but mechanically stomached their samples for 2 min and stated that BPW mitigates formation of the gel coating. The results of this study show that a higher dilution ratio (1:30), the use of filter bags, and stomaching the mixture can result in reliable and sufficient recovery of bacteria from chia seeds.

The homogeneity and stability of moisture and bacterial population in the inoculated chia seed samples are visualized in **Fig. 5.1**. The relatively small standard deviation of bacterial population—maximum of 0.16 $\log_{10}$ CFU/g for both bacteria—indicates good homogeneity of the inoculation. Three days after inoculation, the moisture content and water activity of samples inoculated with either *Salmonella* or *E. faecium* equilibrated and remained stable around 7% and 0.53, respectively. As for bacterial population, *Salmonella* decreased by about 0.4 $\log_{10}$ CFU/g over 7 days before stabilizing to approximately 7.9 $\log_{10}$ CFU/g. *E. faecium* stabilized comparatively faster to approximately 8 $\log_{10}$ CFU/g after only 3 days. Based on these results, the inoculated samples were allowed to equilibrate for at least 3 days before they were used in the isothermal inactivation studies because the water activity was deemed to be the more important parameter. The importance of water activity in the context of bacterial thermal resistance has been shown in various low-moisture foods (*4*, *24*, *30*).

The thermal inactivation curves of both *Salmonella* and *E. faecium* at 80, 85, and 90 °C was plotted in **Fig. 5.2**. In the upper row, the data for all three lots are plotted and fitted to the log-linear and Weibull models. Lot 3 (filled markers) exhibited lower survivors (*i.e.* faster death rate) for both bacteria and at all temperatures, indicating a lower thermal resistance than the other two lots. In fact, because the bacteria in lot 3 were dying at a faster rate than the other two lots, the timepoints for lot 3 had to be adjusted to avoid having a portion of the data under the detection limit. Since lot 3 appeared to be the special case, it was excluded in the lower row of **Fig. 5.2**. The exclusion of lot 3 allowed for a better fit of the models, though the resultant slope or curve of the lines indicate a higher or conservative estimate of thermal resistance. The model parameters for the log-linear and Weibull models with or without lot 3 are compared in **Table 5.2**. The larger values of $D_{80°C}$ and $\alpha_{80°C}$ for models that excluded lot 3 in comparison to the models with lot 3 confirms the observations of higher thermal resistances in **Fig. 5.2**. In addition, the RMSE of the models without lot 3 are always lower than their counterparts with lot 3, indicating better fit. Naturally, the exclusion of an entire set of data to achieve a better model fit is not a productive exercise. However, it should also be noted that without lot 3, the resulting models are more conservative in the sense that they predict a higher thermal resistance, thus requiring harsher pasteurization conditions. In the context of food safety, it is prudent to be conservative. Therefore, both situations (with and without lot 3) are presented in this work to allow judgement and use of either case. Within each situation, the Weibull model always outperformed the log-linear model based on its lower AIC_c values. This is as expected because the Weibull model has been shown to be more favorable than the log-linear model for modeling the thermal inactivation of

microorganisms in most food products (*33*). Interestingly, the Weibull models with lot 3 had smaller values for β than their counterparts without lot 3, indicating a more prominent "tailing off" effect as time goes on. In fact, this can be seen around the 75 min mark of the left column (*Salmonella*) in **Fig. 5.2** where the Weibull line for all lots is just slightly higher than without lot 3. Therefore, caution is advised when extrapolating the models out of the time ranges in this study. Across all the models and the inclusion/exclusion of lot 3, *E. faecium* had higher thermal resistance than *Salmonella*, suggesting its suitability as a conservative non-pathogenic surrogate in thermal pasteurization of chia seeds.

It has been shown that higher water activity at high temperatures usually results in decreased thermal resistance compared to the same sample with lower water activity (*21*, *22*). As a preliminary attempt to understand the cause of the lower thermal resistance for both bacteria in lot 3, the water activity of inoculated samples from all lots were measured from room temperature to the high treatment temperatures used in the isothermal inactivation study (**Fig. 5.3**). The data from the vapor sorption analyzer had good agreement with the custom measurement device at 50 and 60 °C, therefore, both datasets are considered equivalent in subsequent analysis. It can be seen that the water activity of all three lots do increase with temperature up to approximately 0.68 at 80 °C. In addition, the trend and magnitude of water activity with temperature for all three lots are practically the same, with lot 3 having only slightly higher (~0.015) water activity at 80 °C. Therefore, the decreased thermal resistance of lot 3 is unlikely to be due to higher water activity than the other two lots at the treatment temperatures. Since there are some

research suggesting that chia seeds have antibacterial properties, it could be argued that lot 3 may have higher antibacterial properties than the other two lots. However, the scientific consensus on the antibacterial properties of chia seeds is mixed: growth inhibition of *Staphylococcus aureus* (ATCC 10832) and *Escherichia coli* O157:H7 (ATCC 43895) with protein extracts from chia seeds (*2*); no growth inhibition of *Escherichia coli*, *Salmonella* typhi, *Shigella flexneri*, *Klebsiella pneumonia*, *Staphylococcus aureus*, *Bacillus subtilis* and *Streptococcus agalactiae* with chia protein hydrolysates (*28*); no growth inhibition of *Staphylococcus aureus* NCTC 8530, *Bacillus subtilis* NRRL-B209, *Listeria monocytogenes* ATCC 7644, and *Escherichia coli* BL21 with oil extracts from chia seeds (*32*); growth inhibition of various bacteria including *Salmonella typhimurium* ATCC 14028 and *Salmonella enteritidis* ATCC 13076 but no effect for various other microorganisms with chia seed extracts (*19*). In short, the antimicrobial activity of chia seeds may be species- and strain-specific. It should also be noted that the cited studies were investigating growth inhibition; none have investigated inactivation at high temperatures encountered in thermal pasteurization processes. The chia seed samples used in this study are also mixtures of black and white chia seeds which have been shown to have slightly different phenolic contents and antioxidant activities (*32*). Therefore, more work needs to be done to understand how differences between production lots of chia seeds could affect bacterial thermal resistance.

The lipid analysis results of thermally treated chia seeds to achieve approximately 4-log reduction of *Salmonella* are summarized in **Table 5.3**. Overall, there is not a consistently large difference between lot 3 and the other two lots for all the quality

measurements as was previously seen in the thermal inactivation results. The interaction between treatment and lot for PV was found to be significant, therefore lot-specific data within each treatment were then combined for analyzing differences between treatments. At 85 °C, the PV value was significantly different than the control and other two treatments. When pairwise comparisons for PV were done on lots within individual treatments, the differences between lots, in general, are not significantly different. Interestingly, the PV at 90 °C was lower than that of 85 °C even though one would expect more lipid oxidation to occur at higher temperatures. Since there is no clear trend as to how the samples at 85 °C had a higher PV value, it is likely that the abnormally high PV values at 85 °C are due to outlier samples, as indicated by the large standard deviations. The amount of TBARS for all treatments are insignificantly different both statistically and in magnitude. Since PV is a measure of primary lipid oxidation products while TBARS helps in tracking secondary oxidation products (*26*), these results suggest that either the lipid oxidation has not advanced sufficiently to produce secondary oxidation products or that the oxidation advanced through other pathways not detected by the TBARS test. The amounts of Omega-3 and Omega-6 fatty acids in the chia seeds samples after thermal treatment did not change significantly from the control, with exception to the 80 °C treatment. The lower Omega-3 and Omega-6 fatty acid content for the 80 °C treatment may be due to the longer treatment time (70 min 25 s) which is almost twice that of 85 °C (37 min 8 s) and almost quadruple that of 90 °C (14 min 44 s). Imran et al. (*14*) detected a higher reduction in the major Omega-3 fatty acid of chia seeds, ALA, when the seeds were subjected to autoclaving (121 °C, 15 psi, 15 min) as compared to boiling (100 °C, 5 min), and oven drying (105 °C, 1 h). Considering the

different results depending on the nature of heat treatment used, it will be necessary to perform in-depth quality analyses when scaling up and implementing a thermal pasteurization process for chia seeds.

In conclusion, *E. faecium* was found to be a conservative nonpathogenic surrogate for *Salmonella* for thermal processes. The Weibull model predicted thermal inactivation for both *Salmonella* and *E. faecium* better than the log-linear model. The difficulty of preparing chia seeds for dilution in microbial enumeration could be overcome by increasing the dilution factor and using a bag with filter. Future work could investigate factors that could introduce variability into the thermal resistance of microorganisms in chia seeds, as seen in lot 3 in this study.

5.4. Acknowledgements

This material is based upon work that is supported by the National Institute of Food and Agriculture, U.S. Department of Agriculture, under award number 2015-68003-23415 and with partial support from the Nebraska Agricultural Experiment Station with funding from the Hatch Act (Accession Number 1006859) through the USDA National Institute of Food and Agriculture.

5.5. References

1. Coelho, M. S., and M. de las M. Salas-Mellado. 2014. Chemical Characterization of Chia (*Salvia hispanica L.*) for Use in Food Products. 5. *J. Food Nutr. Res.* Science and Education Publishing 2:263–269.

2. Coelho, M. S., R. A. M. Soares-Freitas, J. A. G. Arêas, E. A. Gandra, and M. de las M. Salas-Mellado. 2018. Peptides from Chia Present Antibacterial Activity and Inhibit Cholesterol Synthesis. *Plant Foods Hum. Nutr.* 73:101–107.
3. Coorey, R., A. Tjoe, and V. Jayasena. 2014. Gelling Properties of Chia Seed and Flour. *J. Food Sci.* 79:E859–E866.
4. Finn, S., O. Condell, P. McClure, A. Amézquita, and S. Fanning. 2013. Mechanisms of survival, responses and sources of Salmonella in low-moisture environments. *Front. Microbiol.* 4.
5. Fong, K., and S. Wang. 2016. Strain-Specific Survival of *Salmonella enterica* in Peanut Oil, Peanut Shell, and Chia Seeds. *J. Food Prot.* 79:361–368.
6. Grancieri, M., H. S. D. Martino, and E. G. de Mejia. 2019. Chia Seed (*Salvia hispanica L.*) as a Source of Proteins and Bioactive Peptides with Health Benefits: A Review. *Compr. Rev. Food Sci. Food Saf.* 18:480–499.
7. Greenspan, L. 1977. Humidity Fixed-Points of Binary Saturated Aqueous-Solutions. *J. Res. Natl. Bur. Stand. Sect. -Phys. Chem.* 81:89–96.
8. Guillén-Sans, R., and M. Guzmán-Chozas. 1998. The Thiobarbituric Acid (TBA) Reaction in Foods: A Review. *Crit. Rev. Food Sci. Nutr.* Taylor & Francis 38:315–350.
9. Harvey, R. R., K. E. Heiman Marshall, L. Burnworth, M. Hamel, J. Tataryn, J. Cutler, K. Meghnath, A. Wellman, K. Irvin, L. Isaac, K. Chau, A. Locas, J. Kohl, P. A. Huth, D. Nicholas, E. Traphagen, K. Soto, L. Mank, K. Holmes-Talbot, M. Needham, A. Barnes, B. Adcock, L. Honish, L. Chui, M. Taylor, C. Gaulin, S. Bekal, B. Warshawsky, L. Hobbs, L. R. Tschetter, A. Surin, S. Lance, M. E. Wise, I.

Williams, and L. Gieraltowski. 2017. International outbreak of multiple *Salmonella* serotype infections linked to sprouted chia seed powder - USA and Canada, 2013-2014. *Epidemiol. Infect.* 145:1535–1544.

10. Hildebrandt, I. M., B. P. Marks, V. K. Juneja, M. Osoria, N. O. Hall, and E. T. Ryser. 2016. Cross-Laboratory Comparative Study of the Impact of Experimental and Regression Methodologies on *Salmonella* Thermal Inactivation Parameters in Ground Beef. *J. Food Prot.* 79:1097–1106.
11. Hildebrandt, I. M., B. P. Marks, E. T. Ryser, R. Villa-Rojas, J. Tang, F. J. Garces-Vega, and S. E. Buchholz. 2016. Effects of Inoculation Procedures on Variability and Repeatability of *Salmonella* Thermal Resistance in Wheat Flour. *J. Food Prot.* 79:1833–1839.
12. Horwitz, W., and G. W. Latimer. 2005. Official methods of analysis of AOAC International. AOAC International, Gaithersburg, Md.
13. Hylton, R. K., A. F. Sanchez-Maldonado, P. Peyvandi, F. Rahmany, F. Dagher, C. G. Leon-Velarde, K. Warriner, and A. M. Hamidi. 2019. Decontamination of Chia and Flax Seed Inoculated with *Salmonella* and Surrogate, *Enterococcus faecium* NRRL B-2354, Using a Peracetic Acid Sanitizing Solution: Antimicrobial Efficacy and Impact on Seed Functionality. *J. Food Prot.* 82:486–493.
14. Imran, M., M. Nadeem, M. F. Manzoor, A. Javed, Z. Ali, M. N. Akhtar, M. Ali, and Y. Hussain. 2016. Fatty acids characterization, oxidative perspectives and consumer acceptability of oil extracted from pre-treated chia (*Salvia hispanica L.*) seeds. *Lipids Health Dis.* 15.

15. Jewell, K. 2012. Comparison of 1-step and 2-step methods of fitting microbiological models. *Int. J. Food Microbiol.* 160:145–161.

16. Jin, Y., J. Tang, and M.-J. Zhu. 2020. Water activity influence on the thermal resistance of *Salmonella* in soy protein powder at elevated temperatures. *Food Control* 113:107160.

17. Julio, L. M., V. Y. Ixtaina, M. A. Fernández, R. M. T. Sánchez, J. R. Wagner, S. M. Nolasco, and M. C. Tomás. 2015. Chia seed oil-in-water emulsions as potential delivery systems of ω-3 fatty acids. *J. Food Eng.* 162:48–55.

18. Keller, S. E., N. M. Anderson, C. Wang, S. J. Burbick, I. M. Hildebrandt, L. J. Gonsalves, Q. J. Suehr, and S. M. S. Farakos. 2018. Survival of *Salmonella* during Production of Partially Sprouted Pumpkin, Sunflower, and Chia Seeds Dried for Direct Consumption. *J. Food Prot.* 81:520–527.

19. Kobus-Cisowska, J., D. Szymanowska, P. Maciejewska, D. Kmiecik, A. Gramza-Michałowska, B. Kulczyński, and J. Cielecka-Piontek. 2019. In vitro screening for acetylcholinesterase and butyrylcholinesterase inhibition and antimicrobial activity of chia seeds (*Salvia hispanica*). *Electron. J. Biotechnol.* 37:1–10.

20. Li, C. T., M. Wick, and D. B. Min. 2001. Spectrophotometric determination of lamb tissue peroxide value. 183. Special Circular, Ohio Agricultural Research and Development Center.

21. Liu, S., R. V. Rojas, P. Gray, M.-J. Zhu, and J. Tang. 2018. *Enterococcus faecium* as a *Salmonella* surrogate in the thermal processing of wheat flour: Influence of water activity at high temperatures. *Food Microbiol.* 74:92–99.

22. Liu, S., J. Tang, R. K. Tadapaneni, R. Yang, and M.-J. Zhu. 2018. Exponentially Increased Thermal Resistance of *Salmonella* spp. and *Enterococcus faecium* at Reduced Water Activity. *Appl. Environ. Microbiol.* American Society for Microbiology 84.

23. Peleg, M. 2006. Advanced Quantitative Microbiology for Foods and Biosystems: Models for Predicting Growth and Inactivation1 edition. CRC Press, Boca Raton.

24. Podolak, R., E. Enache, W. Stone, D. G. Black, and P. H. Elliott. 2010. Sources and Risk Factors for Contamination, Survival, Persistence, and Heat Resistance of *Salmonella* in Low-Moisture Foods. *J. Food Prot.* 73:1919–1936.

25. Reyes-Jurado, F., A. R. Navarro-Cruz, J. Méndez-Aguilar, C. E. Ochoa-Velasco, E. Mani-López, M. T. Jiménez-Munguía, E. Palou, A. López-Malo, and R. Ávila-Sosa. 2019. High-Intensity Light Pulses To Inactivate *Salmonella* Typhimurium on Mexican Chia (*Salvia hispanica L.*) Seeds. *J. Food Prot.* Allen Press 82:1272–1277.

26. Schaich, K. M. 2016. Analysis of Lipid and Protein Oxidation in Fats, Oils, and Foods, p. 1–131. *In* M. Hu, and C. Jacobsen (eds.), Oxidative Stability and Shelf Life of Foods Containing Oils and Fats. AOCS Press.

27. Seabold, S., and J. Perktold. 2010. statsmodels: Econometric and statistical modeling with python, 9th Python in Science Conference.

28. Segura-Campos, M. R., I. M. Salazar-Vega, L. A. Chel-Guerrero, and D. A. Betancur-Ancona. 2013. Biological potential of chia (*Salvia hispanica L.*) protein hydrolysates and their incorporation into functional foods. *LWT - Food Sci. Technol.* 50:723–731.

29. Sung, W. C., E. T. Chiu, A. Sun, and H. I. Hsiao. 2020. Incorporation of chia seed flour into gluten-free rice layer cake: Effects on nutritional quality and physicochemical properties. *J. Food Sci.* 85:545–555.
30. Syamaladevi, R. M., J. Tang, R. Villa-Rojas, S. Sablani, B. Carter, and G. Campbell. 2016. Influence of Water Activity on Thermal Resistance of Microorganisms in Low-Moisture Foods: A Review. *Compr. Rev. Food Sci. Food Saf.* 15:353–370.
31. Tamber, S., E. Swist, and D. Oudit. 2016. Physicochemical and Bacteriological Characteristics of Organic Sprouted Chia and Flax Seed Powders Implicated in a Foodborne Salmonellosis Outbreak. *J. Food Prot.* 79:703–709.
32. TunçiL, Y. E., and Ö. F. ÇeliK. 2019. Total phenolic contents, antioxidant and antibacterial activities of chia seeds (*Salvia hispanica L.*) having different coat color. *Akad. Ziraat Derg.* 113–120.
33. van Boekel, M. A. J. S. 2002. On the use of the Weibull model to describe thermal inactivation of microbial vegetative cells. *Int. J. Food Microbiol.* 74:139–159.
34. Verdú, S., J. M. Barat, and R. Grau. 2017. Improving bread-making processing phases of fibre-rich formulas using chia (*Salvia hispanica*) seed flour. *LWT - Food Sci. Technol.* 84:419–425.
35. Verma, T., X. Wei, S. K. Lau, A. Bianchini, K. M. Eskridge, and J. Subbiah. 2018. Evaluation of *Enterococcus faecium* NRRL B-2354 as a Surrogate for *Salmonella* During Extrusion of Low-Moisture Food. *J. Food Sci.* 83:1063–1072.
36. Virtanen, P., R. Gommers, T. E. Oliphant, M. Haberland, T. Reddy, D. Cournapeau, E. Burovski, P. Peterson, W. Weckesser, J. Bright, S. J. van der Walt, M. Brett, J. Wilson, K. J. Millman, N. Mayorov, A. R. J. Nelson, E. Jones, R. Kern, E. Larson, C.

J. Carey, İ. Polat, Y. Feng, E. W. Moore, J. VanderPlas, D. Laxalde, J. Perktold, R. Cimrman, I. Henriksen, E. A. Quintero, C. R. Harris, A. M. Archibald, A. H. Ribeiro, F. Pedregosa, and P. van Mulbregt. 2020. SciPy 1.0: fundamental algorithms for scientific computing in Python. 3. *Nat. Methods*. Nature Publishing Group 17:261–272.

37. Wei, X., S. K. Lau, J. Stratton, S. Irmak, A. Bianchini, and J. Subbiah. 2018. Radio-Frequency Processing for Inactivation of *Salmonella enterica* and *Enterococcus faecium* NRRL B-2354 in Black Peppercorn. *J. Food Prot.* 81:1685–1695.

Table 5.1. Recovery of Salmonella and E. faecium from chia seeds subjected to various inoculation levels and pretreatments.

Bacteria	Inoculation level	Pretreatment	Recovery (log_{10} CFU/g)
Salmonella	High	Purée	7.94 ± 0.09 [a]
		None	7.72 ± 0.06 [b]
		Soak 5 min	7.81 ± 0.04 [b]
	Low	Purée	2.99 ± 0.08 [a]
		None	2.81 ± 0.11 [b]
		Soak 5 min	2.84 ± 0.04 [b]
E. faecium	High	Purée	7.89 ± 0.08 [a]
		None	7.79 ± 0.08 [a]
		Soak 5 min	7.88 ± 0.16 [a]
	Low	Purée	2.77 ± 0.07 [a]
		None	2.69 ± 0.09 [a]
		Soak 5 min	2.78 ± 0.13 [a]

Values are reported as mean ± standard deviation. Within each bacteria-inoculation level combination, means sharing a common letter are not significantly different (α = 0.05).

Table 5.2. Model parameter estimates and corresponding goodness-of-fit measures for thermal inactivation of Salmonella and E. faecium in chia seeds with $\boldsymbol{T_{ref}} = 80°C$.

Bacteria	Model	$D_{80°C}$ or $\alpha_{80°C}$ (min)	z (°C)	β	RMSE ($\log_{10}$ CFU/g)	AIC_c
Salmonella	Log linear	6.41 (0.15)	13.86 (0.50)	-	0.677	-83
	Log linear (excluding lot 3)	6.96 (0.13)	13.35 (0.40)	-	0.479	-108
	Weibull	0.55 (0.11)	14.72 (0.62)	0.57 (0.03)	0.434	-181
	Weibull (excluding lot 3)	0.97 (0.13)	13.70 (0.37)	0.65 (0.03)	0.289	-183
E. faecium	Log linear	10.17 (0.26)	13.80 (0.54)	-	0.784	-49
	Log linear (excluding lot 3)	11.26 (0.16)	13.70 (0.29)	-	0.361	-141
	Weibull	0.77 (0.18)	13.08 (0.58)	0.56 (0.03)	0.541	-130
	Weibull (excluding lot 3)	2.58 (0.26)	13.36 (0.27)	0.77 (0.03)	0.274	-178

Values are reported as parameter estimate (standard error of estimate).

Table 5.3. Quality analysis results of chia seeds subjected to various thermal treatments to achieve approximately 4 log reduction of Salmonella.

Treatment	Lot	Peroxide value (meq peroxide/kg seed)	TBARS (mM/g seed)	Omega-3 fatty acid (mg/g seeds)	Omega-6 fatty acid (mg/g seeds)
Control	1	54.91 ± 15.45 ^{a,A}	0.50 ± 0.15 ^{A}	158.43 ± 7.01 ^{AB}	47.30 ± 1.50 ^{AB}
	2	35.15 ± 3.06 ^{ab}	0.41 ± 0.05	149.69 ± 3.85	44.32 ± 1.22
	3	29.74 ± 2.14 ^{b}	0.34 ± 0.03	156.55 ± 4.00	45.80 ± 0.54
80 °C	1	27.40 ± 13.38 ^{a,A}	0.36 ± 0.11 ^{A}	131.46 ± 18.33 ^{B}	38.93 ± 5.63 ^{B}
	2	25.23 ± 2.17 ^{a}	0.36 ± 0.04	151.90 ± 4.36	45.63 ± 2.18
	3	28.81 ± 7.30 ^{a}	0.42 ± 0.05	121.39 ± 52.98	35.23 ± 15.08
85 °C	1	84.04 ± 16.8 ^{a,B}	0.58 ± 0.09 ^{A}	164.98 ± 4.48 ^{A}	49.64 ± 1.01 ^{A}
	2	48.99 ± 14.66 ^{a}	0.43 ± 0.06	152.18 ± 3.17	45.35 ± 0.91
	3	70.95 ± 11.41 ^{a}	0.43 ± 0.14	155.34 ± 6.06	45.52 ± 2.23
90 °C	1	31.65 ± 1.82 ^{a,A}	0.36 ± 0.07 ^{A}	159.77 ± 3.17 ^{A}	47.40 ± 0.62 ^{A}
	2	29.43 ± 2.58 ^{a}	0.42 ± 0.04	158.28 ± 2.09	46.99 ± 0.85
	3	27.54 ± 2.48 ^{a}	0.44 ± 0.09	159.04 ± 2.52	46.84 ± 1.08

Values are reported as mean ± standard deviation. Uppercase letters compare means of treatments, with all lots within a treatment pooled. Lowercase letters compare means of lots within an individual treatment. Means sharing a common letter are not significantly different ($\alpha = 0.05$). Absence of lowercase letters indicate that no statistical comparison was performed for comparing lots due to non-significant main effect of lots.

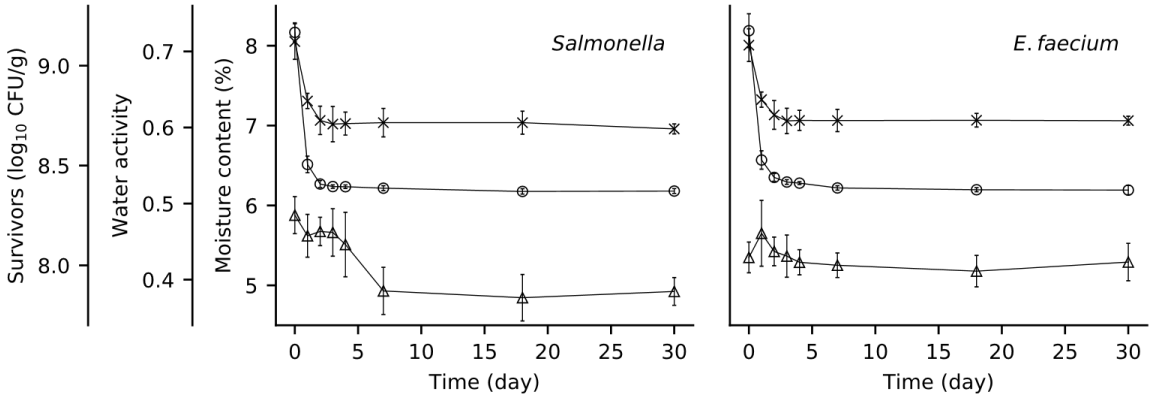

Figure 5.1. Homogeneity and stability of moisture content (×), water activity (○), and inoculum population (△) in chia seed samples inoculated with *Salmonella* and *E. faecium*. Each half of the error bars indicate one standard deviation.

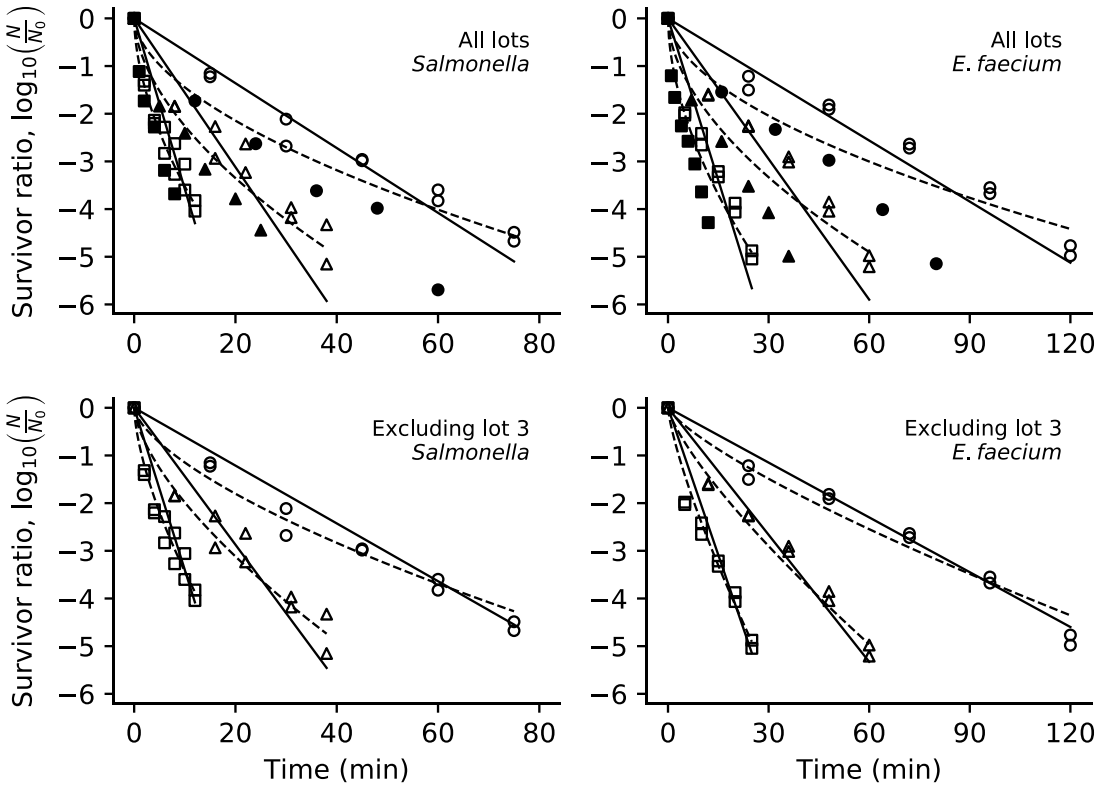

Figure 5.2. Thermal inactivation of *Salmonella* and *E. faecium* in chia seeds at 80 (○), 85 (△), and 90 °C (□). Solid and dashed lines are fitted log-linear and Weibull models, respectively. Data for lot 3 are plotted as filled markers.

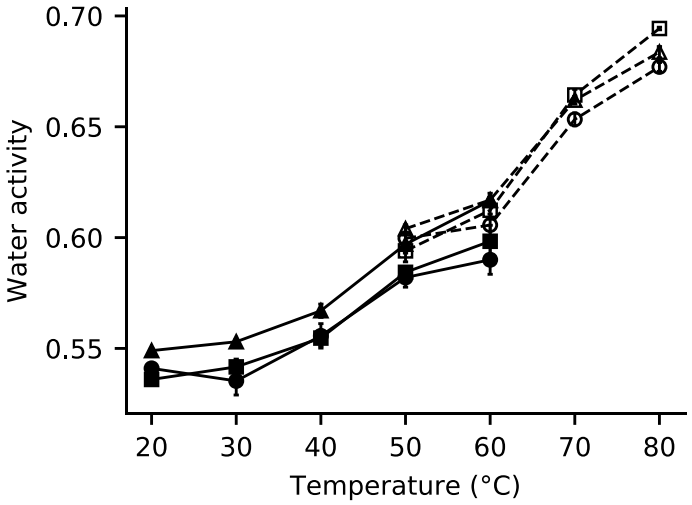

Figure 5.3. Water activity of chia seeds from lots 1 (○), 2 (△), and 3 (□) from 20 to 80 °C measured using a vapor sorption analyzer (filled markers, solid lines) and a custom high temperature water activity meter (empty markers, dashed lines).

Chapter 6: Summary and Recommendations

6.1. Summary

The TDT Sandwich described in Chapter 2 is an open source tool for characterizing the thermal resistance of microorganisms in food. Samples are packed in heat-sealable pouches and heated inside the TDT Sandwich with dry heat. The user can adjust multiple treatment parameters such as temperature, heating duration, and heating rate using a computer program. The TDT Sandwich is capable of operating up to 140 °C and achieving heating rates up to approximately 100 °C/min. Based on results of the characterization study, it is advisable to operate the TDT Sandwich with minimal sample thickness and below 110 °C. Assuming these operation limits are obeyed, the largest temperature nonuniformity of up to 1 °C will be observed between the center and corner of the sample during the initial heating phase. Upon reaching the target temperature, this temperature nonuniformity will degrade to negligible amounts after a sufficient time (~2 min). Once the sample has achieved near-isothermal conditions, the TDT Sandwich is able to maintain the temperature of the sample within 0.2 °C of the target temperature.

Chapter 3 described the development of the HumidOSH, an open source environmental chamber. The system allows users to adjust the water activity of food samples through precise control of relative humidity within the chamber. Other ergonomic and functional features such as overhead lighting, sampling door, and a power outlet are also included. The chambers are self-contained; every part is mounted onto the chamber itself, making it easy to relocate or replace HumidOSH units. Operation of the HumidOSH is performed through a mounted display and keypad for adjusting the target

relative humidity and fan speed. When operated at relative humidity targets of 5 % and 80 % with large amounts of samples (500 g of whole milk powder), the HumidOSH was capable of equilibrating samples to the corresponding water activities (0.05 and 0.80) within three days. The built-in two-point calibration allows users to recalibrate the sensors if the relative humidity readings are inaccurate.

Both of the aforementioned systems were used to prepare and treat samples in the thermal resistance studies of Chapters 3 and 4. The thermal resistance of *Salmonella* in whole milk powder was determined in Chapter 3 with three methods: TDT disk in water bath, pouches in water bath, and TDT Sandwich. The resultant survivor data was fitted to the log-linear and Weibull models, with the latter being the better fit. Analysis of the model parameters also showed insignificant differences between the three thermal treatments, indicating that the TDT Sandwich can be used as a direct replacement for conventional isothermal treatments. In fact, the TDT Sandwich had advantages in certain aspects such as smaller variability in come-up time and less microbial reduction during the come-up phase.

In chapter 4, the thermal resistances of *Salmonella* and a potential surrogate, *Enterococcus faecium* NRRL B-2354, were characterized in whole chia seeds. The unique gel-forming ability of chia seeds upon exposure to water created issues in diluting the sample for microbial enumeration. After investigating three methods of dilution, it was determined that simply increasing the dilution liquid to a 1:30 (w/w) ratio and stomaching in a filter bag resulted in similar recovery to the other two methods that involved puréeing or pre-soaking the chia seeds for 5 min. The survivor data of both

bacteria were fitted to the log-linear and Weibull models, with the latter showing a better fit. Comparison of model parameters showed that *E. faecium* had higher thermal resistance than *Salmonella*, indicating its suitability as a conservative surrogate. Interestingly, one of the chia seed production lot had significantly lower thermal resistance than the other two lots. This lower thermal resistance could not be explained by a difference in water activity at higher temperatures, suggesting that there may be other factors involved in the thermal resistance of microorganisms in low-moisture foods.

6.2. Recommendations for Future Research

The TDT Sandwich and HumidOSH were developed as open source tools in order to provide other researchers with the means of building and using these tools for their own research. There is still a lot of work to be done to fully characterize the thermal resistance of pathogenic microorganisms in low-moisture foods, therefore these tools can be used to make progress in this area. These open source tools can also be used for other purposes. The TDT Sandwich can be adapted for characterizing thermal degradation kinetics of heat-sensitive compounds in foods. The HumidOSH can be used for long-term storage of moisture-sensitive samples or to adjust the moisture content/water activity of samples.

The statistical framework developed in Chapter 4 for comparing the parameters of thermal resistance models can be extended to other food products. The thermal resistance models for both *Salmonella* and *E. faecium* can be used in scaled-up thermal technologies such as retort or radiofrequency heating. The time-temperature profiles of products undergoing these processes can be used as inputs for the developed models to predict

microbial inactivation. The thermal inactivation data for chia seeds in Chapter 5 can be used similarly. In addition to that, the unexplained lower heat resistance in production lot 3 begs for more investigation into additional factors aside from water activity that could affect the heat resistance of microorganisms in low-moisture foods.